8-9-2022

Modeling supercritical fluids and fabricating electret films to address dielectric challenges in high-power-density systems

Farhina Haque
farhina141@gmail.com

Modeling supercritical fluids and fabricating electret films to address dielectric challenges in high-power-density systems

By

Farhina Haque

Approved by:

Chanyeop Park (Major Professor)
Masoud Karimi Ghartemani
Mehmet Kurum
Ryan B. Green
Qian (Jenny) Du (Graduate Coordinator)
Jason M. Keith (Dean, Bagley College of Engineering)

A Dissertation
Submitted to the Faculty of
Mississippi State University
in Partial Fulfillment of the Requirements
for the Degree of Doctor of Philosophy
in Electrical and Computer Engineering
in the Department of Electrical and Computer Engineering

Mississippi State, Mississippi

August 2022

Name: Farhina Haque

Date of Degree: August 9, 2022

Institution: Mississippi State University

Major Field: Electrical and Computer Engineering

Major Professor: Chanyeop Park

Title of Study: Modeling supercritical fluids and fabricating electret films to address dielectric challenges in high-power-density systems

Pages in Study: 177

Candidate for Degree of Doctor of Philosophy

Wide bandgap (WBG) devices and power electronic converters (PEC) that enable the dynamic control of energy and high-power density designs inevitably contain defects including sharp edges, triple points, and cavities, which result in local electric field enhancements. The intensified local electric stresses cause either immediate dielectric breakdown or partial discharge (PD) that erodes electrical insulators and accelerates device aging. With the goal of addressing these dielectric challenges emerging in power-dense applications, this dissertation focuses on 1) modeling the dielectric characteristics of supercritical fluids (SCFs), which is a new dielectric medium with high dielectric strength and high cooling capability; and 2) establishing the optimal fabrication conditions of electrets, which is a new dielectric solution that neutralizes locally enhanced electric fields.

In this dissertation, the dielectric breakdown characteristics of SCFs are modeled as a function of pressure based on the electron scattering cross section data of clusters that vary in size as a function of temperature and pressure around the critical point. The modeled breakdown electric field is compared with the experimental breakdown measurements of supercritical fluids, which show close agreement. In addition, electrets are fabricated based on the triode-corona

charging method and their PD mitigation performance is evaluated through a series of PD experiments. Electrets are fabricated under various charging conditions, including charging voltage, duration, polarity, and temperature with the goal of identifying the optimal condition that leads to effective PD mitigation. The PD mitigation performance of electrets fabricated based on these charging conditions is further assessed by investigating the impact of various power electronics voltage characteristics, including *dv/dt*, polarity, switching frequency, and duty cycle. Electret based electric field neutralization approach is further utilized in increasing the critical flashover voltage associated with the surface flashover voltage. Moreover, due to the high mechanical strength of epoxy composites at cryogenic temperatures, in this dissertation, epoxy-based electrets are fabricated as a solution to PD in high temperature superconducting cables. The experimental demonstrations conducted with electret in this dissertation is dedicated for the establishing the electret based electric field neutralization approach as a dielectric solution for the dielectric challenges in power electronics driven systems.

DEDICATION

To my beloved Family.

ACKNOWLEDGEMENTS

I would express my sincere gratitude to my advisor Dr. Chanyeop park for his continuous supports and inspiration to achieve my goal. His advice and motivation have made me to reach at this position. I would also thank my previous advisor Dr. Joni Kluss who gave me the opportunity to join the High Voltage Lab.

Apart from my advisor, I would like to express my sincere gratitude to my committee members Dr. Masoud Karimi, Dr. Mehmet Kurum, and Dr. Ryan Green. There valuable feedback on my research helped me to broaden my knowledge. I would like to express my appreciation to the rest of the team (both present and past) in High Voltage Lab, especially Dr. David Wallace, Dr. Zeeshan, Dr. Mojtaba, Dr. Kamran, Omar, Pradip, Bobby, Rashid, Tahir, and Avri. I am thankful to my friends Tashfin, Farzana, Kemi, Sudipto, and others in Starkville for their supports. Last but not the least, I would like to acknowledge all my family member from my parents and siblings to all my uncle, aunts, and cousins for their love, supports, and prayers.

TABLE OF CONTENTS

LIST OF TABLES

LIST OF FIGURES

CHAPTER I

INTRODUCTION

1.1 Problem statement

The high efficiency, high electric field, and high-power density provided by wide bandgap (WBG) semiconductors and advanced power electronic converter (PEC) topologies enable the dynamic control of power in medium to high voltage systems. WBG semiconductors outperform the conventional Silicone (Si) based devices in terms of voltage rating, switching speed, and efficiency. The increased voltage handing properties, high dv/dt, and compact device packaging enable all-electric ship, more-electric aircraft, and automotive vehicle where major goal is to provide high-power density and high-efficiency with a reduction in weight and size. However, high electric field generated by thin laminated structures, high voltage blocking capabilities, and fast switching frequency cause inevitable dielectric challenges in these modern power-dense applications. The presence of sharp edges in bonded wires, triple points at the metallization layers, and defects including cracks, bubbles, and airgaps in the interfaces of the laminated structure cause local electric field enhancements. The intensified electric field promotes partial discharge (PD) and surface flashover (SFO) that accelerate dielectric material ageing and reduce device lifetime. New dielectric media and solutions are required to address the dielectric challenges emerging in the PEC driven systems. Supercritical fluids (SCFs), a new dielectric medium with high dielectric strength and low viscosity, show steep decrease in the dielectric strength near the critical point. In this dissertation, the dielectric strength variation of SCFs near the critical point is modeled based

on the electron scattering cross section data of various cluster sizes of SCFs. In addition, electrets, a new dielectric solution to neutralize the localized electric field, mitigate partial discharge (PD) effectively when fabricated at an optimum charging condition. This dissertation demonstrates the performance of electrets when fabricated under various charging conditions. Based on the analysis, electret-based electric field neutralization is utilized in PD mitigation caused by various power electronics parameters and surface flashover improvement.

1.2 State of the art

1.2.1 Sulfur Hexafluoride (SF_6): traditional dielectric medium

Sulfur Hexafluoride (SF_6) is a man-made gas with non-toxicity, non-flammability, low boiling point, thermal stability, and chemically inert property [1]. The high gas density maintained at low temperatures and tightly bounded electrons provide SF_6 high dielectric strength [2], which is 2.5-3 times higher than air [3]. Owing to the high dielectric strength along with other excellent properties, e.g., good heat transfer capability, interruption of electric arcs, strong dielectric recovery strength provided by SF_6, it has been considered as the most efficient gaseous dielectric medium for medium to high voltage applications for many decades [1], [3]–[5].

1.2.1.1 Dielectric properties of SF_6

Electron kinetic process is utilized to analyze the electrical breakdown characteristics of gaseous medium. Every gaseous medium has its own set of electron-scattering cross section data that has impact on the electron energy distribution function and the electron kinetic process. Electron scattering cross section data is utilized for Boltzmann analysis to determine the ionization and attachment coefficients of the gaseous medium. The critical electric field, at which the ionization process is in equilibrium with the electron attachment process, has been used as the

metric of comparing the dielectric strength of various gas media in numerous studies. Figure 1.1 shows the electron scattering cross section data of SF_6 extracted from PHELPS database [6]. It is observed that SF_6 has a high elastic electron scattering cross section data over the entire energy range. Ionization collisions occur only with electron energies greater than 15.7 eV. On the other hand, attachment collision takes place with electron energy greater than only 0.001 eV. This implies that SF_6 has high electron affinity that makes SF_6 a dielectrically strong gaseous medium.

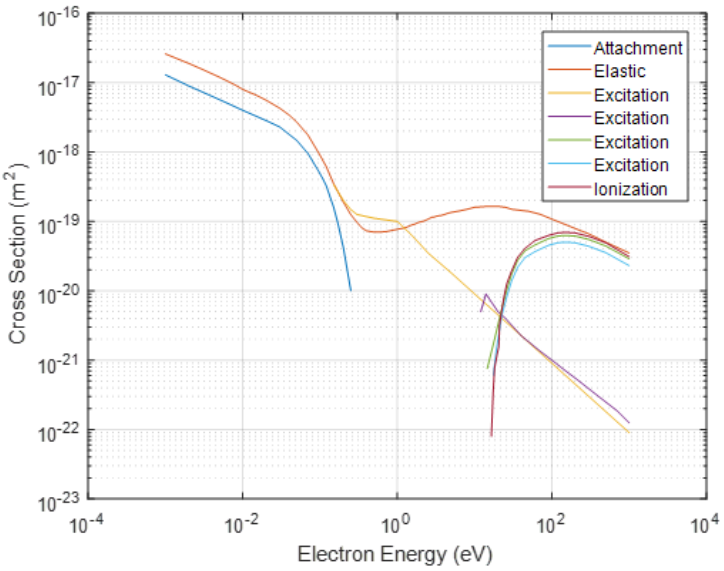

Figure 1.1 Electron scattering cross section data of SF_6.

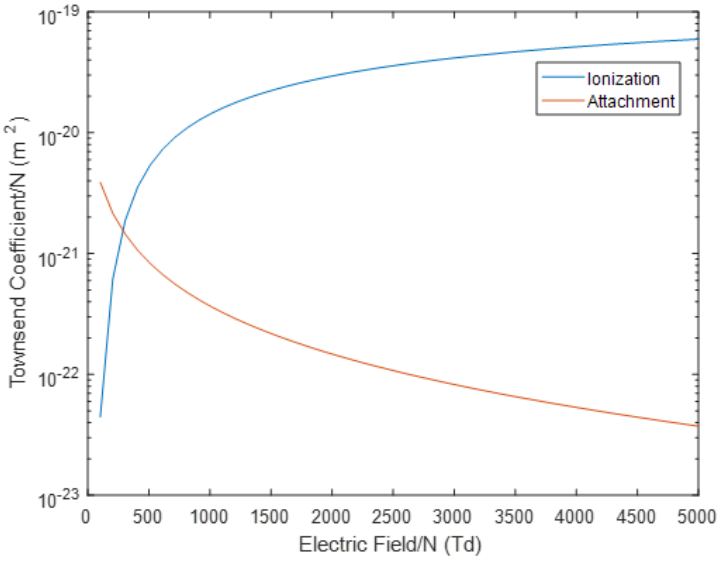

Figure 1.2 Density reduced ionization coefficient (α/N) and density reduced attachment coefficient (η/N) of SF_6.

The dielectric strength of SF_6 estimated based on the electron kinetic processes, density reduced ionization coefficient (α/N) and density reduced attachment coefficient (η/N), is shown in Figure 1.2. The density reduced critical electric field ($(E/N)_{cr}$) at which the rate of ionization and attachment process are equal is used to estimate the dielectric strength of SF_6. The $(E/N)_{cr}$ of SF_6 is 300 Td. The significantly high $(E/N)_{cr}$ of SF_6 implies that SF_6 is a gaseous dielectric medium with high dielectric strength. For this reason SF_6 is considered in the power industry as the electrical insulation and arc quenching medium for medium to high voltage equipment such as gas circuit breakers (GCBs), gas insulated switchgears (GISs), gas insulated transmission lines (GILs), and gas insulated transformers (GITs) [3], [5].

1.2.1.2 Environmental effects of SF_6

Table 1.1 Physical properties of SF_6 [4], [7]

Properties	SF_6
Atmospheric lifetime	3200 years
Global Warming Potential (GWP)	22,800
Boiling Point	-64 ^oC
Ozone depletion potential (ODP)	0

Although SF_6 has been used as a dielectric medium in electrical power applications for decades, it has been recognized as a potent greenhouse gas for its physical properties presented in Table 1.1. SF_6 has significantly high Global Warming Potential (GWP), which is the index that provides the relative measure of the climate impact of a compound that acts as a greenhouse gas in the atmosphere [7]. The main reason for having such high GWP is the strong infrared absorption of SF_6 and its long atmospheric lifetime [1]. For this reason, the utilization of SF_6 gas as insulation medium has been reduced and the search for an environmental-friendly substitute for SF_6 has been pursued for the last two decades. In [5], authors outlined the following requirements that SF_6-alternative gases should exhibit:

- Environmentally friendly, i.e., low GWP and ODP.
- Low toxicity
- Thermally and chemically stable
- High dielectric strength and thermal conductivity
- Excellent arc quenching capability
- Low boiling point

1.2.2 Supercritical fluid (SCF): a new dielectric medium

Supercritical fluid is the state of a substance at which the temperature and pressure of the fluid are above the critical point showing viscosity and diffusivity compared to gas state and density and solvating property compared to liquid state. Owing to these properties, SCF are considered for use as a new dielectric fluid that can replace SF_6 with high dielectric strength, low viscosity, and efficient heat transfer capability.

1.2.2.1 Fluid properties of SCF

1.2.2.1.1 Transport properties

SCF is the intermediate phase of matter between liquid and gaseous phases achieved at temperature and pressure above the critical point. For example, the critical point of CO_2 is T_c = 304.15 K and P_c = 7.37 MPa [8]. In Figure 1.3(a), density-pressure diagram of CO_2 in three different states has been plotted. It is observed that at the critical point, for a small change in the pressure there is a large change in the density. In Figure 1.3(b), viscosity of CO_2 in different states have been plotted, and it is observed that viscosity at supercritical condition remains between liquid and gaseous phases. Near the critical point, diffusion coefficient and surface tension of materials also have values between liquid and gaseous phases [8]. However, there are some properties, *e.g.*, thermal conductivity, heat capacity, and compressibility, that have a maximum value near the critical point [8]. Figure 1.3(c) and Figure 1.3(d) shows the thermal conductivity and heat capacity of CO_2, and it is observed that at the critical point, they are maximized.

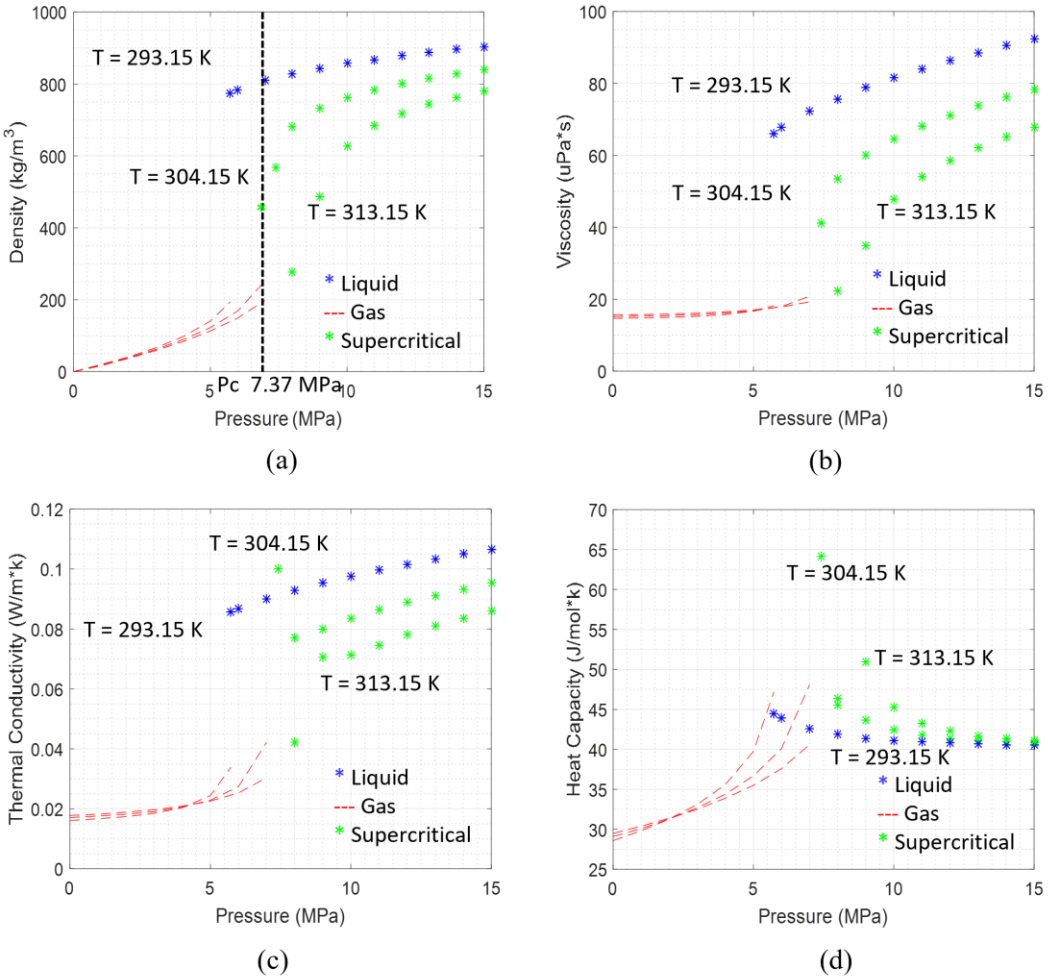

Figure 1.3 Comparison of (a) density, (b) viscosity, (c) thermal conductivity, (d) heat capacity of CO_2 in three different states (liquid, gaseous, and supercritical) [9]

1.2.2.1.2 Structural characteristics

Supercritical fluids are historically called “cluster fluid” [10] due to the nature of cluster formation in different sizes having weak intermolecular forces near the critical point as shown in the phase diagram as function of pressure and temperature in Figure 1.4. The formation of clusters causes higher density fluctuation (F_D) in the substances. The value of F_D is a measure of local density enhancement that is defined by [8]

$$F_D = \frac{\ll N \gg}{< N >} = \frac{< (N - < N >) * (N - < N >) >}{< N >} = \frac{k_T}{k_T^0} \tag{1.1}$$

where N is the total number of particles in an arbitrary volume V and <N> the average, k_T is the isothermal compressibility of the fluid and k_T^0 the isothermal compressibility of a perfect gas. The formation of clusters greatly influences the transport properties and the structures of SCFs. Similar anomalies have also been reported in the electrical discharge area. For example, the decrease of breakdown voltages for micrometer-scale gap electrodes [10]–[12].

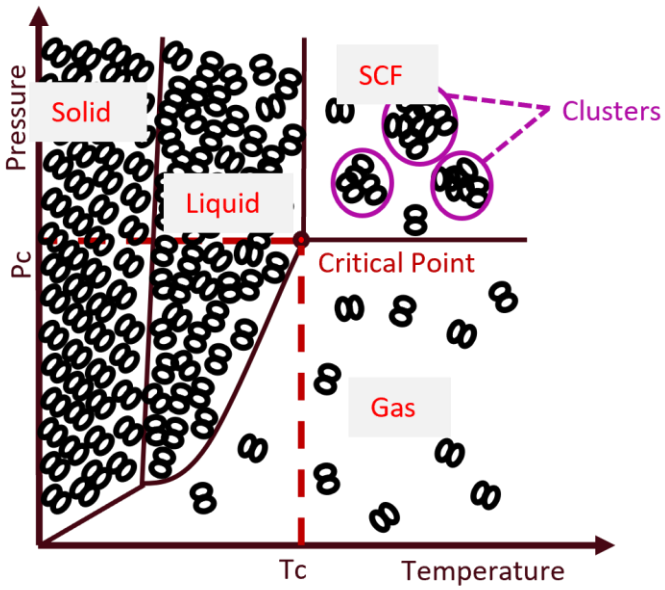

Figure 1.4 Phase diagram

1.2.2.2 Dielectric properties of SCF

Traditional gas discharge theories known as Townsend theory and Paschen's law describe the electrical breakdown characteristics at low pressure. According to the conventional gas discharge theory, under uniform electric field, the breakdown voltage V_{bd} is expressed as

$$V_{bd} = BPd * \frac{1}{ln\left[APd * \frac{1}{ln\left(\frac{1}{\gamma}\right)}\right]} \tag{1.2}$$

where A and B are constants about a specific gas type determined by experiments, γ is the third Townsend ionization coefficient which represents the average of secondary electron emissions per positive ion hitting the cathode, P is the pressure, and d is the electrode gap. SCF, which is a state of material achieved above the critical points, discharge happens in a highly pressurized condition. The electrical breakdown characteristics in such high pressurized conditions deviate from the values estimated from Paschen's law. In [10], [11] the electrical breakdown characteristics of SCF CO_2 have been reported, and a significant decrease in the local breakdown voltage has been observed near the critical point. Similar breakdown characteristics have been reported in [12] for SCF H_2O and SCF Xe and in [13] for SCF He. In the vicinity of the critical point, the density fluctuation F_D increases significantly due to the molecular clustering, and the breakdown voltage of the material becomes lower compared to the gas discharge theory described by Paschen's law. Hence, the breakdown voltage V_b and density fluctuation F_D are correlated by the following expression in [10]–[13].

$$V_b = \alpha V_p F_D^{\beta} \quad (1.3)$$

where α and β are fitting parameters, and Vp is the breakdown voltage according to the classical Townsend theory for gas discharges in Eq. (1.2), and density fluctuation is F_D calculated based on isothermal compressibility k_T of the fluid.

1.2.2.3 Dielectric breakdown characteristics of binary mixtures of SCF

a. Dielectric strength investigation on the SC CO_2-C_2H_6 azeotropic mixture: Wei *et al.* investigated the breakdown strength characteristics of CO_2 and C_2H_6 mixtures and their azeotropic mixtures under supercritical conditions [14]. The breakdown voltage was measured in a 0.1 mm gap with a uniform electric field over a wide range of mixture ratios and fluid densities. The observed breakdown strength characteristics of CO_2 and C_2H_6 mixtures showed similar anomality near the critical point as seen in pure SC CO_2. This analogous behavior in discharge phenomenon showed by the CO_2 and C_2H_6 mixtures was explained by the unstable molecular clustering near the critical point. This investigation suggests that the mixtures of SCFs show tunable combination of properties that allow them to use in broader range of applications.

b. Dielectric strength investigation on the SCF mixture: CF_3I-CF_3I that has high dielectric strength is a potential replacement of SF_6 in power systems and was mixed with SC CO_2 in [15]. Here, the same authors reported the dielectric strength SC CO_2-CF_3I under supercritical condition. By changing the mixing ratio, the author achieved dielectric strength of SC CO_2-CF_3I as high as 350 kV/mm, which is comparable to solid insulating materials. This implies that by

changing the mixing ratio, SCFs mixtures can be used as dielectric medium in power dense applications.

1.2.2.4 Applications of SCF as dielectric medium

Traditionally SCFs have been used in chemical processes which includes the extraction of solids and liquids, polymer processing, chemical, and biochemical reactions, and drying and cleaning [16]. In addition, SCFs have been used as the coolant fluid in air conditions and refrigeration systems [16]. Moreover, they have been used in other applications in the energy sector, for instance, as heat transfer fluids in solar power, solar water heater, and carbon capture and storage[17]. More recently, researches have proposed to utilize SCFs as dielectric media [14], [15], [17]–[21]. Four potential applications of SCFs as a dielectric medium are discussed below.

a. Ultra-fast switchgear – SCFs have high dielectric strength and low viscosity, which allow them to reduce contact travel time and therefore faster switching operation can be achieved. For this reason, in non-arcing disconnect switches with piezoelectric actuator SCFs can be used as an insulating medium for enhanced performance [17].

b. Electrostatic rotating machine – Electrostatic machines require dielectric medium that has both high dielectric strength and low viscosity to spin at a very high speed and develop power. SCFs have liquid-like density and gas-like viscosity. These properties of SCFs allow them to be used as a potential dielectric medium in electrostatic rotating machine [17].

c. Van de Graff generators – SCFs could potentially be used as a dielectric medium in van de Graff generators. The high dielectric strength would shrink the size of the generators and accelerators that rely on these generators thereby reducing the cost. The use of SCFs in van de Graff generators would benefit both high energy physics research and medical applications [17].

d. High temperature superconducting (HTS) technology – High temperature superconducting (HTS) technology provides promising solutions to emerging aerospace and naval power applications that require light weight, high efficiency, and high-power-density. Conventionally, cryogenic conditions required by HTS applications have been achieved by using liquid nitrogen (LN_2) owing to its effective heat transfer properties and dielectric strength. In recent years, however, research efforts have been made to replace LN_2 with gaseous cryogens to take advantage of the broader temperature range of operation and the reduced risk of asphyxiation [22]–[25]. The wide temperature range provided by gaseous cryogens enables HTS cables and machines to carry higher current density and facilitates the integration of multiple cryogenic power devices into fewer cooling loops, which is systematically more efficient. As a part of this effort, the development of cryogenic power electronics [26]–[28], cryogenic switchgear [29], and HTS cables [30] have been researched. However, gaseous cryogens introduce two major shortcomings – i) low heat capacity, ii) low dielectric strength. Studies have shown that the low heat capacity can be partially resolved by increasing the pressure of the gas-cooled cryogenic system[31]. As a replacement for these gaseous cryogens, SCF He could be used in HTS technology which would provide both high dielectric strength and high heat capacity [21].

1.2.3 Conventional partial discharge (PD) mitigation approaches

Partial discharge (PD) is a chronic dielectric issue that partially bridges the insulation between conductors. PD is mainly caused by the enhancement of local electric fields due to the presence of inevitable manufacturing defects, including sharp edges, triple points, airgaps, bubbles, etc. PD activities caused by the intense local electric field initiate electrical treeing, reduce device lifetime, accelerate dielectric material aging, and increase the chance of device failure. PD mitigation in medium to high voltage applications has drawn attention from researchers, and

numerous studies on reducing PD on sharp edges and triple points have been reported in the literature. The reported methods are largely classified into geometry- and material-based approaches.

1.2.3.1 Geometry-based approaches

Various geometry-based PD mitigation approaches have been reported in the literature. These are discussed briefly in this section [32].

a. Corona ring method – Corona discharges occur around the sharp points or rough surface of electrodes where the intensity of the electric field at the tip of electrode increases and causes the degradation of insulating material by gas ionization and streamer discharges. In the case of the corona ring PD mitigation approach, the large radius and smooth surface of the corona ring is utilized to distribute the electric field and reduce the field stress around the sharp points and rough surfaces. Figure 1.5 shows an insulator that is surrounded by a corona ring to improve the electric field distribution. However, the implementation of the corona ring increases the overall weight and volume of a system [32]. In addition, there is no standard for the design and location of corona rings, which would lead to premature failure of the insulators [33], [34].

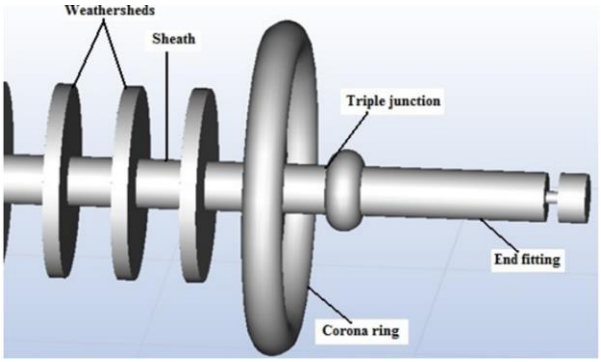

Figure 1.5 Corona ring method to mitigate PD [33]

b. Combined insulator assembly – A new optimized structure combining the use of non-ceramic insulator and glass insulator showed significant reduction in the electric field when tested under several voltage levels [35]. Figure 1.6 shows a system that combine the use of porcelain insulator and glass insulator. However, a complete reduction in the electric field is not achieved with this proposed approach. It has been reported in [36] that only 40% reduction in the electric field is achieved when combined insulator assembly approach is utilized.

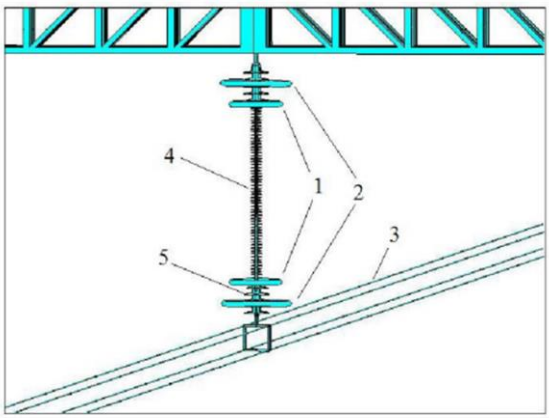

Figure 1.6 Combined insulator string assembly to mitigate PD [36].

c. Optimized end-fitting design – Small radius elements, sharp edges, triple points must be avoided in insulator design of power modules to avoid the enhancement of local electric field. The geometric solution proposed in [37] avoids creating sharp edges by rounding the edges of metallization layers and protrudes ceramic substrate layer to relocate triple point and to avoid tangential electric field. Figure 1.7(a) shows that in an industrial substrate, sharp edges are unavoidable in the metallization due to the etching process and cause an electric field of 42 kV/mm. However, with the protruding structure shown in Figure 1.7(b), triple point is moved away from the edge of the metallization, and the metallization has round edges to limit the field enhancement. This structure results in an electric field of 11 kV/mm, which is notably lower than the field in Figure 1.7(a). Although this approach is effective in theory, they are limited to manufacturing tolerance that creates sharp edges eventually.

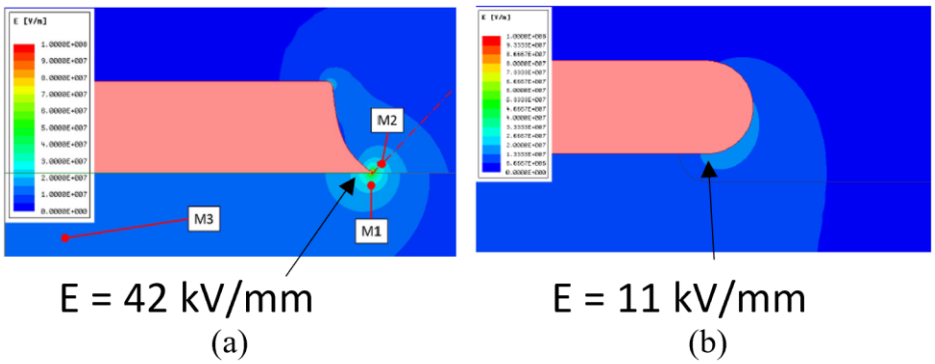

Figure 1.7 Electric field neutralization by rounding the sharp edges. (a) Industrial structure showing field enhancement at the sharp edges, (b) protruding structure with rounded edges [37].

1.2.3.2 Material-based approach

Many studies have been conducted on field grading material (FGM) to reduce the locally enhanced electric field in power module. The main two types of FGM are resistive field grading material and capacitive field grading material [32].

a. Resistive field grading – Resistive field grading materials have the non-linear conducting behavior where the conductivity varies with the electric field [32]. The non-linear behavior is achieved by filling the base polymer (epoxy resin) with inorganic fillers such as ZnO. When the electric field strength exceeds the switching field, the non-linear grading material becomes conductive and impedes the field enhancement effects. Figure 1.8 shows the schematic view of the resistive field grading method. One of the major disadvantages of this method is the Joule heating caused by the conductivity of the resistive materials.

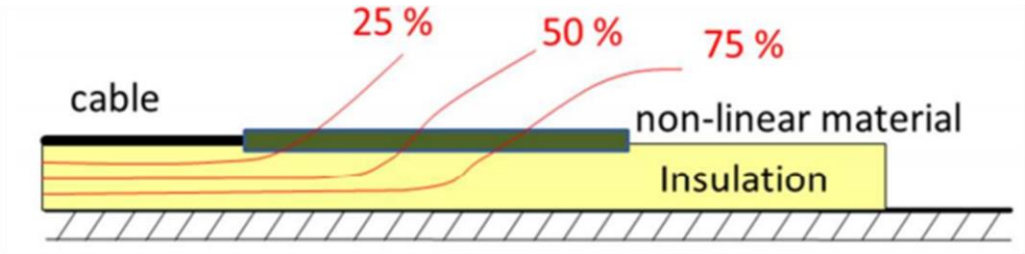

Figure 1.8 Resistive field grading based electric field neutralization [38]

b. Refractive field grading – Refractive field grading materials can be obtained by introducing various fillers to the host matrix. The fillers increase the relative permittivity of the dielectric material. The electric field is regulated when passing over different dielectric materials having various dielectric constant values. The schematic view of the capacitive field grading method is shown in Figure 1.9.

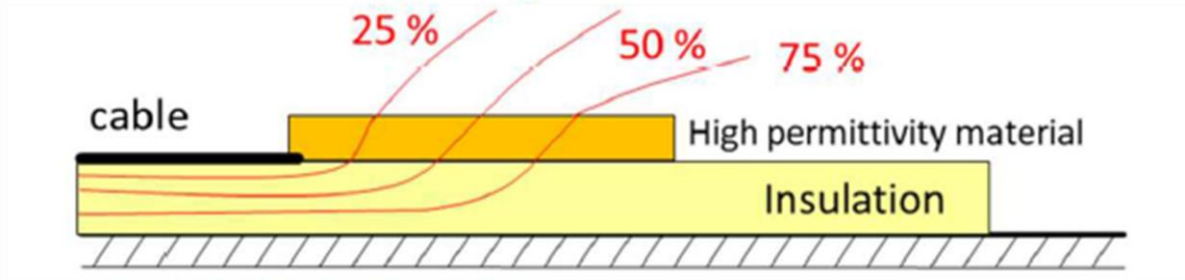

Figure 1.9 Refractive field grading based electric field neutralization [38]

1.2.4 Electret based partial discharge mitigation

1.2.4.1 Definition of electret

An electret is a dielectric material embedded with charge. Electrets emit electric fields due to the embedded charge or dipole orientation. Electrets can be made of various materials, including silicon dioxide (SiO2)-based inorganic materials and polymer-based organic materials such as polytetrafluoroethylene (PTFE), high-density polyethylene (HDPE), polyimide (PI), and polyvinylidene fluoride (PVDF).

1.2.4.2 Fabrication methods of electrets

The SiO_2-based inorganic materials or polymer-based organic materials used for the fabrication of electrets should have a form of a sheet, a ribbon, or a film-coated on the electrode or firmly attached on the electrode. Electrets are fabricated based on five different charge poling methods – thermal poling, electron-beam charging, optical poling, liquid-contact, and corona charging method [39]–[41] as described below.

a. Thermal poling method – The thermal poling method, also known as thermo-electrical method, is the oldest electret fabrication method [39]. In this method, a dielectric material is heated while it is kept under applied electric field for a fixed duration and then cooled to normal ambient temperature while the electric field is being applied. The thermal poling of charge can be achieved by arranging electrodes in one of the three ways as shown in Figure 1.10. In one type, metallic electrodes are deposited on both surfaces of the dielectric material, as shown in Figure 1.10(a), where the dielectric material is a dipolar molecule. In the second case, one side of the dielectric material is in intimate contact of the metallic electrode while keeping an air gap between the other side and electrode as shown in Figure 1.10(b). In the third case, air gaps are present on both sides of the dielectric material as shown in Figure 1.10(c). In the later cases, in Figure 1.10(b)

and Figure 1.10(c), the dielectric material is non-dipolar molecule, where real charge storage is essential to form electret. The air gap in one side or both side ionizes the air under high electric field and real charges are deposited on the bare surface of the dielectric material [41].

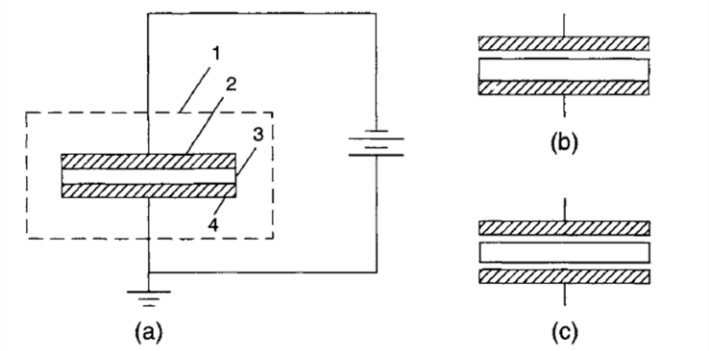

Figure 1.10 Schematic diagram of thermo-electret formation showing various electrode arrangement [41]. (a) dielectric material in intimate metallic electrode contact, (b) metallic electrode only one side of the material and the other surface is bare, (c) both side of the dielectric material are bare. 1: Heating chamber, 2: upper metallic electrode, 3: dielectric material, 4: lower dielectric material.

b. Optical poling – In this method, dielectric material is charged by the displacement of charge carriers generated by penetrating radiation, *e.g.*, x-rays, ultraviolet, or visible lights, under externally applied electric field [41]. The materials, e.g., polycrystalline sulfur, used in this method generally have photoconductivity. Figure 1.11shows the photo-electret formation process. One surface of the dielectric material is in contact with metallic electrode while the other one has transparent electrode so that light can illuminate the material through it. When external electric field is applied, the photogenerated carriers move towards the electrodes and are trapped near the electrode to create space charge. The electret generated through this method has less charge stability because polarization decays gradually under illumination when external field is removed.

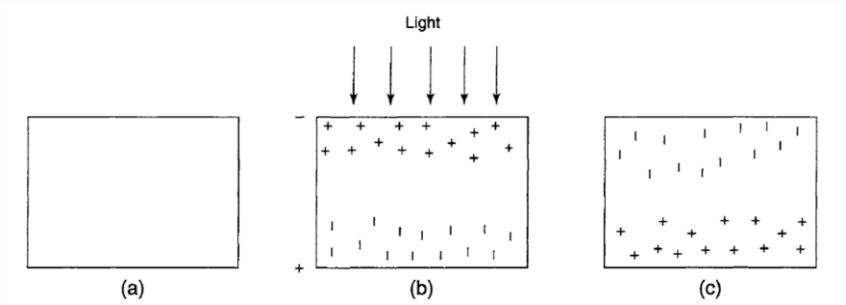

Figure 1.11 Electret fabrication with optical poling. (a) Before applying light and electric field, (b) displacement of photo-induced charges under light and field, (c) charge distribution after poling [41].

c. Electron beam charging – By injecting low-energy electron beam with electron gun, real charge penetrates into the bulk of the dielectric material. The energy of the electron beam is in the order of 10-50 keV and controlled according to the structure and thickness of the dielectric material so that the beam can cause damage to the dielectric material [41]. Figure 1.12 shows the schematic diagram of the electron-beam method in fabricating electret film. The advantage of this method is the controllability of the density, location, and distribution of the injected negative charges.

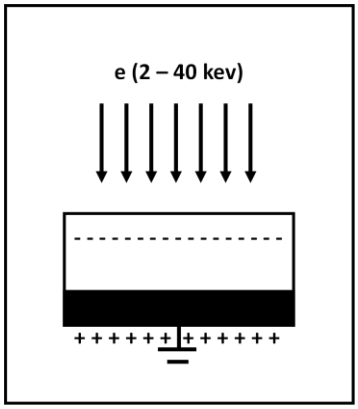

Figure 1.12 Electret fabrication based on electron beam method [41]

d. Liquid-contact method – In this method, the top surface of the dielectric material is in contact with an electrode made of fabric wetted with conductive liquid. When electric field is applied between these two electrodes, the charges will be transferred from the top wetted electrode to the dielectric material surface. Since the top wetted electrode can slide on the material surface, this method can be used to transfer charges over a large area of the material surface. Figure 1.13 shows the schematic diagram of the liquid-contact charging method.

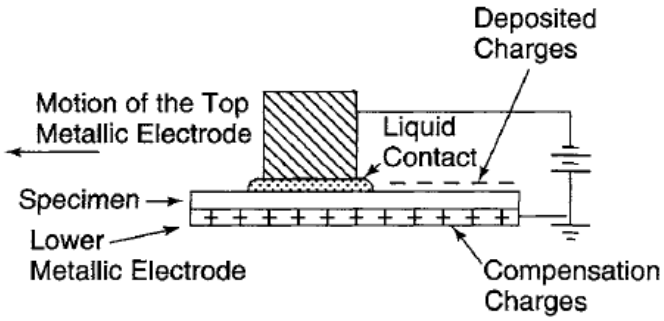

Figure 1.13 Electret fabrication based on liquid contact method [41]

e. Corona charging method – If a sufficiently high voltage is applied between asymmetric electrodes, *e.g.*, point-plane electrodes, an electrical discharge is formed near the tip of the electrode. This controllable and non-disruptive electrical discharge is known as corona discharge [42]. Because of the controllability, simplicity, and low cost, the corona discharge has been used widely to charge polymers and dielectrics [42], [43]. In the early days, the corona charging setup consisted of a needle electrode placed above the dielectric material on a flat electrode. However, this method lacks uniformity when charging a dielectric sample. For this reason, a metallic grid with uniform mesh is placed just above the dielectric sample, as shown in Figure 1.14, to improve the uniformity of charging and control the surface potential of the electret. This needle-grid-plane system is called triode corona system. Ions produced by the needle electrode are transferred at the surface and into the bulk of the sample to be charged and convert the sample into electret.

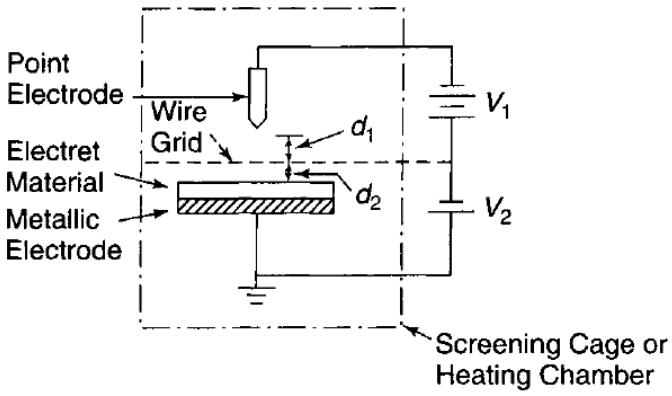

Figure 1.14 Electret fabrication based on corona charging method [41].

1.2.4.3 Conventional applications of electrets

Any external force caused by mechanical compression, heat, sound wave, electricity, light, or radiation interact with the stored charges in electrets [41]. For this reason, most common applications of electrets are transducer and sensors [39], [41]. There are many commercially available electret device, including micro-electro-mechanical systems [40], [43], air filters [44], radiation dosimeter [41], acoustic transducer [41], actuators [39], [45]. The long-term charge stability of electrets enables them to be used in these applications. Recently, an electret-based field neutralization approach is reported in [46], [47] where locally enhanced electric fields due to the presence of sharp edges, triple points, and cracks and bubbles are neutralized by incorporating an electret layer.

1.2.4.4 Electret for PD mitigation

1.2.4.4.1 Theoretical framework

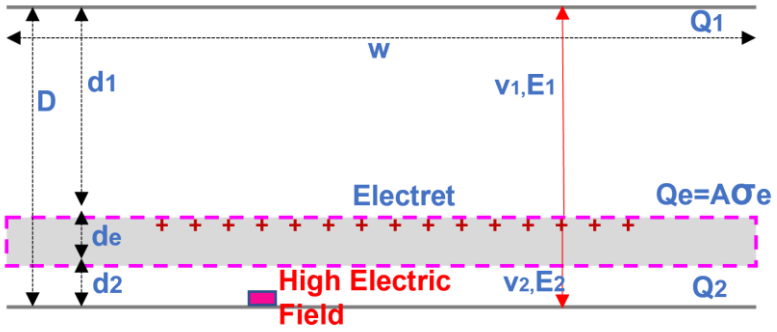

Figure 1.15 Model used to understand electric field neutralization process by the electret film

To describe local electric field neutralization achieved by using electrets, we use a model shown in Figure 1.15 where the top and bottom surfaces have Q_1 and Q_2 charges [46]. The electret layer

has a surface charge density of σ_e on its top surface. The distance between the top surface and top of the electret layer is d_1, the thickness of the electret layer is d_e, and the distance between the bottom layer and the bottom of the electret layer is d_2. The electric potential difference between the top surface and the top of the electret is v_1, and electric field E_1 across it points towards the top surface. Again, the electric potential difference between the top of the electret and the bottom surface is v_2, and the electric field E_2 points towards the bottom surface. We assume that all surfaces have equal area of A, which quantifies the total amount of charge in the electret as $Q_e = A\sigma_e$. With the presence of the electret layer, the electric potential between the top and bottom surface is

$$v_1 - v_2 = v \tag{1.4}$$

The induced charge on the top and bottom surface and the total charge of the electret are equal in magnitude but opposite in polarities. Therefore, the net charge in the system is zero and is represented as

$$Q_1 + Q_2 + Q_e = 0 \tag{1.5}$$

We assume that C_1 and C_2 are the capacitance across v_1 and v_2 and express (2.5) as follows.

$$\frac{\in_0 \in_{r1} v_1}{d_1} + \frac{\in_0 \in_{re} \in_{r2} v_2}{d_e \in_{r2} + d_2 \in_{re}} - \sigma_e = 0 \tag{1.6}$$

Solving (1.4) and (1.6) for v_2 and by the definition of the electric field, $E_2 = \frac{v_2}{d_2}$, we can write as follows,

$$E_2 = \frac{1}{d_2} \frac{d_1 d_e \in_{r2} + d_1 d_2 \in_{re}}{\in_0 \in_{r1} (d_e \in_{r2} + d_2 \in_{re}) + \in_0 \in_{re} \in_{r2} d_2} (\sigma_e - \frac{\in_0 \in_{r1}}{d_1} v) \quad (1.7)$$

A point of local high electric field is assumed to be on the bottom surface, and the goal is to nullify the electric field. Therefore, we solve the surface charge density σ_e, such that it satisfies the condition of $E_2 = 0$. Therefore, σ_e is expressed as follows.

$$\sigma_e = \frac{\in_0 \in_{r1} v}{d_1} \quad (1.8)$$

Based on (1.8), we can design the surface charge density of the electret to neutralize the local electric field, which consequently mitigates the partial discharge in high-power-density applications.

1.2.4.4.2 Numerical validation

Figure 1.16 shows the numerical validation of the proposed electret-based PD mitigation approach. The figure shows the neutralization of the local electric fields with the incorporation of electrets. The high electric field of 114.2 kV/mm generated around the triple point (Figure 1.16 (a-1)) is reduced to 15.8 kV/mm with the incorporation of 0.1mm thick electret layer as shown in Figure 1.16 (a-2). The inclusion of electret layer causes an 86% reduction in the locally enhanced electric field. In this numerical analysis, we applied 24 kV across a 2 mm-thick aluminum nitride (AlN) layer and our calculated surface charge density σ_e was 1,006 μC/m^2 according to (5), which

is higher than the value achieved in the lab. Figure 1.16 (b) shows the effectiveness of the electret-based approach in reducing the high electric field in cavities. The high electric field of 53.8 kV/mm due to bubbles and airgaps in the insulation layer without the electret layer is reduced to 4.4 kV/mm with the inclusion of the electret layer. In this case, a 92 % reduction in the electric field is achieved when an electret layer is inserted below the epoxy layer. This reduction in the high electric field by the incorporation of the electret layers consequently eliminates the PD activities in high-power density applications.

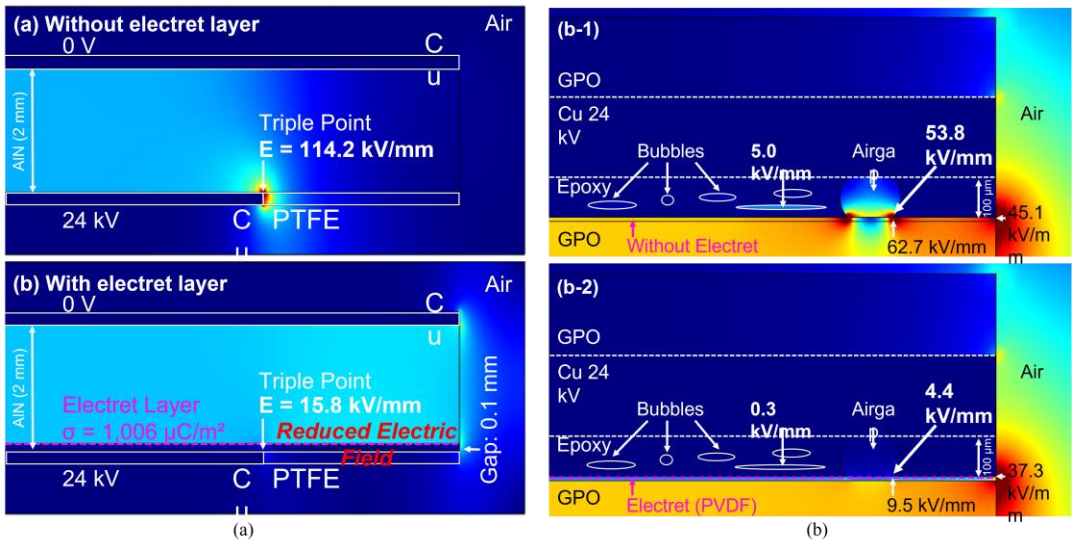

Figure 1.16 Numerical validation of electret-based approach in PD activities mitigation. (a) Electric field reduction due to triple point on the bottom surface, (b) electric field reduction due to bubbles and airgaps in the laminated busbar [46], [47]

1.3 Research objectives

The goal of this research is to model the breakdown characteristics of SCFs near the critical point and fabricate electret under an optimum condition that can effectively mitigate PD regardless of PD sources and power electronics voltage parameters. This indicates that this dissertation has two parts. In the fast part, the dielectric breakdown characteristics of SCFs are modeled and compared with the experimental data. In the second part, electret-based electric field neutralization has been utilized to mitigate PD.

The primary objectives of this dissertation are:

- **Accurate dielectric modeling of supercritical fluids:** The drastic degradation in dielectric strength occurring near the critical point has been confirmed by experimental measurements. The authors of those works have utilized the correlation between the density fluctuation caused by cluster formation near the critical point and breakdown voltage to explain the extreme degradation of dielectric strength. The reported correlation and models proposed in these studies mainly rely on the data of isothermal compressibility, which also vary near the critical point, retrieved from the NIST database. However, difficulties may arise for modeling the dielectric strength of the fluids whose isothermal compressibility data are not available. To overcome the potential limitations, in this dissertation, a correlation between the breakdown characteristics of SCFs and the clustering effect is developed.

- **Electret-based electric field neutralization**

    - **Utilizing electret for mitigating PD caused by the local enhancement of electric field:** Electrets are fabricated from polyvinylidene (PVDF) based on the simple, inexpensive, and controllable triode-corona charging method. A series of experiments on surface discharge around triple points and cavity discharge in bubbles are conducted under high-*dv/dt* square voltage stimuli.

The PD signals at the rising edge of the square voltage waveforms are recorded without and with the incorporation of electrets fabricated under the various charging conditions. The surface charge density and the PD mitigation performance of electrets in mitigating surface discharge caused by triple points and cavity discharge caused by airgaps and bubbles are analyzed.

- **Utilizing the electret-based field neutralization in mitigating surface flashover:** The electret based electric field neutralization approach is utilized to increase the critical flashover (CFO) associated with surface flashover and thus enhance the dielectric robustness of the insulation materials. The CFO of dielectric materials with and without the incorporation of electret film is compared by conducting surface flashover experiments under power electronics switching voltages.

- **Utilizing epoxy-based electret as a solution to PD at cryogenic temperatures:** Epoxy-based composites exhibit mechanical compatibility at cryogenic temperatures. Owing to these properties, composites based on epoxy are used as electrical insulators in high temperature superconducting (HTS) power applications. The PD mitigation performance of electrets fabricated from epoxy resin in analyzed, which is suitable for cryogenic power applications.

- **Investigating the electret fabrication conditions for effective PD mitigation:** Electrets are fabricated based on the triode corona charging method under various charging conditions, including charging voltage, charging duration, charging polarity, and charging temperature to establish an electret fabrication condition, through which PD can be optimally mitigated.

- **Utilizing the electret-based field neutralization approach in power electronics converters:** The PD mitigation performance of electret under various power electronics switching voltage parameters including rise time, switching voltage frequency, voltage polarity, and duty

cycle is evaluated. For this purpose, we conduct a series of PD experiments with uncharged PVDF and charged PVDF (electret) films under unipolar and bipolar square voltage waveforms while varying the voltage parameters and compare their performance in mitigating PD.

CHAPTER II

DIELECTRIC STRENGTH MODELING OF SUPERCRITICAL FLUID

This part of the dissertation has been published in two journals and one conference paper. [20] and [48] includes the dielectric strength modeling of SCF CO_2 and electron scattering cross section data of CO_2, respectively and [21] includes the dielectric strength modeling of SCF He and SCF Xe near the critical point.

2.1 Motivation

Near the critical point, the gas molecules of form clusters of various sizes. The dielectric property, which can be determined by Boltzmann analysis, changes with the formation of cluster. To perform Boltzmann analysis to estimate the critical electric field, the electron scattering cross section data of clusters are needed. However, the electron scattering cross section for clusters are not directly available but could be derived from the gas molecule cross section data.

2.2 Developing electron scattering cross section data of SCF

2.2.1 Modeling approach

For the simplicity of our electron scattering cross section data modeling approach, we assume a sphere with radius R_c as the cluster of both He and Xe near the critical point as shown in Figure 2.1. At point *A,* electron enters the cluster and the traverses following the horizontal trajectory. Collisions occur between points *B* and $B^{'}$ distanced by *dx* as the electron travels along the trajectory. The electron scattering cross section is multiplied by the cluster impact parameter,

h, which is the normal distance between the center of the cluster and the electron trajectory. The total electron scattering cross section, σ for cluster size N is derived by applying the following equation[20], [21], [48], [49]

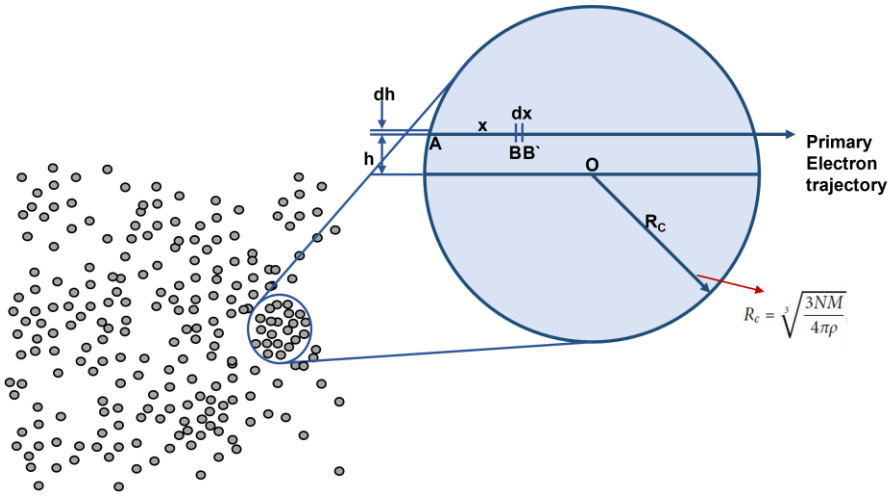

Figure 2.1 Spherical electron-cluster collision model.

$$\sigma(N, W_{e0}) = \frac{[2\pi \int_0^{R_c} h\{1 - \exp[-n_0 \int_0^{2\sqrt{(R_c{}^2 - h^2)}} \sigma_0(1, W_e(x))F(x)\,dx]\}dh]}{N} \qquad (2.1)$$

where W_{e0} is the initial electron energy upon impact, $\sigma(N, W_{e0})$ is the electron scattering cross section data of the cluster, n_0 is the molecular density of the cluster, $\sigma_0(1,\ W_e(x))$ is the electron scattering cross section data of gaseous He and Xe, and $F(x)$ is the probability of secondary electrons being produced by ionization collisions escaping out of the cluster. It should be noted

that $F(x)$ is only relevant to the ionization collision process. For this reason, for cross sections except for the ionization cross section, e.g., momentum transfer and excitation, $F(x)$ is not applicable. In our study, we define $F(x)$ with a three-dimensional spherical model, as shown in Figure 2.2. We have assumed that clusters are spherical in shape. To model the probability of electron escaping out of the cluster after an ionization collision, we assumed a sphere at the position of the electron on the trajectory inside the cluster. The escaping probability of an electron asymptotes to unity as the ionization occurs closer to the surface of the cluster. In this work, the probability of escaping out of the cluster due to ionization is formulated as the ratio of the spherical volume travelled by the electron to the total volume of the spherical cluster. The following equation represents the probability function [20]:

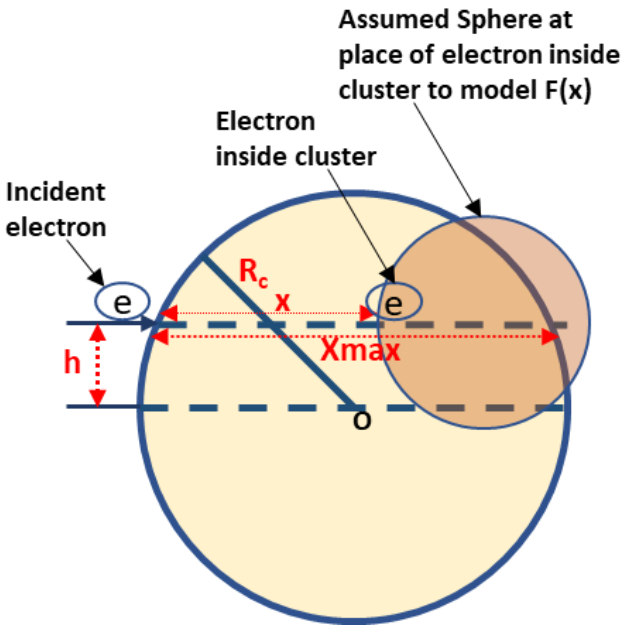

Figure 2.2 Spherical model used for escape probability function *F(x)*.

$$F(x) = (V_{cluster} - V_{sphere})/V_{cluster} \tag{2.2}$$

where $V_{cluster}$ is the volume the spherical cluster and V_{sphere} is the volume of a sphere that evolves with radii $(x_{max} - x)/2$ with the traversing electron as shown in Figure 2.2 and defined as

$$V_{sphere} = \frac{4}{3}\pi\left(\frac{x_{max} - x}{2}\right)^3 \tag{2.3}$$

where x is the distance traveled by the electron inside the cluster along the trajectory, and x_{max} is the maximum length electron can travel with a cluster impact parameter h defined as equation (1.4).

$$x_{max} = 2\sqrt{(R_c^2 - h^2)} \tag{2.4}$$

where R_c is the radius of the cluster. The radius of the cluster shows a correlation with the cluster size N by the following equation [49]

$$R_c = \sqrt[3]{\frac{3NM}{4\pi\rho}} \tag{2.5}$$

where M is the mass of the gas molecule, and ρ is the specific mass of the cluster. Figure 2.3 shows the probability function $F(x)$ as a function of the position of the electron along the trajectory of

supercritical He. As shown by the figure, the probability increases as the ionization collision takes place closer to the vicinity of the cluster surface. The electron scattering cross section data of clusters in our model includes the electron energy $W_e(x)$ at position *x* inside the cluster. Electron energy gradually decreases from its initial energy W_{e0} while traversing along the trajectory inside the cluster. At any position *x* on the trajectory, $W_e(x)$ is modeled as

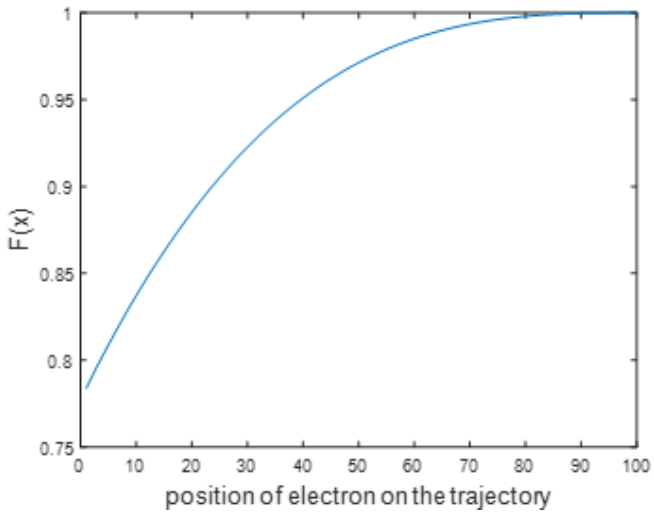

Figure 2.3 Escaping out probability function *F(x)* of supercritical fluid

$$W_e(x) = W_{e0} - \int_0^x \left(\frac{dW_e}{ds}\right) ds \tag{2.6}$$

where W_{e0} is electron energy at the moment of impact with the cluster, and dW_e/ds is the energy loss rate of electron traversing in the cluster. The energy loss rate of an electron inside the cluster

shows different behavior for different energy levels. For an electron energy level higher than 80 eV, the behavior of the energy loss rate is modeled by the Bethe's formula. However, when the electron energy level falls below the mean excitation energy, Bethe's formula does not agree well with the experiment. That is, at low electron energy level, Bethe's formula calculates lower electron energy loss rate than actual values which cannot be explained. For this reason, for energy level lower than 80 eV, all the energy loss mechanisms including ionization, excitation, and momentum transfer processes, are taken into account in modeling the electron energy loss rate. The electron energy loss rate we develop in our study is described as follows.

$$\frac{dW_e}{ds} \cong \begin{cases} -\dfrac{\alpha_1 z}{W_e}\ln\left(\dfrac{\alpha_2 W_e}{z}\right) \text{ eV } m^{-1}, & W_e \geq 80\ eV \ \ (a) \\ -n\sigma_\tau\left((V_i + W_{s0})\alpha_i + \displaystyle\sum_{m,n} V_{m,n}^{*}\, a_{m,n} + 2\frac{m_e}{M}W_e\alpha_d\right)\text{eV } m^{-1}, & W_e \leq 80\ eV \ \text{(b)} \end{cases} \tag{2.7}$$

where in the first equation $\alpha_1 = k_1 q^2 n/(8\pi\varepsilon_0)$, W_e is electron energy, n is the density of the cluster, k_1 is the empirical factor of correction, z is the atomic number, and q is elementary charge. For both He and Xe, we use 0.5 for k_1. In the second equation, σ_τ is the total collision cross section, $\alpha_i\sigma_\tau$ is the ionization cross section, W_{s0} is the mean initial energy of an electron ejected by an ionization collision, $\alpha_{m,n}\sigma_\tau$ is the excitation cross section, $\alpha_d\sigma_\tau$ is the momentum transfer cross section, V_i is the ionization potential, $V_{m,n}$ is the excitation potential, m_e is the mass of an electron, and M is the mass of a neutral. To show the effect of electron energy level on the rate of electron energy loss, the reduction of the electron energy inside the He cluster is represented in Figure 2.4. It is observed from the figure that the electron loses energy as it travels along the trajectory. It decreases rapidly when the energy level is high, and after a certain distance when energy falls

below 80 eV, the energy loss rate reduces. For Xe, the electron energy inside the cluster shows a similar trend – if energy is higher than 80 eV loss rate follows Bethe's formula and when it falls below 80 eV, all energy loss mechanisms are used to calculate the energy loss rate. The number density n_0 of a cluster is higher than that of gas. Since ideal gas law becomes less applicable as it gets closer to the critical point, we modified the equation of state to account for the particle number density near the critical point. For this purpose, in our cross section data modeling, we introduce a density correction factor ρ_f. The ideal gas density is multiplied by the density correction factor and the cross section data of a cluster containing a single particle are obtained. When the ideal gas density is multiplied by ρ_f, ionization coefficient values obtained from the cross section data of the one-particle cluster should agree with those obtained from the cross section data of the gas. For this reason, in our model, the value of ρ_f is different for different species. The following equation is used to define the number density.

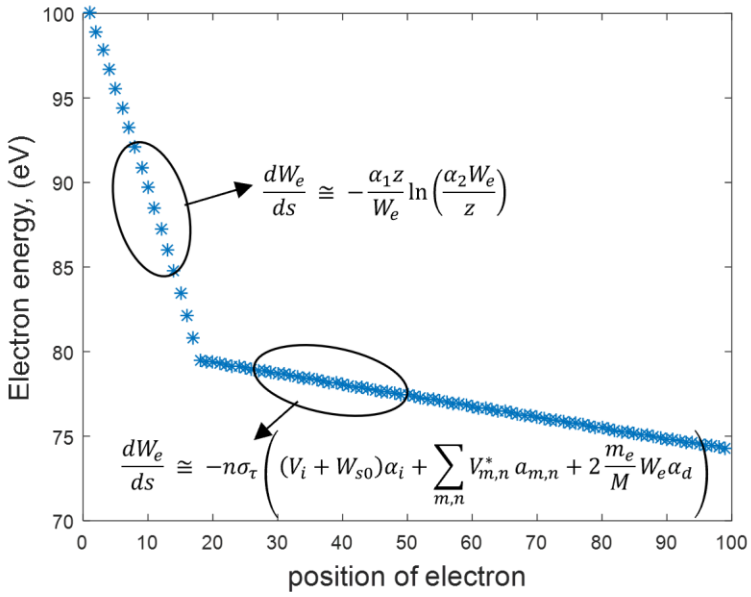

Figure 2.4 Electron energy loss inside a cluster

$$n_0 = \frac{\rho_f P_c}{kT_c} \tag{2.8}$$

where, T_c is the critical temperature, P_c is the critical pressure, k is the Boltzmann constant, and ρ_f is the density correction factor. The ionization coefficient for a cluster containing one particle (i.e., cluster size 1) should be identical to that of the gaseous molecule of the same species. For this reason, a density correction factor ρ_f is determined for each species such that when the ideal gas density of the cluster with one particle is multiplied by ρ_f, it results in the same ionization coefficient as that of the gaseous molecule. Based on our modeling, ρ_f is 2 for He, 6 for Xe and 4 for CO_2.

2.2.2 Modeled cross section data

Table 2.1 Supercritical fluids, their critical points, and name of cross section database

Supercritical fluids	Critical Temperature (K)	Critical Pressure (Mpa)	Cross Section Database
CO_2	304.25	7.39	MORGAN [50]
He	5.25	0.227	PHELPS [51]
Xe	289.733	5.842	SIGLO [52]

We model the dielectric strength of supercritical CO_2, supercritical He, and supercritical Xe. The critical points of all three supercritical fluids are given in Table 2.1. Based on Eq. (1), the electron scattering cross section data of supercritical CO_2, supercritical He, and supercritical Xe clusters near its critical point are derived from those of gaseous CO_2, He, and Xe. The databases used to retrieve the electron scattering cross section data of gaseous CO_2, He, and Xe are listed Table 2.1.

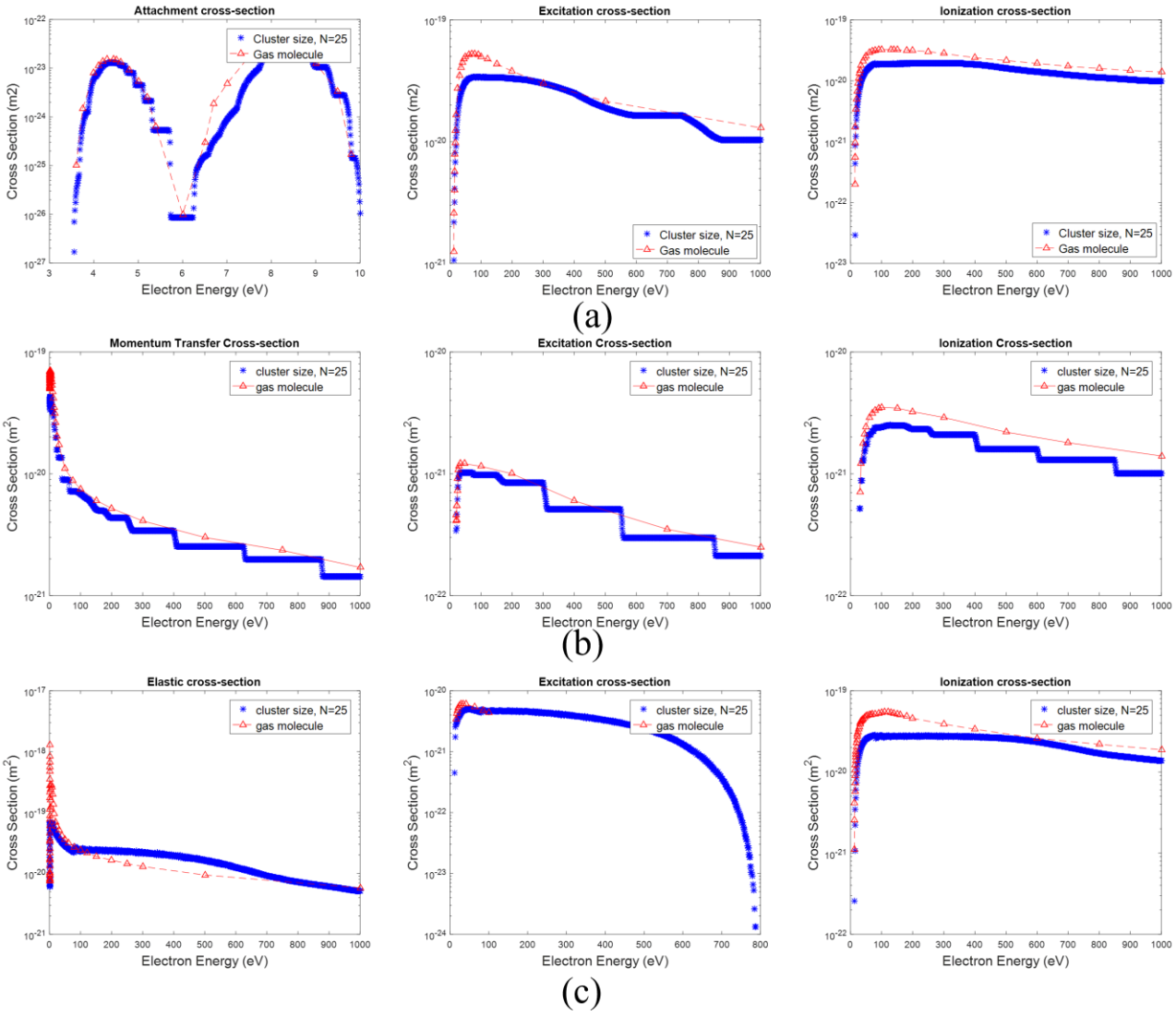

Figure 2.5 (a) Attachment, excitation, and ionization cross section of CO_2 cluster with respect to initial electron impact energy, (b) Momentum transfer, excitation, and ionization cross section of He cluster with respect to initial electron impact energy, (c) Elastic, excitation, and ionization cross section of Xe cluster with respect to initial electron impact energy.

Figure 2.5(a) shows the attachment, ionization, and excitation cross sections of supercritical CO_2 with cluster size 25 as a function of electron energy. The cross-section data of cluster size 25 are compared with those of gaseous CO_2. According to the figure, it is confirmed that the cross-section data of clusters decrease from those of gases. The trend is in agreement with published reports in the literature, in which authors experimentally showed that the electron scattering cross sections of clusters decrease from those of gas species [53], [54]. In addition, the authors modeled the breakdown voltage of supercritical CO_2, He, Xe, and H_2O around critical point based on electron scattering cross section, ionization potential, and secondary Townsend coefficient [8], [10]–[12], [55]. These studies also reported that electron scattering cross section decreases as the cluster size increases around critical point. The momentum transfer, excitation, and ionization cross section data of supercritical He with cluster size N =25 and the corresponding cross section data of gaseous He in Figure 2.5(b) and the elastic, excitation, and ionization cross section data of supercritical Xe with cluster size N=25 and the corresponding cross section data of gaseous Xe in Figure 2.5(c). A reduction in the cross sections is observed with the increasing cluster size from that of gaseous He and gaseous Xe.

2.3 Density reduced critical electric field for various cluster size

Boltzmann analysis performed based on the electron scattering cross section data is a widely used method for obtaining ionization coefficient and attachment coefficient [22]–[25]. For any occurrence of collisions by electron in molecule, Boltzmann analysis determines the rate coefficients and the transport coefficients by solving the following equation known as Boltzmann equation [56].

$$\frac{\partial f}{\partial t} + \vartheta . \Delta f - \frac{e}{m} E . \nabla_v f = C[f] \tag{2.9}$$

where f is the electron distribution function in phase space, ϑ is the velocity vector, e is the elementary charge, m is the mass of electron, E is the electric field, ∇_v is the velocity gradient, and $C[f]$ is the rate of change in f due to collision. We numerically solve the Boltzmann equation with BOLSIG+ solver to obtain the density- normalized ionization coefficient (α/N`), density-normalized attachment coefficient ($\eta/N$`), and density-normalized effective ionization coefficient ((α-η)/N`). It has been reported that the two-term approximation method is less reliable at high $E/N$`, in which the inelastic collision process is dominant, and the electron distribution is highly anisotropic [56]. The Boltzmann analysis of the present study involves gas species that have large elastic momentum-transfer electron scattering cross sections and $(E/N`)_{cr}$ as high as 63 Td for $CO_2$ 46 Td for Xe and 17 Td for He. The analysis results describe the kinetic processes of electrons that are represented by density reduced ionization coefficient $\alpha/N$` and density reduced attachment coefficient η/N`. The critical electric field, at which the ionization process is in equilibrium with the electron attachment process, has been used as the metric of comparing the dielectric strength of various gas media in numerous studies. α/N and η/N obtained from the Boltzmann analysis are plotted in Figure 2.6 as function of E/N for both gaseous CO_2 and the supercritical CO_2 of cluster size 25. Breakdown strength is represented by $(E/N)_{cr}$. In Figure 2.6, it is shown that $(E/N)_{cr}$ of supercritical CO_2 with cluster size 25 decreases to 55.6 Td from the 77.8 Td of gaseous CO_2.The values of α/N` of supercritical He clusters and supercritical Xe clusters are plotted as a function of density reduced electric field $E/N$` to describe the kinetic process of electron as shown in Figure 2.7. He and Xe are non-electronegative gases. Hence, attachment cross section data are not

available for He and Xe. Thus a constant attachment process is assumed for both supercritical He and Xe – the value used for He is 3.5×10^{-23} m^2 and the value used for Xe is 1×10^{-23} m^2, as shown in Figure 2.7. In this study, our objective is to model the dielectric strength variation of supercritical fluids which shows good agreement with the experimental data. $\alpha/N`$ for each cluster sizes are already obtained based on the electron scattering cross section data. Therefore, $\eta/N`$ is modeled such that the resulting dielectric strength variation shows close agreement with the experimental data. Figure 2.7(a) shows that $(E/N`)_{cr}$ decreases from 17 Td to 15.84 Td with increasing cluster sizes of supercritical He when $\eta/N`$ is modeled as 3.5×10^{-23} m^2. Similarly, in Figure 2.7(b) $(E/N`)_{cr}$ decreases from 30.56 Td to 17.67 Td when cluster size of supercritical Xe increases while $\eta/N`$ is kept at 1×10^{-23} m^2.

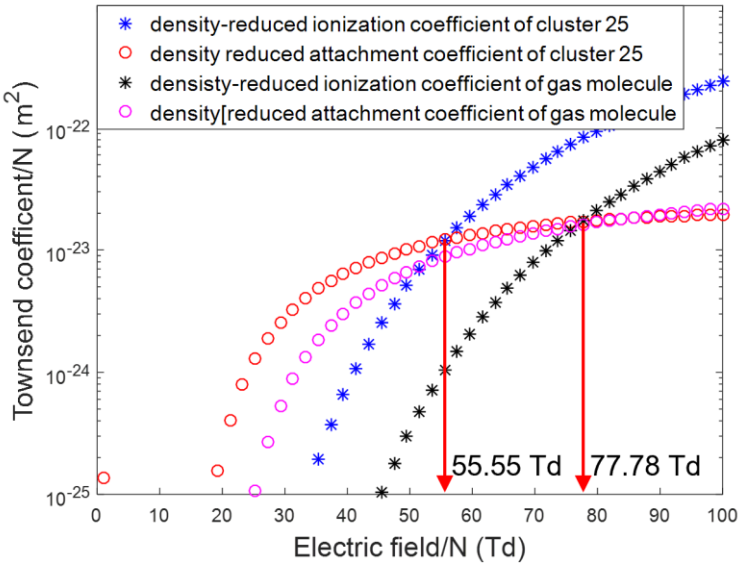

Figure 2.6 Density-reduced Townsend coefficients of CO_2 gas module and CO_2 cluster

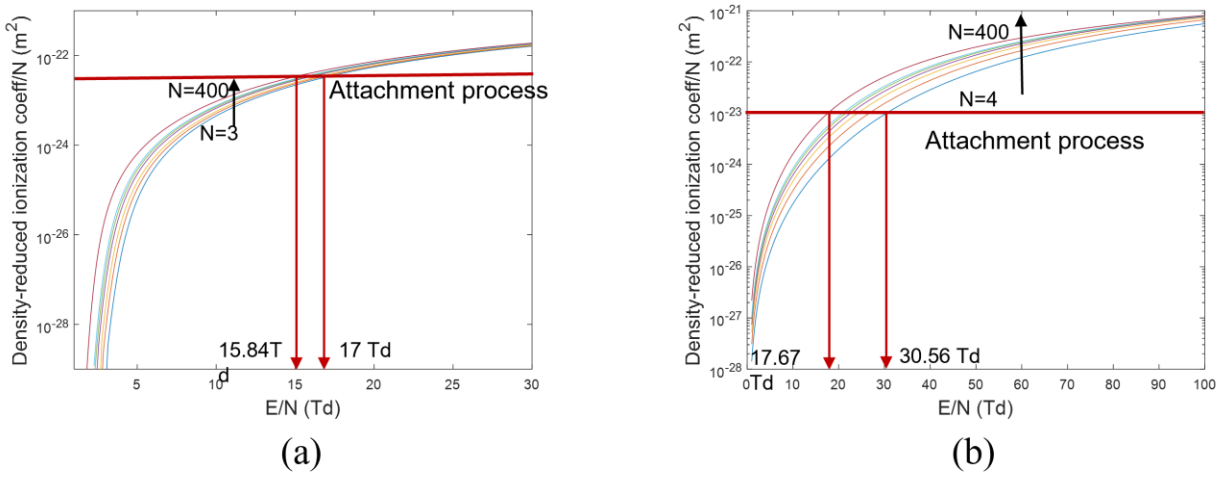

Figure 2.7 Density- reduced ionization coeeficient for various cluster sizes, (a) supercritical He and (b) supercritical Xe

2.4 Estimated dielectric strength variation and experimental verification

The reduction in $(E/N)_{cr}$ is mainly due to the effect of density fluctuation caused by the formation of clusters near critical point. Consequently, the dielectric breakdown characteristics of supercritical fluids shows the steep reduction near critical point, much lower than the breakdown strength of gas estimated by Paschen's law. Critical electric field E_{cr} derived from various cluster sizes near critical point are plotted as a function of pressure in Figure 2.8. Figure 2.8(a-1) shows the E_{cr} of supercritical CO_2 derived from various cluster sizes near the critical point. The modeling was conducted assuming a constant temperature of 304.25 K, which is the critical temperature of CO_2. The figure shows that the critical electric field slightly increases with increasing pressure (*i.e.*, Paschen's law), but a sharp decrease occurs as pressure becomes close to the critical point of CO_2 (*i.e.*, cluster formation). We compared the critical electric field values of our model with the experimental values reported in the literature. The experimental values includes those corresponding to temperatures from 306 K to 313 K. As shown in Figure 2.8(a-1), relatively

pronounced dielectric strength decline is observed in the cases of 306 K, 308 K, and 310 K because they are near the critical point. However, almost no decline in dielectric strength is observed in the case of 313 K most likely because the temperature is farther away from the critical point. The modeled dielectric strength of supercritical CO_2 show the trend of decreasing dielectric strength near the critical point similar to those shown by the experimental data reported in the literature [10], [11]. However, there are some discrepancies between the modeled data and experimental data shown by the root mean square error in Figure 2.8 (a-2) as there is no literature that reports the actual molecular cluster size near the critical point. In Figure 2.8(b-1), E_{cr} of supercritical He is plotted over a constant temperature of 5.25 K. It is observed from Figure 2.8(b-1) that near the critical pressure, a steep decline in the breakdown electric field occurs. Compared to the experimental data in the literature [55], the modeled data of this study show close agreement in dielectric strength near the critical pressure. Similarly, experimental data of breakdown electrical fields at temperatures 5.10 K and 5.40 K, reported in [55] are plotted as a function of pressure in Figure 2.8. It is observed that at temperature below and above critical point, comparatively less steep decline in dielectric strength is observed. The root mean square error in Figure 2.8(b-2) shows the discrepancies between the modeled data and experimental data. In Figure 2.8(c-1), E_{cr} of supercritical Xe for a constant temperature of 289.73 K is plotted and a steep decline of the breakdown electric field is observed near the critical pressure. The modeled data based on the cross section data of clusters are compared with the experimental values measured at a temperature of 292.15 K [12]. It is observed that, our approach of modeling the dielectric variation of supercritical Xe near the critical point results in very close agreement with the experimental data with some discrepancies showed by the root mean square error in Figure 2.8(c-2).

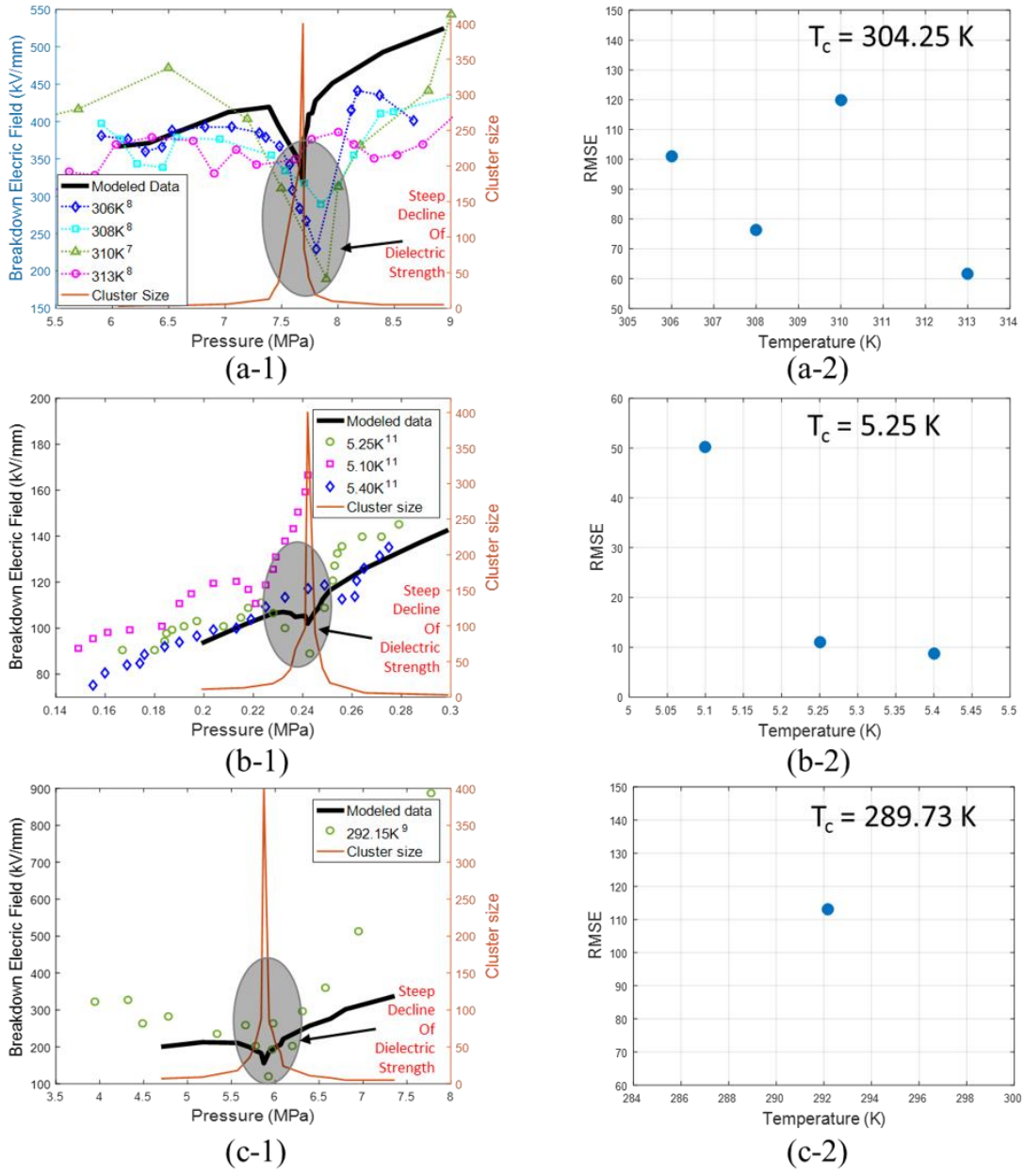

Figure 2.8 Dielectric strength of supercritical fluids near critical point. (a) SCF CO_2, (b) SCF He, and (c) SCF Xe. Modeled results agree well with the experimental data.

2.5 Summary

It is worth noting that that proposed approach of modeling the sharp decline in the breakdown electric field near the critical point is based on the electron scattering cross section data of various sizes of clusters. The approach is different from previously reported modeling methods that rely on the isothermal compressibility data. However, due to the lack of reported experimental data on the cluster sizes of supercritical fluids near critical point, in this study we assumed the cluster sizes as shown in Figure 2.8. Although we were able to fine tune the cluster sizes of supercritical fluids to achieve closer agreement with the experimental data, we did not do so because the major focus of our study is introducing the new modeling approach. That is, the discrepancies between the modeled data and the reported experimental data can be minimized with more accurate cluster size data. Furthermore, even with more accurate cluster size data, there would always be some level of discrepancies between data of the model and experimental measurements due to the stochastic nature of dielectric breakdown phenomena and finite accuracies in the experimental measurements.

CHAPTER III

ELECTRET: A NOVEL SOLUTION TO DIELECTRIC CHALLENGES

This part of the dissertation has been published in 3 different conferences. In [57], the performance of electret in PD mitigation caused by triple points and cavities are experimentally demonstrated. [58] experimentally shows the electrets performance in increasing the critical flashover voltage in the surface flashover occurrence. In [59], which is accept but not available online yet, epoxy-based electret as a solution to PD at cryogenic temperature.

3.1 Electrets for surface discharge and cavity discharge mitigation

3.1.1 Motivation

Triple points, where three different type of material coexists, generate high electric fields because of the differences in the conductivity and permittivity of the materials. This high electric field causes surface partial discharge around the triple points. Cavities including bubbles and airgaps are formed in solid insulators or in adhesive layers during the bonding process and are filled with gas, which typically show low relative permittivity. These cause high electric fields in the cavities and promote internal PD. The presence of triple points, sharp edges, and cavities is a very common phenomenon in any power device, making PD an inevitable dielectric challenge. The effectiveness of electret fabricated in mitigating PD activities caused by the triple points (surface discharge), and cavities and airgaps (cavity discharge) by neutralizing the locally enhanced electric field are discussed in this section.

3.1.2 Fabrication of electrets

If a sufficiently high voltage is applied between asymmetric electrodes, *e.g.*, point-plane electrodes, an electrical discharge is formed near the tip of the electrode. This controllable and non-disruptive electrical discharge is known as the corona discharge[42]. Because of the controllability, simplicity, and low cost, the corona discharge has been used widely to charge polymers and dielectrics [42], [43]. In the early days, the corona charging setup consisted of a needle electrode placed above the dielectric material on a flat electrode. However, this method lacks uniformity when charging a dielectric sample. For this reason, a metallic grid with uniform mesh is placed just above the dielectric sample, as shown in Figure 3.1(a), to improve the uniformity of charging and control the surface potential of the electret. This needle-grid-plane system is called triode corona system. Ions produced by the needle electrode are transferred at the surface and into the bulk of the sample to be charged and convert the sample into electret as shown in Figure 3.1(b).

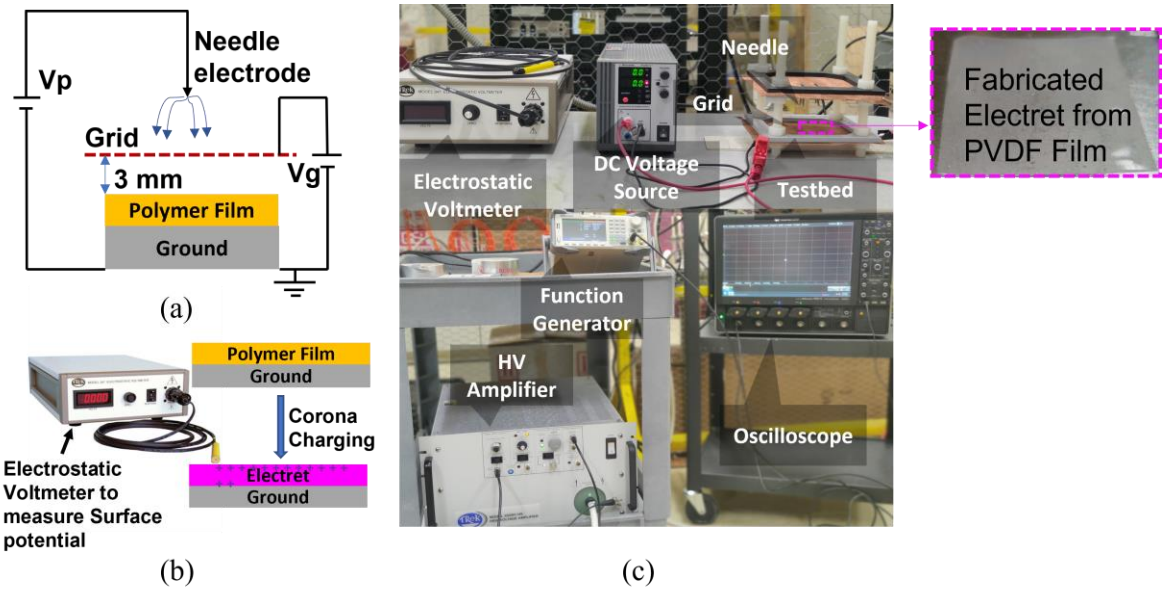

Figure 3.1 (a) Schematic diagram of triode corona charging method, (b) conversion of a PVDF film into an electret based on triode corona charging method and measuring the surface potential with an electrostatic voltmeter, (c) experimental setup

The surface charge density of the electrets cannot be measured directly. For this reason, an electrostatic voltmeter is used to measure the surface potential, which is then used to calculate total deposited surface charge density based on Gauss's law of a sheet of charge [60]. Equation (3.1) defines the surface charge density of the electret sheet of thickness d for the measured surface potential, V,

$$\sigma_s = \frac{\epsilon_0 \epsilon_r V}{d} \tag{3.1}$$

Electret films are prepared based on the triode corona charging method described in the previous section. Figure 3.1(c) shows the experimental setup for the fabrication of the electrets from the PVDF films in the lab [57], [61], [62]. For the electret preparation, two separate high voltage

supplies are used – needle voltage supply and grid voltage supply. The needle voltage is as high as 20 kV DC, which is generated by amplifying 2,000 times the low voltage signal formed by a function generator through a high voltage amplifier (Trek Model 20/20C-HS-L). The copper mesh grid is supplied directly from a DC voltage source and the applied 600 V for 20 minutes. The PVDF films that are used to be charged to prepare electrets have a thickness of 25.4 μm. The distance between the needle and the grid surface is 3.5 cm while the distance between the grid and the PVDF film is only 3 mm. Once charging is completed, the surface potential is measured with an electrostatic voltmeter and converted into surface charge density based on 5.1.

3.1.3 PD detection circuit

The performance of electret mitigating PD in power electronic driven system application is evaluated by conducting a series of PD measurements. The PD measurement circuit is designed in accordance with the IEC standard 60270 [63] as shown in Figure 3.2(a). The experimental setup is shown in Figure 3.2(b) [57], [61], [62]. The high voltage is supplied to the high voltage electrode was generated by amplifying the low voltage of a function generator through a high voltage amplifier (Trek Model 20/20 CHS-L). PD caused by the triple points and cavities are detected with the coupling capacitor and PD detecting device that has a measurement impedance (quadrupole). For each PD, the quadrupole causes a voltage drop across it which is then converted in apparent charge through Omicron MPD 600. Surface discharge caused by triple points and cavity discharge caused by internal cavities of the dielectric sample were monitored through a computer-based software provided by Omicron.

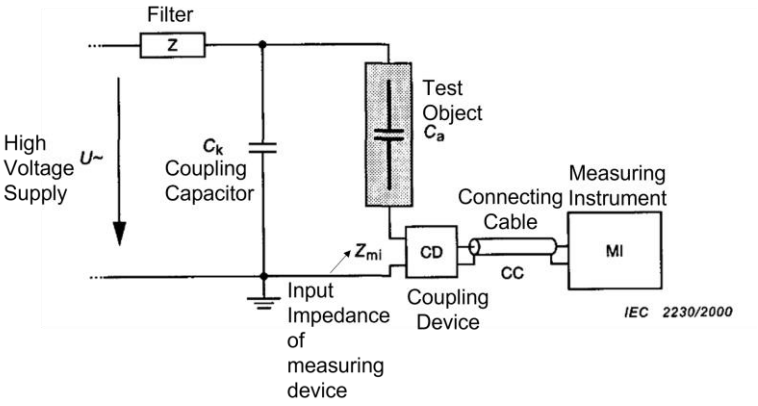

(a)

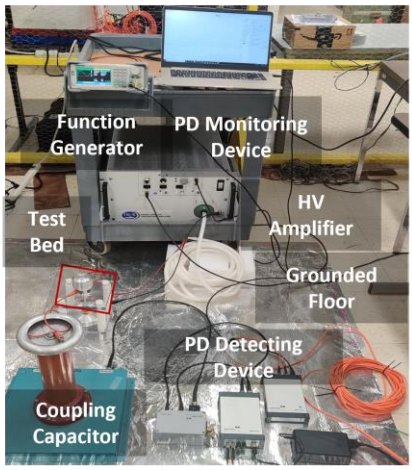

(b)

Figure 3.2 (a) Partial discharge measurement based on IEC standard 60270 [63] and (b) experimental setup of PD measurement.

3.1.4 Surface discharge mitigation performance

3.1.4.1 Testbed configuration

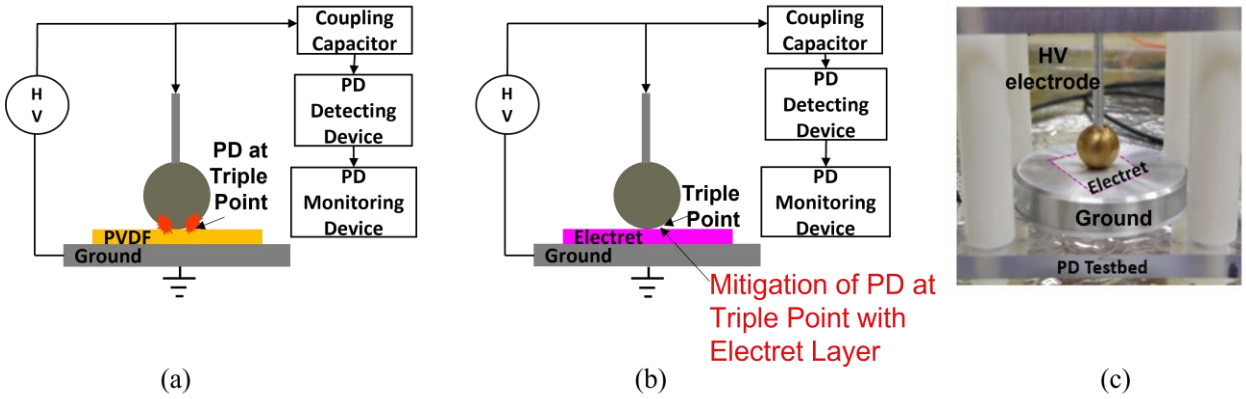

Figure 3.3 Experimental setup developed and used to compare PD mitigation performance with PVDF films and the electret layer caused by triple points. Schematic diagram of PD measurement (a) with uncharged PVDF, (b) with charged PVDF (electret), (c) testbed used for PD measurement.

Figure 3.3 shows the experimental setup that is used for demonstrating the PD mitigation performance of electrets at triple points. The testbed consists of a spherical electrode, where high voltage is applied to, and a flat electrically grounded disk. The spherical electrode is used as the high voltage electrode to avoid any enhancement of electric field caused by the sharp edges. Both the PVDF film and the electret film were placed between the two electrodes respectively to compare the effectiveness of the electret layer in mitigating PD activities caused by the presence of triple points. The spherical electrode was supplied with square voltage waveform with magnitude varying from 0 V to 2 kV or 2.5 kV and maintaining a constant *dv/dt* ratio of 50 V/μs for each voltage magnitude. The rise time was increased from 40 μs to 50 μs to maintain constant *dv/dt* ratio. A function generator is used to generate the square voltage which is then amplified 2,000 times with a high voltage and high frequency amplifier. The interfaces of the high-voltage electrode, PVDF film, and air generate a triple point, which causes high local electric fields and

promotes PD activities. Coupling capacitor and PD detecting device MPD 600 is used to detect PD signals. PD signals are monitored using a computer-based software provided by OMICRON.

3.1.4.2 Experimental result

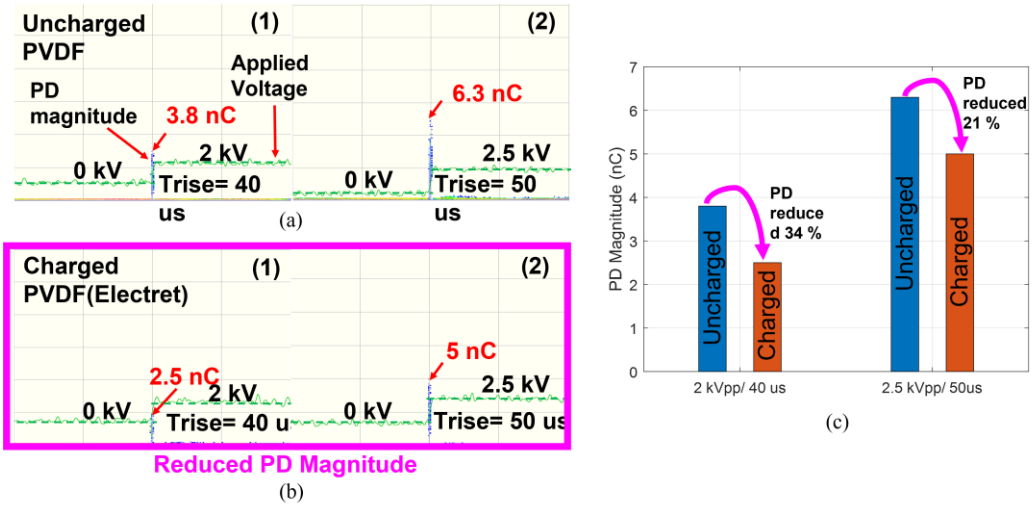

Figure 3.4 Partial discharge magnitudes caused by the triple points at the interface of electrode, dielectric material and surrounding air. The applied square voltage is increased from 2 kV to 2.5 kV and the rise time is from 40 µs to 50 µs to maintain constant *dv/dt* ratio. (a) PD magnitudes with uncharged PVDF film. (b) PD magnitudes charged electret layer, (c) PD magnitudes as a function of square voltage magnitude and rise time.

Figure 3.4shows the PD activities at the triple point in the presence of a PVDF film (Figure 3.4(a)) and an electret layer (Figure 3.4(b)). In Figure 3.4(a), when uncharged dielectric film is used, PD magnitudes caused by the triple points are 3.8 nC for 2 kV_{pp} and 6.3 nC for 2.5 kV_{pp}. However, when the uncharged dielectric film is replaced with the charged electret, as shown in Figure 3.4(b), PD is reduced from 3.8 nC to 2.5 nC when the applied voltage is 2 kV_{pp} and from

6.3 nC to 5 nC when the applied voltage is 2.5 kV_{pp}. A maximum of 35% reduction in the PD magnitude is achieved when an electret with surface charge density of 892 $\mu C/m^2$ is used. The reduction of the PD magnitudes implies that the high electret field generated due to the triple point is reduced by the embedded surface charge in the electret layer. Figure 3.4(c) summarizes the PD magnitudes of resulting from the uncharged PVDF and the charged electrets caused by the presence of triple points as a function of voltage magnitudes and rise time.

3.1.5 Cavity discharge mitigation performance

3.1.5.1 Testbed configuration

Figure 3.5 represents a testbed that is used for measuring PD signals that occur in cavities. Airgaps and bubbles in an insulator or between dielectric layers cause high electric fields and promote PD activities. For the experiment, a 1 mm-thick dielectric sample is 3D printed in the lab, which inherently contains micro scale cavities. The dielectric material is placed above the PVDF film as shown in Figure 3.5(a) and Figure 3.5(b). To observe the PD signals caused by the cavities in the dielectric material, the same PD measurement setup is used. The square voltage waveform applied to the spherical electrode had magnitudes varying between 5 kV_{pp} and 6 kV_{pp} and maintained a constant *dv/dt* ratio of 1,000 V/μs. For this reason, when voltage level was 5 kV_{pp}, rise time was 5 μs, and when voltage level was 6kV_{pp}, rise time was 6 μs. PD measurements are conducted for both uncharged PVDF and charged electret separately and their PD magnitudes are compared to observe the effectiveness of electrets in mitigating PD activities caused by cavities inside the solid insulator. PD signals caused by the cavities are detected with the same coupling capacitor and MPD 600.

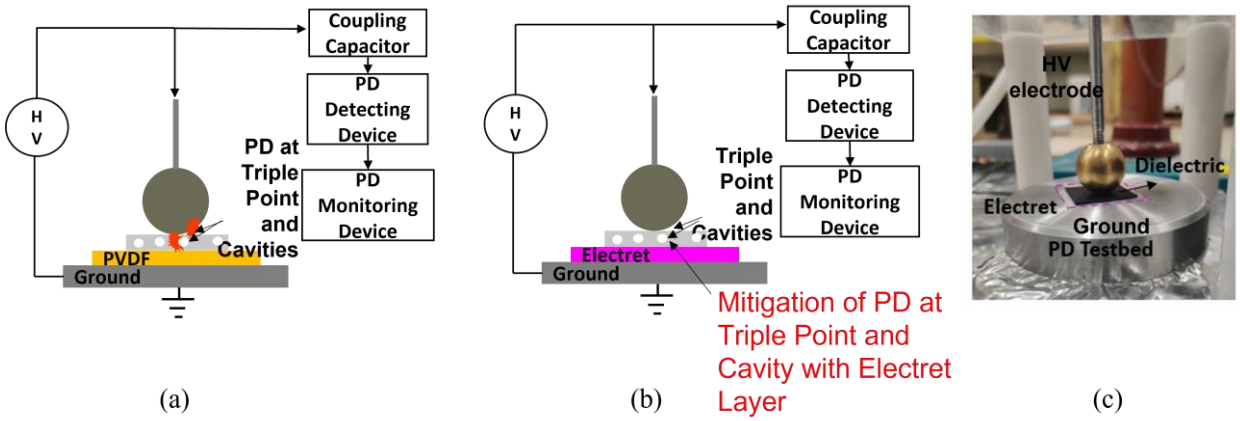

Figure 3.5 Experimental setup to compare PD mitigation performance with PVDF films and the electret layer caused by cavities. Schematic diagram of PD measurement (a) with uncharged PVDF (b) with charged PVDF (electret), (c) testbed used for PD measurement.

3.1.5.2 Experimental results

Figure 3.6 shows the effectiveness of the electret-based approach in mitigating PD occurrence caused by the cavities inside solid insulators. Figure 3.6(a) is the case, where an uncharged PVDF is placed below the solid insulator and PD magnitudes are recorded due to the cavity discharge. It is observed that with the uncharged PVDF film, the PD magnitudes caused by the micro scale cavities are 5.4 nC for 5 kV_{pp} and 9.4 for 6 kV_{pp}. Later, when uncharged PVDF is replaced with the charged electret having a surface charge density of 892 $\mu C/m^2$, a significant reduction in the PD magnitudes is observed. PD magnitude is reduced to 1 nC when applied voltage is 5 kV_{pp} and 4 nC when applied voltage is 6 kV_{pp}. The charge embedded in the electret surface neutralizes the high electric field caused by the cavities and mitigate the PD activities. Figure 3.6(c) summarizes the performance of electret in mitigating PD activities as a function of voltage magnitude and rise time.

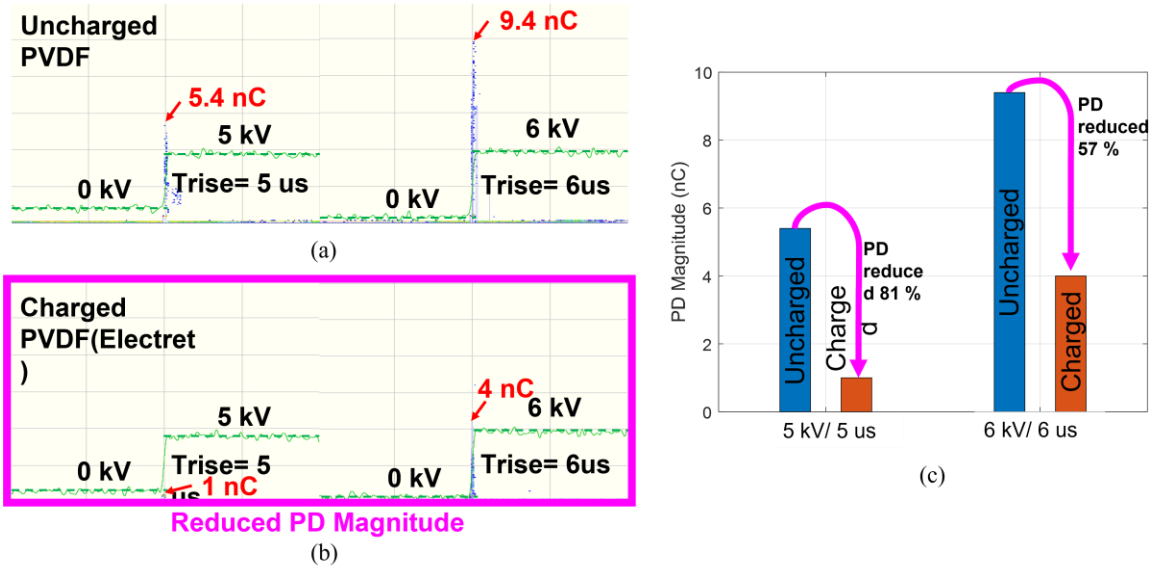

Figure 3.6 Partial discharge magnitudes caused by the triple points at the interface of electrode, dielectric material and surrounding air. The applied square voltage is increased from 2 kV to 2.5 kV and the rise time is from 40 µs to 50 µs to maintain constant *dv/dt* ratio. (a) PD magnitudes with uncharged PVDF film. (b) PD magnitudes charged electret layer, (c) PD magnitudes as a function of square voltage magnitude and rise time

3.1.6 Summary

In this section, we experimentally demonstrated that the locally enhanced electric fields around the triple point and cavities can be reduced significantly with the incorporation of electret films and hence mitigate PD activities. The results show the potential of using electrets to solve PD in power electronic converters and laminated busbars, where triple points and cavities are unavoidable. Electrets with tailored surface charge density would lead to high-power density systems with the complete mitigation of PD activities. Therefore, fabricating electrets with the

right amount of surface charge density creates tremendous prospects in the next-generation of technological advancements.

3.2 Epoxy electret for partial discharge mitigation at cryogenic temperature

3.2.1 Motivation

Epoxy-based composites exhibit mechanical compatibility at cryogenic temperatures. Owing to these properties, composites based on epoxy are used as electrical insulators in high temperature superconducting (HTS) power applications. However, the inevitable presence of voids in solid insulators, triple points, and airgaps at high-voltage conductor-insulator interfaces increase electric fields locally. The intensified electric field around these defects and interfaces is the main cause of partial discharge (PD), which is a dielectric challenge for numerous power applications including HTS cables. Electret has been introduced as a promising solution to mitigate PD activities caused by voids and triple points. In this section, the PD mitigation performance of electrets fabricated from epoxy resin in analyzed, which is suitable for cryogenic power applications.

3.2.2 Partial discharge source in HTS power applications

In the recent increasing electric demand, HTS power cables are preferable over conventional cables because of the high-power density provided by them. All electric shipboards and electric aircraft power system, where high-power ratings with reduced weight and size are primary concerns, are based on HTS power technology. In the gaseous He (GHe) cooled HTS power cable, the widely used electrical insulation is the lapped tape [64]. This lapped tape insulation is helically wrapped around the cable and to avoid mechanical stress, butt gaps are introduced as shown in Figure 3.7. These intentional butt gaps are filled with coolants with lower

permittivity than the insulation tape. This causes local field enhancements. In intensified local electric field causes partial discharge that leads to dielectric material ageing and the increased risk of device failure.

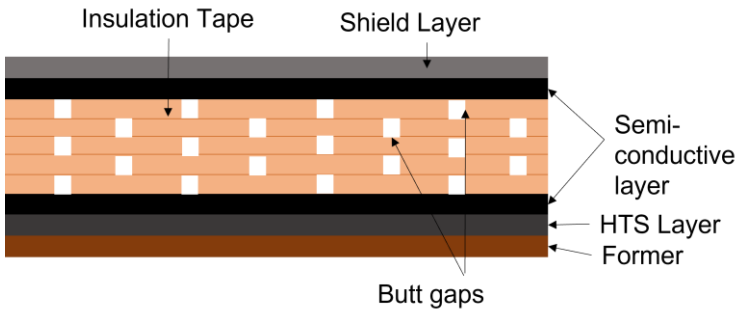

Figure 3.7 PD source in HTS power cable[65].

3.2.3 Fabrication of epoxy-based electret

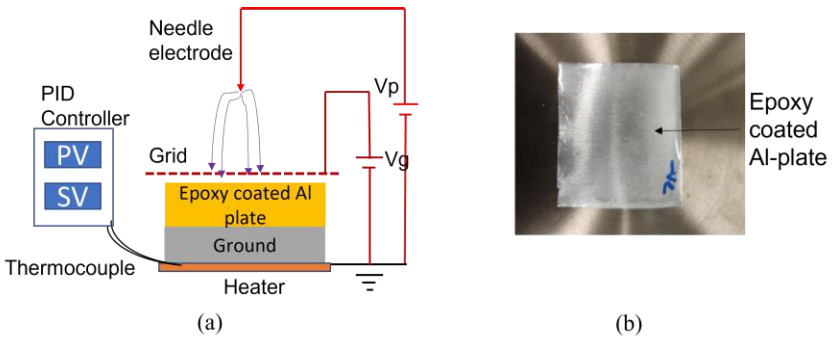

Figure 3.8 Fabrication of electret from epoxy-based composites. (a) Schematic diagram charging epoxy coated aluminium plate at elevated temperature, (b) epoxy electret

An aluminium (Al) plate with thickness 0.25 mm was coated with a thin layer of epoxy. The epoxy used for this purpose was 820 resin that is a very low viscosity resin, and 824 hardener of minimum cure schedule 24 hours was added to the resin in 5:1 volumetric ratio for the curing purpose. The thickness of the epoxy coating was 0.2 mm. Once the coating was done, the Al-plate was placed on an induction heater controlled by a PID controller to accelerate the curing process of the epoxy in air. The epoxy layer was charged based on the triode-corona charging method during the whole curing process. In Figure 3.8(a), the schematic diagram of the triode-corona charging method along with the temperature control system is shown. Temperature was kept at 60 ^{o}C to accelerate the curing process and to increase the stability of the surface charge by allowing charged particles to penetrate into deep traps. After the curing process, the charging process was stopped and measured the surface potential with an electrostatic voltmeter. The surface potential of the epoxy electret achieved by this process was 164 V, which translates 26.17 μC/m^2 surface charge density. To compare the effectiveness of epoxy electret in mitigating PD activities, an uncharged epoxy coated Al-coated sample was prepared and cured under the same temperature.

3.2.4 PD mitigation by epoxy electret

3.2.4.1 Testbed description

With the uncharged epoxy layer and charged epoxy layer, a series of PD experiments under same square voltage waveform were conducted and PD signals were compared. The presence of triple points at the interface of metal electrode, dielectric material, and surrounding medium (air) cause local field enhancements and promote PD occurrence. A 3D printed solid insulator was used as the dielectric material as shown Figure 3.9. The micro-scale cavities inherently created in the 3D printed solid insulator are the main sources of PD activities. Below the 3D printed solid insulator, the uncharged epoxy layer was placed. A function generator was used to generate the

square voltage, which is amplified with a high voltage amplifier and supplied to the high voltage electrode. PD activities caused by the presence of triple points and cavities are detected with the coupling capacitor and PD detecting device (Omicron MPD 600). PD signals achieved with the uncharged epoxy were recorded with a computer-based software provided by Omicron. Later, uncharged epoxy was replaced with the charged epoxy (electret) and PD signals under same square voltage were recorded. Figure 3.9 shows the testbed used to conduct the PD measurements.

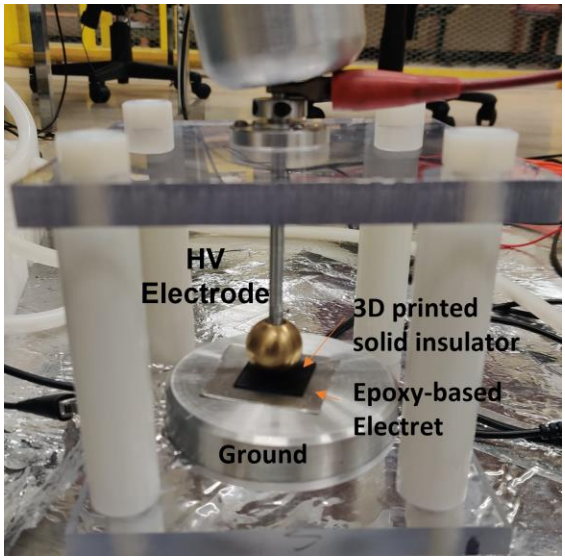

Figure 3.9 PD measurement testbed used to evaluate the performance of epoxy-based electret

3.2.4.2 Comparison of PD mitigation performance

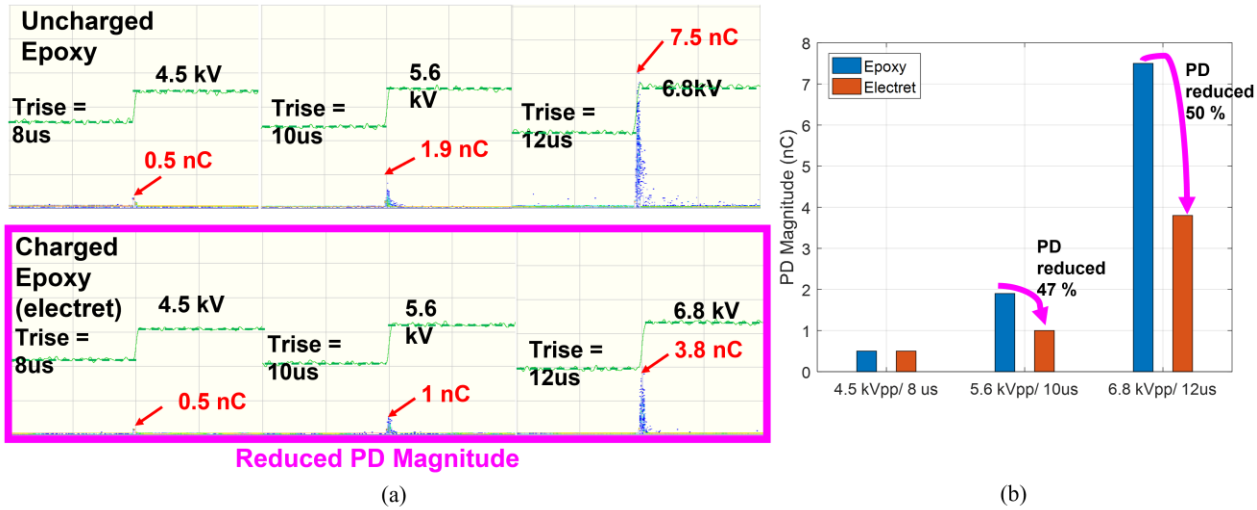

Figure 3.10 The PD mitigation performance of uncharged epoxy and charged epoxy stressed under three different square voltage stimuli. In each case, the *dv/dt* was maintained at a constant value. (a) PD signals with uncharged epoxy and epoxy electret, (b) Comparison of PD magnitudes

PD measurements were conducted with uncharged and charged epoxy (electret) layers under same unipolar square voltage waveforms. Three different square voltage levels on the high voltage electrode were applied and maintained a constant *dv/dt* of 560 V/µs for all voltage levels. To this end the square voltage magnitude and rise time were both increased systematically. The PD signals achieved at each voltage level with uncharged and charged epoxy are presented in Figure 3.10. It is shown that when square voltage magnitude varies between 0 to 4.5 kV with a rise time 8 µs, both uncharged and charged epoxy caused same PD magnitudes of 0.5 nC. Subsequently, the voltage was increased to 5.6 kV and to maintain same *dv/dt* ratio, rise time was set to 10 µs. It is observed that, PD magnitude with uncharged epoxy (1.9 nC) is 90 % higher than

that of the charged electret (1 nC). Once the voltage level is further increased and set to 6.8 kV with the rise time of 12 μs, there is a drastic rise in PD magnitudes in the case of the uncharged epoxy (7.5 nC). However, PD magnitudes achieved with the charged epoxy is 3.8 nC which only 50% of the PD magnitude resulted with the uncharged epoxy. Figure 3.10(b) shows the relative comparison of PD magnitudes with and without electret. This significant reduction in the PD magnitudes achieved with the electrets fabricated from epoxy suggests that the charge stored in the electret surface neutralizes the high electric field caused by triple points and cavities.

3.2.5 Summary

In this section, the performance of epoxy-based electrets in mitigating PD activities caused by the presence of triple points and cavities is experimentally demonstrated. The results show that electrets with a surface charge density of 26.17 $\mu C/m^2$ can reduce PD magnitude by 50%. Epoxy-based electrets are fabricated using the triode corona charging method while curing without any degassing prior to casting. The objective of this study is to prepare epoxy-based electret and observe if they can mitigate PD. Several samples of charged and uncharged epoxy sheets were cured under identical condition that did not involve a degassing process. Despite the possibility of having bubbles, the results show that epoxy-based electrets can mitigate PD. Further improvements in PD mitigation are expected as improved epoxy-based electrets are developed. With higher surface charge density and increased stability, the epoxy-based electrets will enable PD-free conditions in cryogenic and HTS power applications.

3.3 Electret for surface flashover improvement

3.3.1 Motivation

Surface flashover is another chronic dielectric issue associated in medium to high voltage devices and power electronics driven system that threaten the emerging technologies. The high voltage rating, high power density, and high *dV/dt* provided by the advanced power electronics driven system increases the risk of surface flashover. For this reason, critical flashover (CFO) voltage associated with surface flashover event should be improved. In this section, the electret based electric field neutralization approach is utilized to increase the CFO and thus enhance the dielectric robustness. The CFO of dielectric material with and without the incorporation of electret film is compared by conducting surface flashover experiments under power electronics switching voltages.

3.3.2 Surface flashover theory

Surface flashover occurs along the surface of an electrical insulation or dielectric medium. The field emission electron generated at the triple points initiates the surface flashover process. The field emission electrons collide with the insulator surface and produce more electrons. When some of these secondary electrons strike the insulator surface, the results in the emission of more electrons and the process continues causing a cascading effect along the surface. This process is called secondary electron emission avalanche (SEEA) that eventually cause surface flashover [66], [67].

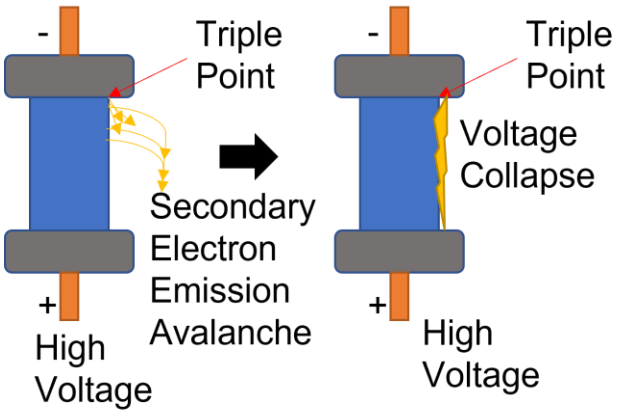

Figure 3.11 Secondary electron emission avalanche (SEEA)

3.3.3 Electret based surface flashover improvement

According to Secondary Electron Emission Avalanche theory, surface flashover happens on the insulator surface because of the high electric field around the triple point. This indicates that electret-based dielectric approach is applicable to improve the critical flashover voltage (CFO) since it can neutralize the intensified electric field around triple points [58], [68].

3.3.3.1 Testbed description

Figure 3.12 shows the schematic diagram where triple points are formed at interfaces of high voltage electrode, sample films, and air. Figure 3.12(a) is the case when an uncharged PVDF is on top of a dielectric material. The local electric field around the triple point is so high that surface flashover takes place when the applied voltage is not sufficiently high. This is called the critical flashover voltage (CFO). We placed the cylindrical electrode close to the one corner of the PVDF film so that surface flashover can take place in one direction. In Figure 3.12(b), the uncharged PVDF film is replaced with the positively charged PVDF (electret) and all the

experimental conditions are kept exactly same as before. The charge embedded on the surface of the electret build a counter electric field that neutralizes the enhanced electric field due to the triple point. This helps the surface flashover to take place at much higher voltage than the case earlier.

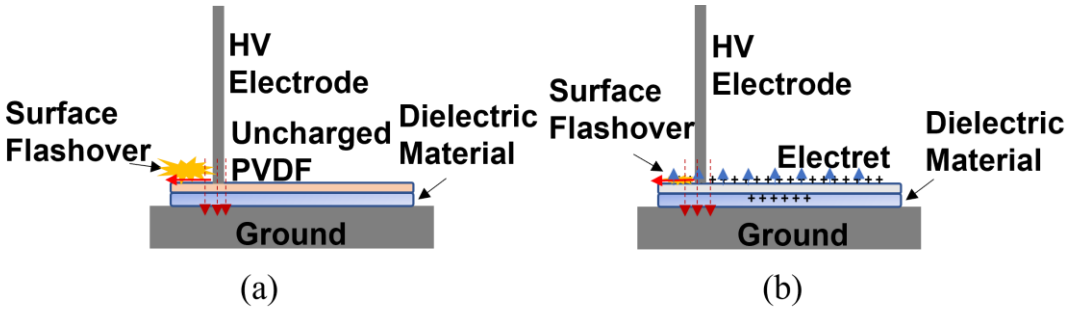

Figure 3.12 Schematic diagram to compare electrets performance in improving CFO, (a) Uncharged PVDF, (b) electret

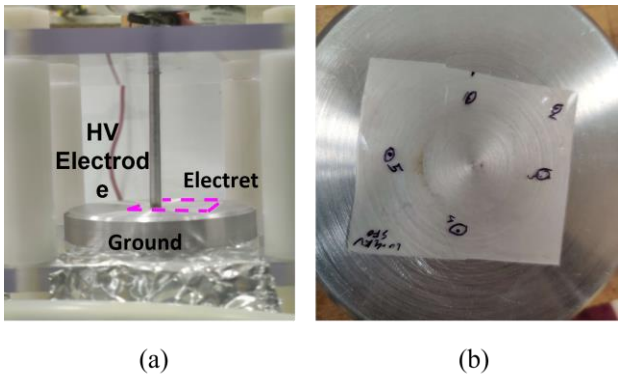

Figure 3.13 (a) Surface flashover experiment testbed, (b) different position on the uncharged PVDF film to be conducted surface flashover experiment

The actual testbed to demonstrate the effectiveness of electret in improving CFO is shown in Figure 3.13(a). A PVDF film of 100 μm thickness is used as the dielectric material as shown in Figure 3.12. The sample PVDF films of 25 μm is placed on top of the dielectric material. To observe surface flashover at different point on the PVDF film, we marked five different position on the PVDF film shown in Figure 3.13(b) and conducted surface flashover experiment separately for each position. We used five different electret samples that are charged under same condition as mentioned in section III. On each electret sample we marked a position that matches one of the positions on uncharged PVDF and surface flashover experiments are conducted on each sample separately to determine the CFO.

3.3.3.2 Results

The cylindrical electrode as shown in Figure 3.13(a) are supplied with the square voltage waveforms with rise time 40 μs and duty cycle 50%. The magnitude of the voltage is increased very slowly from 200 V_{pp} up to the voltage where the surface flashover event takes place. The CFO voltage for each of the surface flashover events with the uncharged PVDF films and electrets are recorded. Table 3.1 shows all the CFO voltage for each position as shown in Figure 3.13(b). The CFO value achieved with the electrets are higher than the values associated with the uncharged PVDF films. The CFO are increased by 20% with the incorporation of electret layer on the dielectric material. Although this percentage is not very impressive, CFO voltage can be improved further if the electrets are fabricated in a more developed system. Figure 3.14summarizes the experimental results.

Table 3.1 Critical flashover (CFO) voltage of uncharged PVDF and electret

Electrode position	PVDF CFO (kV)	Electret CFO (kV)	Percentage Improvement
Position-1	6.2	7.2	16%
Position-2	4.8	5.8	20%
Position-3	6.8	8	18%
Position-4	6.4	7	9%
Position-5	6.4	7	9%

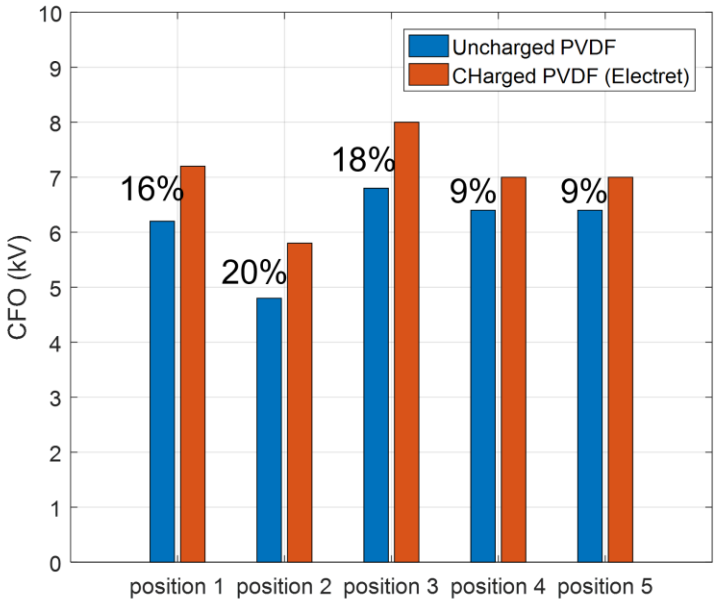

Figure 3.14 Critical flashover (CFO) voltage of uncharged PVDF and electret.

3.3.4 Summary

In this study, it is experimentally demonstrated that the inclusion of electret layers in medium to high voltage application leads to improve surface flashover voltage by neutralizing the high electric field around triple point. The surface flashover experiment shows that the CFO voltage associated

with the surface flashover events can be increased by 20% when electret layer is placed on a dielectric material. For this reason, the dielectric improvements provided by the electret-based approach are expected to facilitate the materialization of PEC driven system with ensured dielectric integrity.

CHAPTER IV

FABRICATION CONDITIONS FOR ENHANCED ELECTRET PROPERTIES

This part of the dissertation has been accepted in IEEE Transaction on Industrial Electronics [69].

4.1 Motivation

In the electret-based dielectric solution charge embedded in electrets is utilized for the neutralization of harmful locally enhanced electric field. For this reason, the optimum amount of surface charge density and high charge stability are required to properly mitigate PD. In this section, electrets are fabricated based on the widely used triode corona charging method under various charging conditions that includes charging voltage, charging duration, charging polarity, and charging temperature with the goal of establishing an electret fabrication process that yields high-quality electrets. A series of experiments on surface discharge and cavity discharge are conducted under high- *dv/dt* square voltage stimuli. PD signals are recorded at the edges of the square voltage waves without and with the incorporation of PVDF based electrets fabricated under the various charging conditions. The surface charge density and the PD mitigation performance of electrets are analyzed and reported to evaluate the performance of electrets fabricated under various charging conditions.

4.2 Impact of charging voltage

Charging voltage is determined by the grid voltage. To observe the impact of applied grid voltage on the performance of electret, PVDF films are charged for 20 minutes under various charging voltage magnitudes by varying the grid voltage from 100 to 600 V DC in the steps of 100 V. The needle voltage is kept at a constant voltage of 20 kV DC to ionize air and create charged particles. Table 4.1 summarizes the charging conditions applied in this section. The surface charge density and PD magnitude performance achieved by each electret fabricated under the various charging voltages are discussed below.

4.2.1 Surface discharge

Table 4.1 Electret fabrication under various charging voltage

Needle Voltage (kV DC)	Grid Voltage (V DC)	Charging Duration (minutes)	Charging Temperature (^{o}C)
20	100	20	30
	200		
	300		
	400		
	500		
	600		

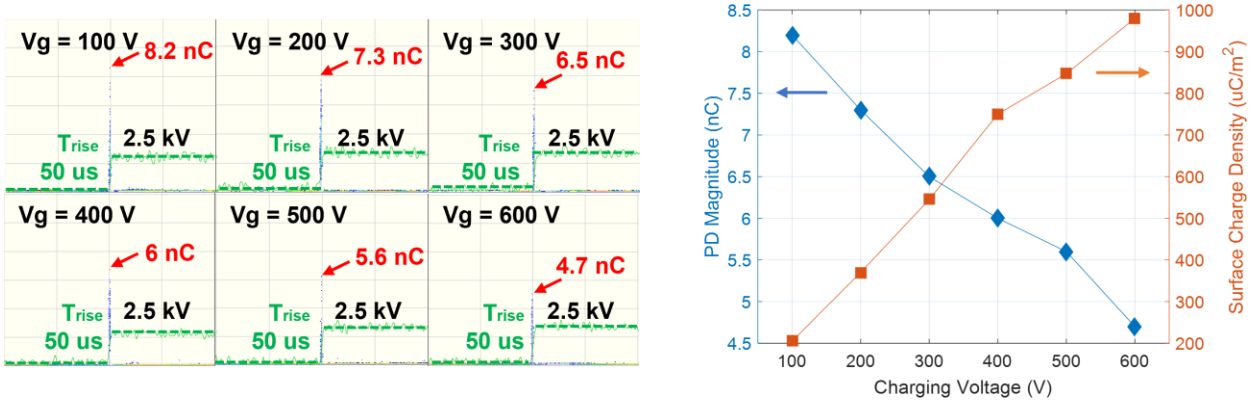

(a) (b)

Figure 4.1 Impact of charging voltage in mitigating surface discharge. PVDF films are charged for 20 minutes under various charging voltage magnitudes varying the grid voltage from 100 to 600 V DC in the steps of 100 V. (a) Surface discharge measured while the electrets prepared at various charging voltages (100-600 V DC) were stressed under the square voltage 2.5 kV with 50 µs rise time, (b) PD magnitude and electret surface charge density as a function of charging voltage.

The effects of charging voltage on the surface discharge mitigation performance of electrets are observed by conductive PD experiments under square voltage waveform. The results are shown in Figure 4.1(a). The square voltage with a 50 µs rise time was applied to the testbed and it was observed that when PD started to occur as voltage magnitude reached 2 kV. Therefore, a square voltage with 2.5 kV voltage magnitude was utilized to clearly observe surface PD. When the square voltage waveform that varies between 0 to 2.5 kV with the rise time 50 µs was applied to the electrets fabricated under various charging voltage magnitudes varying from 100 to 600 V DC, distinct levels of surface discharge occurred as voltage switches from 0 to 2.5 kV as shown in Figure 4.1(a). A decreasing trend in surface discharge magnitude with increasing grid voltage used for fabricating the electrets is observed. It is noted that, a reduction of 43 % in the surface discharge magnitude is achieved with the electret fabricated under 600 V grid voltage compared to the case

where the electret is fabricated under 100 V grid voltage. Figure 4.1(b) summarizes the surface discharge magnitude and shows the achieved surface charge density of the electrets as a function of charging voltage. The figure shows that the surface charge density of electrets increases while the surface discharge magnitude decreases with increasing charging grid voltage.

4.2.2 Cavity discharge

The impact of charging voltage on the cavity discharge mitigation performance of electrets under square voltage waveform is observed in Figure 4.2(a). In this case, a square voltage of rise time 6 μs is applied to the testbed and it is observed that PD started to occur as the square voltage peak value reached to 5 kV. Therefore, to clearly observe surface PD, a square voltage with 6 kV voltage magnitude was utilized. When the square voltage waveform that varies between 0 to 6 kV with the rise time 6 μs was applied to the electrets fabricated under various charging voltage magnitudes varying from 100 to 600 V DC, distinct levels of surface discharge occurred as voltage switches from 0 to 6 kV as shown in Figure 4.2(a). The figure shows a decreasing trend in surface discharge magnitude with increasing grid voltage used for fabricating the electrets. A reduction of 68 % in the cavity discharge magnitude is achieved with the electret fabricated under 600 V grid voltage compared to the case where the electret is fabricated under 100 V grid voltage. Figure 4.2(b) summarizes the cavity discharge magnitude and shows the achieved surface charge density of the electrets as a function of charging voltage. The figure shows that the surface charge density of electrets increases while the cavity discharge magnitude decreases with increasing charging grid voltage.

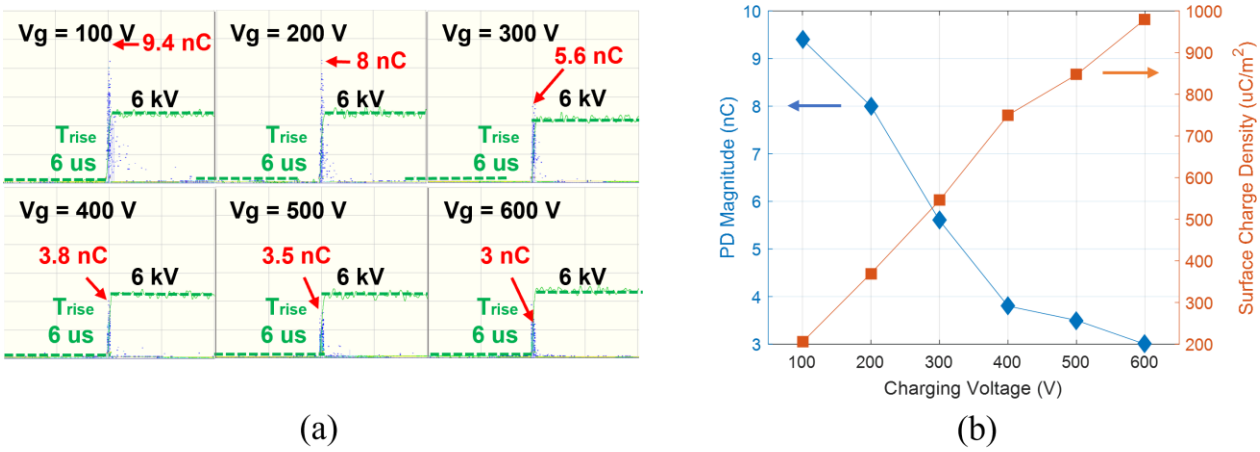

(a) (b)

Figure 4.2 Impact of charging voltage in mitigating cavity discharge. PVDF films are charged for 20 minutes under various charging voltage magnitudes varying the grid voltage from 100 to 600 V DC in the steps of 100 V. (a) Cavity discharge measured while the electrets prepared at various charging voltages (100-600 V DC) were stressed under the square voltage 6 kV with 6 µs rise time, (b) PD magnitude and electret surface charge density as a function of charging voltage.

4.3 Impact of charging duration

In this section, PVDF films were charged for various duration ranging from 10 minutes to 35 minutes. PD experiments are conducted to assess the PD mitigation performance of electrets. For these fabrication condition, the grid voltage and the needle voltage were kept at a constant level and the charging duration is varied from 10 minutes to 35 minutes. The grid voltage was kept at 600 V DC and the needle electrode voltage was kept at 20 kV DC for electret fabrication. Table 4.2 summarizes the charging conditions applied in this section.

4.3.1 Surface discharge

Table 4.2 Electret fabrication under various charging duration

Needle Voltage (kV DC)	Grid Voltage (V DC)	Charging Duration (minutes)	Charging Temperature (^oC)
20	600	10	30
		15	
		20	
		25	
		30	
		35	

Figure 4.3(a) shows the effects of charging duration on the surface discharge mitigation performance of electrets under square voltage waveform. Distinct levels of surface discharge occurred as voltage switches from 0 to 2.5 kV as shown in Figure 4.3(a) when the square voltage waveform that varies between 0 to 2.5 kV with the rise time 50 µs was applied to the electrets fabricated under various charging duration varying from 10 to 35 minutes. The figure shows that the PD magnitudes are relatively high when the charging duration is 10 minutes and 15 minutes. The PD magnitude is lowest in the case of electrets fabricated with a charging duration of 20 minutes which is 4.7 nC. However, as the charging duration further increases beyond 20 minutes, PD magnitudes are observed to increase again. The surface discharge magnitude as well as the achieved surface charge density of the electrets as a function of charging duration is plotted in Figure 4.3(b). The figure shows that the surface charge density of electrets increases while the surface discharge magnitude initially decreases and then increases with further increasing charging duration.

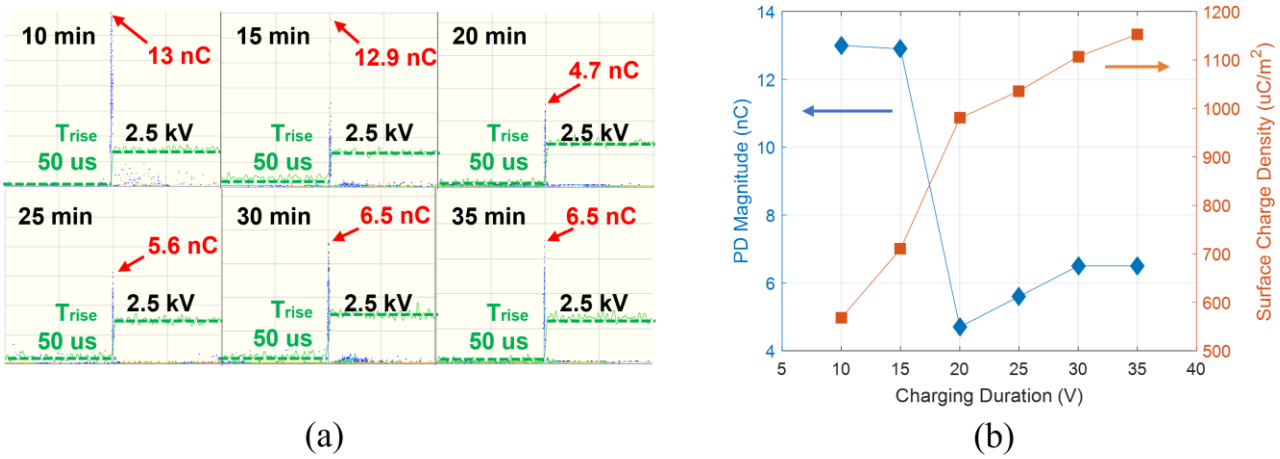

Figure 4.3 Impact of charging duration in mitigating surface discharge. PVDF films are charged for various duration varying from 10 minutes to 35 minutes, the applied grid voltage was 600 V Dc and the needle electrode was 20 kV DC to fabricate electrets. (a) Surface discharge measured while the electrets prepared at various charging duration (10-35 minutes) were stressed under the square voltage 2.5 kV with 50 µs rise time, (b) PD magnitude and electret surface charge density as a function of charging duration.

4.3.2 Cavity discharge

The effects of charging duration on the cavity discharge mitigation performance of electrets under square voltage waveform is shown in Figure 4.4(a). When the square voltage waveform that varies between 0 to 6 kV with the rise time 6 µs was applied to the electrets fabricated under various charging duration varying from 10 to 35 minutes, distinct levels of cavity discharge occurred as voltage switches from 0 to 6 kV as shown in Figure 4.4(a). The figure shows that when the charging duration is 10 minutes and 15 minutes, the PD magnitudes are relatively high. The PD magnitude is lowest in the case of electrets fabricated with a charging duration of 20 minutes which is 3 nC. However, as the charging duration further increases beyond 20 minutes, PD magnitudes are observed to increase again. Figure 4.4(b) summarizes the cavity discharge

magnitude and shows the achieved surface charge density of the electrets as a function of charging duration. The figure shows that the surface charge density of electrets increases while the cavity discharge magnitude initially decreases and then increases with further increasing charging duration.

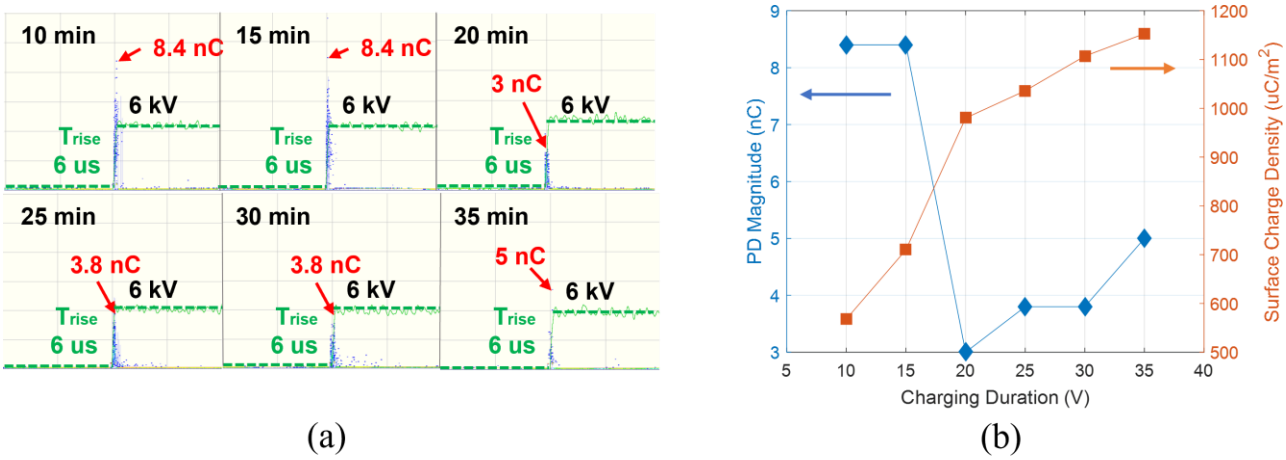

Figure 4.4 Impact of charging duration in mitigating cavity discharge. PVDF films are charged for various duration varying from 10 minutes to 35 minutes, the applied grid voltage was 600 V DC and the needle electrode was 20 kV DC to fabricate electrets. (a) Cavity discharge measured while the electrets prepared at various charging duration (10-35 minutes) were stressed under the square voltage 6 kV with 6 µs rise time, (b) PD magnitude and electret surface charge density as a function of charging duration.

4.4 Impact of charging polarity

In this section, electrets are fabricated under positive and negative voltage polarity utilizing the triode corona charging method and their PD mitigation performance is compared by conducting

a series of PD experiments. First, a PVDF film is charged with both the needle voltage and the grid voltage being positive. Later, another PVDF is charged while both the needle electrode and the grid electrode are supplied voltage of same magnitude and negative polarity. In both cases, PVDF films are charged for 20 minutes, and the grid voltage and the needle voltage are at 600 V DC and 20 kV DC, respectively. The charging conditions are shown in Table 4.3. The resulting electret surface charge densities and PD magnitudes are shown in the following figures.

4.4.1 Surface discharge

Table 4.3 Electret fabrication under various charging polarity

Needle Voltage (kV DC)	Grid Voltage (V DC)	Charging Duration (minutes)	Charging Temperature (^{o}C)
20	600	20	30
-20	-600		

The surface discharge mitigation performance of positively charged electret film is presented in Figure 4.5 (a). The effectiveness of a positively charged electret in PD mitigation is evaluated by comparing the PD magnitudes of an uncharged PVDF film and the positively charged electret. In this case. Both uncharged PVDF and electret are stressed under the same square voltage waveform. PD magnitudes are monitored for two different voltage levels with magnitudes varying from 0 to 2.5 kV and 0 to 3 kV while dV/dt is kept at 50 V/µs. A substantial reduction in the PD magnitude is observed when the uncharged PVDF is replaced with the charged PVDF electret. In Figure 4.5(b), the effectiveness of the negatively charged electret in mitigating surface discharge is compared with the uncharged PVDF. The figure shows that when the uncharged PVDF is replaced with the negatively charged electret, a maximum of 46 % reduction in PD magnitude is achieved whereas only 22 % reduction is achieved in the case of the positively charged electret

under the square voltage magnitude of 2.5 kV. Similarly, when the square voltage magnitude is increased 3 kV while keeping the *dV/dt* same, PD magnitude is reduced by 24 % achieved with the negatively charged electret while a 15 % reduction in the PD magnitude is achieved with the positively charged electrets. The figure shows that the surface charge density magnitude of the electret is higher (-976 $\mu C/m^2$) when it is charged under negative polarity than when it is charged under positive polarity (892 $\mu C/m^2$).

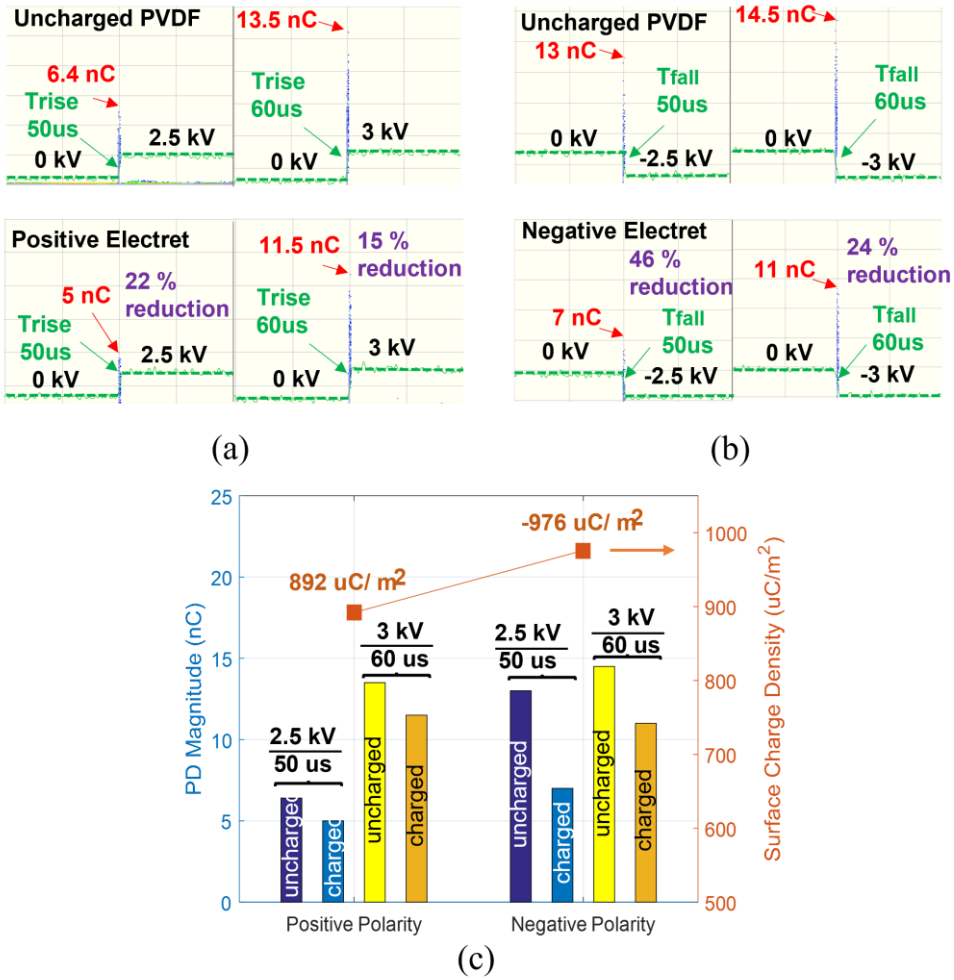

Figure 4.5 Comparison of surface discharge mitigation performance of electrets charged under different charging polarity. (a) comparing PD magnitudes with uncharged PVDF and positively charged electret, (b) comparing PD magnitudes with uncharged PVDF and negatively charged electret, (c) comparing surface charge density and PD mitigation performance of positively charged electret and negatively charged electret.

4.4.2 Cavity discharge

PD magnitudes in the presence of cavities with an uncharged PVDF, a positively charged electret, and a negatively charged electret are reported in Figure 4.6. Figure 4.6 (a) shows the case

of uncharged PVDF and positive electret. PD signals of cavity discharge measured while an uncharged PVDF film or a positively charged electret film is placed beneath the 3D printed solid dielectric sample containing micro scale cavities. Similarly, Figure 4.6(b) shows the PD signals of cavity discharge measured while an uncharged PVDF film or negatively charged electret film is placed beneath the 3D printed dielectric sample containing cavities. The figure shows that a 40 % reduction in PD magnitude is achieved under a square voltage waveform varying between 0 to 6 kV with a rise time of 6 μs while a 50 % reduction in PD magnitude is achieved under a square voltage waveform varying between 0 to -6 kV with a fall time of 6 μs. The figure shows that 25 % reduction is achieved under a square voltage waveform varying between 0 to 7 kV with the rise time of 7 μs in the case where the positively charged electret film is inserted under the 3D printed dielectric samples while a 32 % reduction is achieved under a square voltage waveform varying between 0 to -7 kV with the fall time 7 μs in the case where the negatively charged electret film is inserted under the 3D printed dielectric sample. Figure 4.6(c) summarizes the PD magnitudes recorded and shows the surface charge density achieved in the positively and negatively charged electrets.

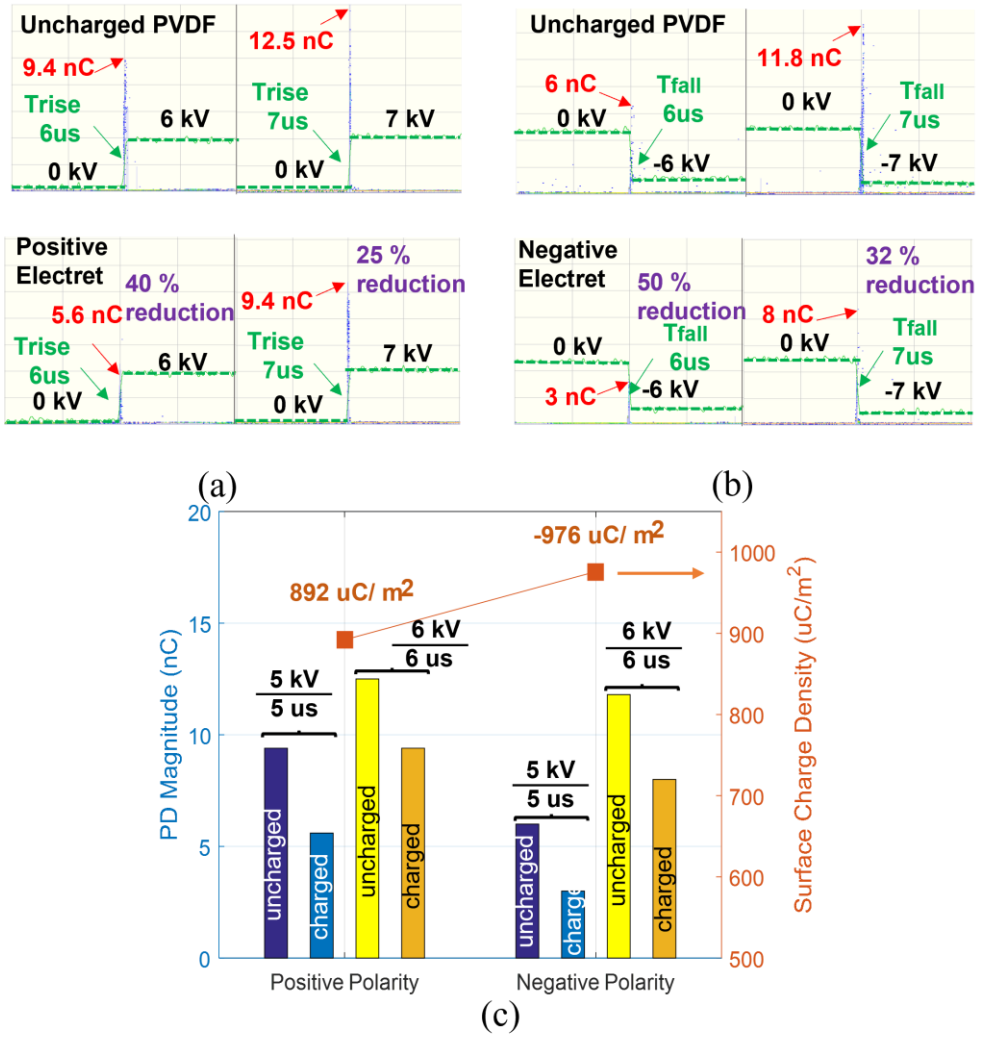

Figure 4.6 Comparison of cavity discharge mitigation performance of electrets charged under different charging polarity. (a) comparing PD magnitudes with uncharged PVDF and positively charged electret, (b) comparing PD magnitudes with uncharged PVDF and negatively charged electret, (c) comparing surface charge density and PD mitigation performance of positively charged electret and negatively charged electret.

4.5 Charging temperature

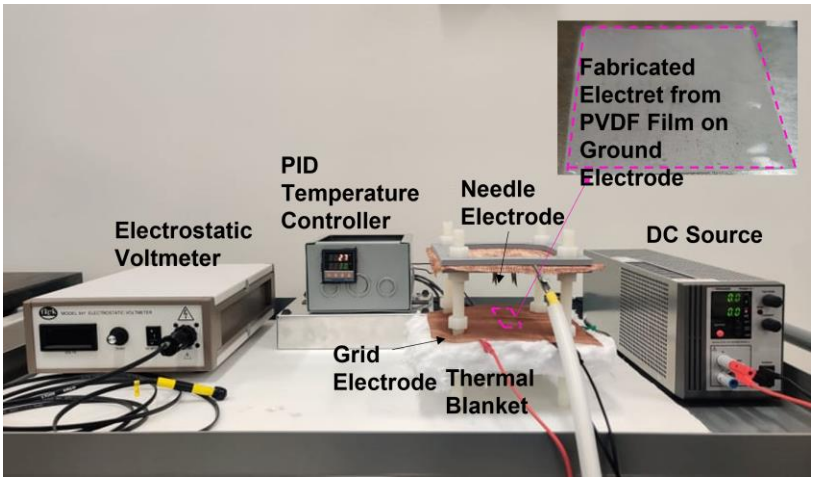

Figure 4.7 Experimental setup used for fabrication of electret at elevated temperatures.

When dielectric films are charged at elevated temperature, charged particles to penetrate into deeper traps that provides higher stability for electrets [70]. In this section, the surface and cavity discharge mitigation performance of electrets prepared at various elevated temperature is reported. For this purpose, the testbed used for electret fabrication is modified slightly. A flat electrically grounded aluminum plate is placed on top of an induction heater of 2”x2” dimension. The induction heater is controlled by a PID controller. The experimental setup used for charging the electret films at elevated temperatures is shown in Figure 4.7. A k-type thermocouple is attached to the ground electrode for the temperature reading as shown in Figure 4.7. PVDF films are attached to the ground plate using polyimide (Kapton) tape so that they are placed flat on the hot plate. For the study, PVDF electret films were fabricated at 30 ^{o}C, 60 ^{o}C, 90 ^{o}C, and 120 ^{o}C. It

should be noted that the PVDF films deformed substantially at temperatures above 130 ^{o}C. For this reason, temperature above 120 ^{o}C is not used for electret fabrication. Electrets charged at 30 ^{o}C were charged for 25 minutes. However, the electrets fabricated at temperature above 30 ^{o}C, the PVDF films were charged at the respective temperatures (60 ^{o}C, 90 ^{o}C, and 120 ^{o}C) for 10 minutes and charged at 30 ^{o}C for the remaining 15 minutes. This procedure allows to maintain the charging process until the PVDF films are completely cooled and ensures charged particles to be embedded firmly into dielectric films. The charging procedure described above is summarized in Figure 4.8 and Table 4.4.

4.5.1 Surface discharge

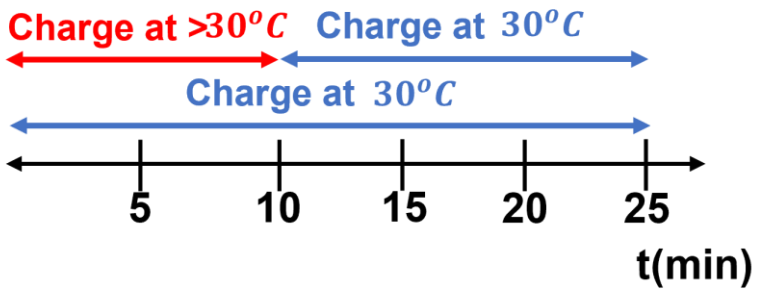

Figure 4.8 Charging conditions.

Table 4.4 Electret fabrication under various charging temperatures

Needle Voltage (kV DC)	Grid Voltage (V DC)	Charging Duration (minutes)	Charging Temperature (^oC)
20	600	20	30
			60
			90
			120

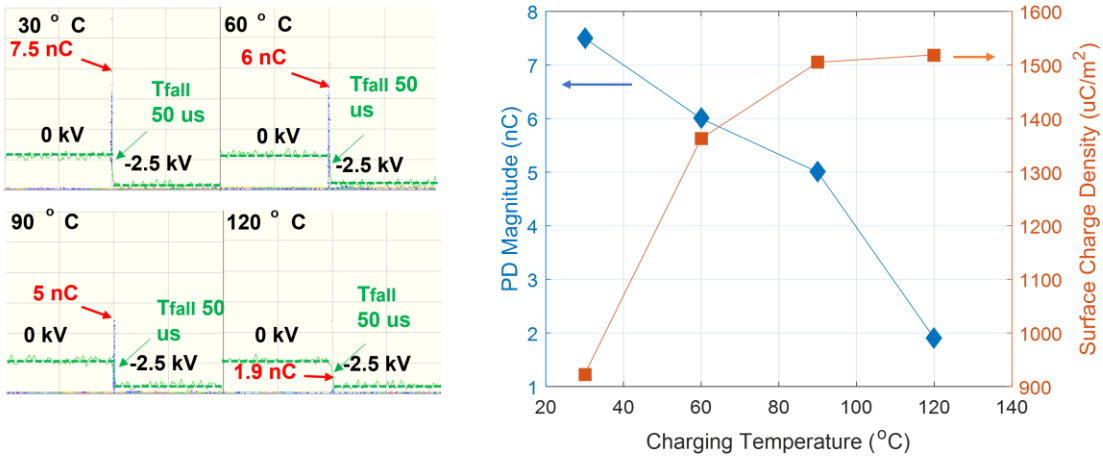

Figure 4.9 Impact of charging temperature in mitigating surface discharge. PD signals measured with electrets prepared under various charging temperature (30 ^oC, 60 ^oC, 90 ^oC, and 120 ^oC). (a) Surface discharge measured under square voltage varying from 0 to -2.5 V with 50 µs fall time, (b) summary of PD magnitude and electret surface charge density as a function of charging temperature.

Figure 4.9 (a) shows the effect of charging temperature on electret surface charge density and their performance in mitigating surface discharge caused by the presence of triple points. Figure 4.9 (a) shows that electrets fabricated at higher temperature has comparatively low PD magnitudes caused by surface discharge. Figure 4.9 (b) shows that the surface charge density of electret increases with increasing temperature. Electrets prepared at 120 ^oC showed surface charge

density higher that 1500 μC/m^2 and comparatively low PD magnitude of 1.9 nC. The figure also shows that the rate of increase in surface charge density decreases with increasing temperature, which indicates that there is a limit to which charging temperatures alone can enhance the surface charge density of electrets.

4.5.2 Cavity discharge

The performance of electrets fabricated at various temperature in mitigating cavity discharge is shown in Figure 4.10 (a). The figure shows that PD magnitudes reduce significantly with electrets fabricated at 120 ^{o}C. The reduction in PD magnitude is achieved due to the high surface charge density and increased surface charge stability of electrets fabricated at a high temperature. The surface charge density of electrets achieved at various charging temperatures is plotted with corresponding PD magnitudes in Figure 4.10 (b). When electrets are charged at high temperature, charge particles penetrate into deeper energy traps and consequently achieve increased surface charge stability.

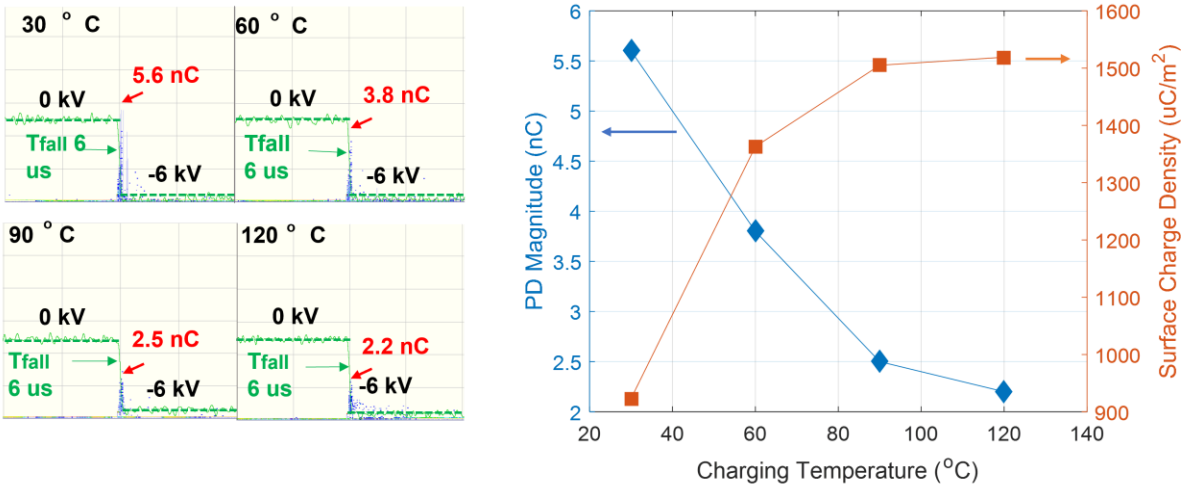

(a) (b)

Figure 4.10 Impact of charging temperature in mitigating cavity discharge. PD signals measured with electrets prepared under various charging temperature (30 ºC, 60 ºC, 90 ºC, and 120 ºC). (a) Cavity discharge measured under square voltage varying from 0 to -2.5 V with 50 µs fall time, (b) summary of PD magnitude and electret surface charge density as a function of charging temperature.

4.6 Discussion

4.6.1 Surface charge density

The charging voltage, i.e., the grid voltage is one of the factors that affects surface charge density. As shown in Figure 4.1(b) and Figure 4.2(b), the surface charge density of electrets increases with charging voltage. The electric field between the grid electrode and the base electret material increases when the grid voltage increases. This allows charged particles to gain more kinetic energy and charged particles embedded in the deeper traps of the base electret materials. Consequently, higher surface charge density is achieved with more charged particles and this neutralizes the harmful local electric field formed at triple points and in the cavities more effectively. Due to the neutralization of the harmful fields achieved with high surface charge density, PD caused by triple points and cavities decreased with increasing charging voltage.

Another factor that has impact on the surface charge density is charging duration. As shown in Figure 4.3(b) and Figure 4.4(b), the surface charge density of electrets increases as charging duration increases. A significant trend in these figures is that both surface discharge and cavity discharge magnitude initially drop as the charging duration increases but increase as the charging duration exceeds 20 minutes mark. This trend implies that although the surface charge density increases, the charge stability is not achieved with increasing charging duration.

Furthermore, Figure 4.5 and Figure 4.6 show that charging polarity has an impact on surface charge density. Under the same conditions of charging voltage magnitude, charging duration, and charging temperature, the surface charge density is higher when electrets are fabricated with negative voltage polarity than those made with positive polarity. This is mainly because electrons gain much higher kinetic energy under a given electric field owing to its higher drift velocity than positive ions. The highly energized electron can more effectively penetrate into the deep traps of the base electret material resulting in higher surface charge density. The results suggest that distinct charging conditions should be applied to fabricate positive electrets that have the same degree of surface density as the negative counterpart.

4.6.2 Surface charge stability

In Figure 4.3(b) and Figure 4.4(b), it is observed that the surface charge density increases as the charging duration increases. It is also noted that, the PD magnitude shows a downward trend up to the charging duration 20 minutes. Beyond 20 minutes charging duration, there is an increasing trend showed by the PD magnitude as the charging duration increases. This increasing trend of PD magnitudes beyond 20 minutes mark suggests that the lack of surface charge stability. It implies that there is a limit to which the ionized particles are able to stably penetrate into the PVDF based electret films when the charging duration is simply extended. The unstable charged

particles eject out from the electret film when stressed under square voltage stimuli and are measured in terms of increasing PD.

The surface charge stability can further be explained by comparing Figure 4.3, Figure 4.4, Figure 4.9, and Figure 4.10. According to Figure 4.9(b) and Figure 4.10(b), it is observed that as the charging temperature increases the surface charge density increases and reaches to 1500 $\mu C/m^2$ and both surface discharge and cavity discharge decreases. The fact that both discharges continue to decrease even though the surface charge density exceeds 1000 $\mu C/m^2$ that is the inflection point shown in Figure 4.3(b) and Figure 4.4(b). This confirms that the excessive surface charge density showed by the electrets fabricated at increased charging duration in not cause of the increasing PD trend in Figure 4.3(b) and Figure 4.4(b). Studies have shown that charged particles tend to fill in deeper traps of dielectric materials when charged at elevated temperatures [70]. As charged particles are able to penetrate into deep energy levels, charge stability increases at elevated temperatures. Therefore, it is clear that when electrets are fabricated at elevated temperature both high surface charge density and high stability can be achieved.

Figure 4.11shows the temporal evolution of electret surface charge density both without and with exposure to PD. The surface charge density of four electrets is plotted as a function time. To observe the effect of elevated temperature in surface charge stability, two electrets are fabricated at 120 ^oC and the other two were fabricated at 30 ^oC. Of the two sets of electrets fabricated at different charging temperatures, one of them was exposed to high power electronics voltage with maximum magnitude 8.6 kV and rise time 10 μs that caused PD over the duration of experiment while the other one was not applied with any voltage stress. Surface charge density and PD magnitudes are measured in every five minutes throughout the experiments and plotted in Figure 4.11. It is observed in the figure that, surface charge density of electrets fabricated at 120

^{o}C is significantly higher than the electrets fabricated at the room temperature. Furthermore, PD magnitudes are comparatively low in the case of electrets fabricated at elevated temperature. In case of electrets those fabricated at 120 ^{o}C, exposure to PD seems to have no significant impact on the degradation of surface charge density with time. However, it is observed from the figure that with the exposure to PD, electret fabricated at 30 ^{o}C shows a notable decrease in the surface charge density at 25 minutes. This implies that exposure to PD accelerates the degradation of surface charge density when fabricated at room temperature. It is also observed that for all the four cases, the surface charge density initially reduced but stabilized after 40 minutes.

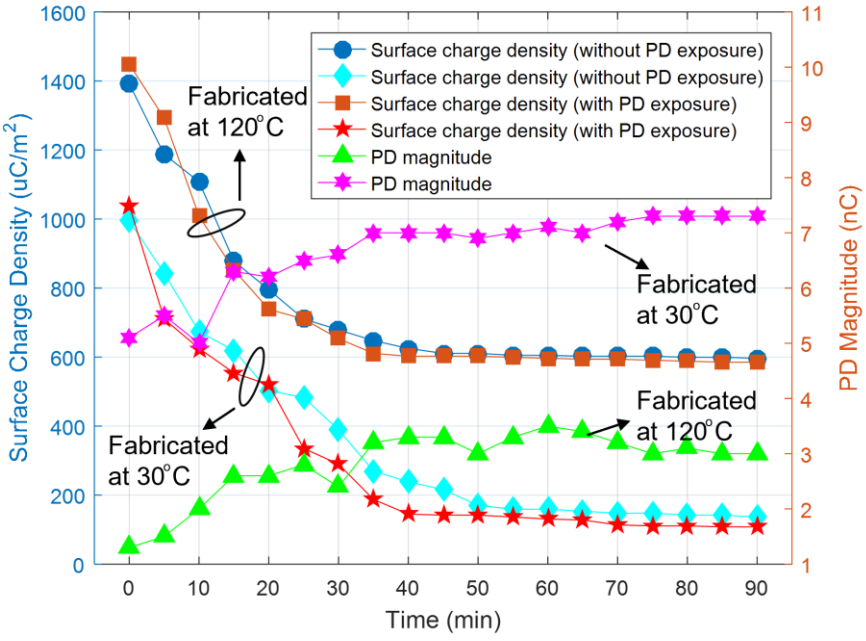

Figure 4.11 Temporal evolution of electret surface charge density and corresponding PD magnitudes.

4.7 Summary

In this section, electrets are fabricated with thin PVDF films under various charging conditions including charging voltage, charging duration, charging polarity, and charging temperature to elucidate their effects on the surface charge density, charge stability, and PD mitigation performance of electrets. To assess the PD mitigation performance, two types PD were considered; surface discharge and cavity discharge. It is experimentally demonstrated that electret those fabricated under negative polarity and at elevated temperature show better performance in terms of surface charge density, charge stability, and PD mitigation. It is also observed that with high surface charge density, increased charge stability is required for the electret-based PD solution to be useful. The findings of this study serve as useful indicators that point out to the next steps required in this research efforts.

CHAPTER V

ELECTRET PERFORMANCE IN POWER ELECTRONICS DRIVEN SYSTEMS

5.1 Motivation

The electrification of transport including electric vehicle, ship, and aircraft is progressing with the technological advancements in power electronics. The fast-switching frequency, high voltage blocking capacity, and high efficiency provided by power electronic driven systems enable designs with high gravimetric and volumetric power density. However, local electric field enhancements occur with the increasing power density, and the PWM voltage stresses increase the risk of PD, which accelerates dielectric material aging and increases the risk of device failure. In electric vehicles, electric motors are fed by PWM inverters that generates high *dV/dt* voltage pulses, which cause large voltage difference between the turns of motor winding and overvoltage at the terminals of electric motors. These lead to increased electric stress in the insulation system and cause PD in the winding. There are various parameters including, rising time, duty cycle, switching frequency, and voltage polarity associated with the study of PD in power electronic driven systems. In this section, the impact of these voltage parameters on PD and the effectiveness of electrets in mitigating PD is discussed. In this section, electrets are fabricated based on the optimum charging condition discussed in the previous section. For each of the parameter, surface discharge and cavity discharge experiments are conducted, and electrets-based PD solution is applied.

5.2 Impact of *dV/dt*

PD experiments with and without electrets are conducted at various rise time varying from 10 µs to 90 µs and a constant voltage level (4 kV_{pp} for surface discharge and 9.6 kV_{pp} for cavity discharge) to analyze the electret-based PD mitigation performance for various *dV/dt*. In this section, electrets are fabricated from the PVDF film under the optimum charging conditions described in the previous section. Both positive polarity electret and negative polarity electret are utilized for the experiments to evaluate their PD mitigation performance at various *dV/dt* under various voltage polarity stress, i.e., positive, negative, and bipolar voltage stress.

5.2.1 Surface discharge

Surface discharge experiments are conducted with same testbed as described in Chapter V in Figure 3.3. Both positive and negative polarity electrets are fabricated, and their PD mitigation performance is compared with the uncharged PVDF films. The *dV/dt* is varied from 40 V/µs to 400 V/µs by varying the rise time from 10 µs to 90 µs with a step of 20 µs and keeping the square voltage magnitude at 4 kV_{pp}. To observe the performance of electret under various voltage polarity stress, both positive polarity and negative polarity electrets are stressed under positive, negative, and bipolar voltage stresses.

5.2.1.1 Positive polarity electret

In this case, electrets are fabricated based on the triode corona charging method with PVDF film of thickness 25.4 µm. For fabricating electrets, the charging conditions maintained are described in the Table 5.1. PD magnitude and repetition achieved with both uncharged PVDF and electrets are compared under various voltage polarity stress.

Table 5.1 Electret Charging Conditions

Needle Voltage	20 kV
Grid Voltage	600 V
Charging Polarity	+ ve
Charging Temperature	120 ^{o}C

a) Positive polarity stress

An uncharged PVDF and positively charged electret are stressed under positive polarity square voltage stimuli with magnitude varying between 0 to 4 kV at distinct *dV/dt*. Figure 5.1shows the PD achieved with uncharged PVDF (Figure 7.1 (a)) and electret (Figure 5.1 (b)) where the square voltage has the rise time of 50 µs and duty cycle of 90 %. To evaluate electrets performance, both maximum PD magnitudes and repetition rate with PVDF and electret are compared. Figure 5.2 (a) compares the maximum PD magnitudes and Figure 5.2 (b) compares the PD repetition rate per cycle with PVDF and electrets at distinct *dV/dt*. It is observed in Figure 5.1 that there is a substantial reduction in the PD magnitude as well as PD occurrence when PDVF is replaced with positive polarity electret when positive polarity voltage is applied. Figure 5.2 shows that as the *dV/dt* increases, both PD magnitude and repetition rate show increasing trend. This phenomenon is previously recognized in [47], [71]–[73] that as the *dV/dt* increases, dielectric materials are more stressed and their life time decreases. In Figure 5.2, it is observed that although PD magnitude and repletion rate increases as *dV/dt* increases with uncharged PVDF film, when replacing with the electret fabricated under an optimum condition described in Table 5.1, there is a significant reduction in the PD magnitude as well as in the repetition rate per cycle.

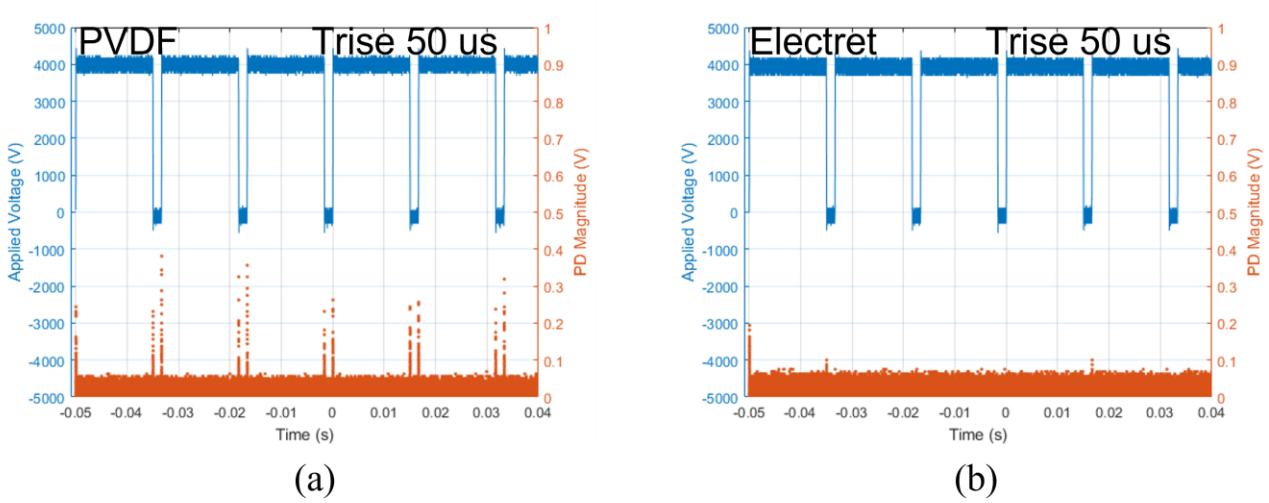

Figure 5.1 PD signal caused by surface discharge under square voltage stimuli with magnitude 4 kV_{pp}, rise time 50 µs, and duty cycle 90 %. (a) Uncharged PVDF, (b) Positive polarity electret

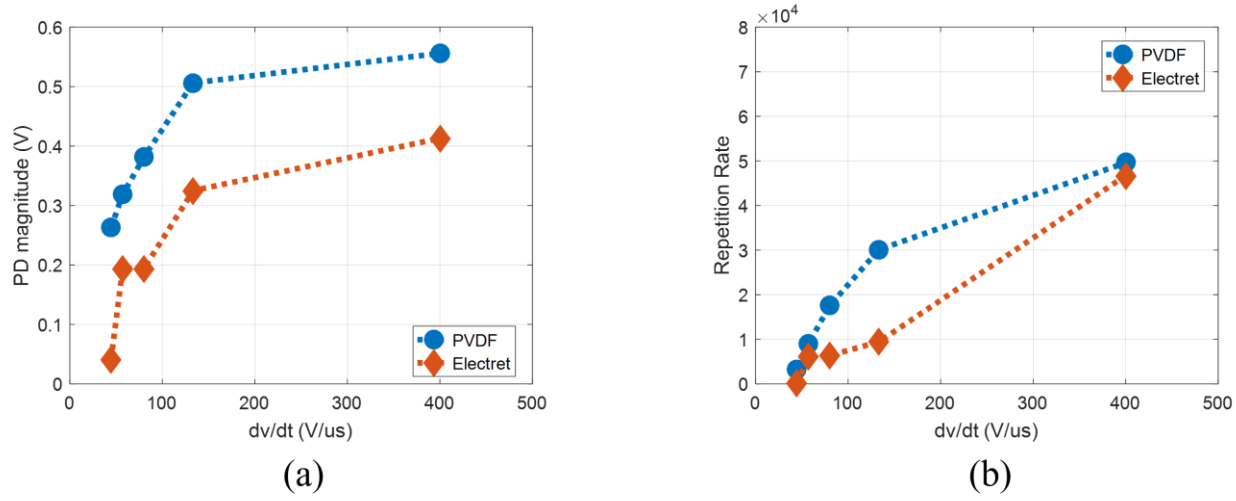

Figure 5.2 Comparison of surface discharge performance of uncharged PVDF and positively charged electret at various *dVdt* under positive voltage. (a) Maximum PD magnitude, (b) Repetition rate.

b) Negative polarity stress

An uncharged PVDF and positively charged electret are stressed under negative polarity square voltage stimuli with magnitude varying between 0 to -4 kV at distinct *dV/dt.* Figure 5.3 shows the PD discharge achieved with uncharged PVDF (Figure 5.3 (a)) and electret (Figure 5.3 (b)) where the square voltage has the rise time of 50 µs and duty cycle of 90 %. To evaluate electrets performance, both maximum PD magnitudes and repetition rate with PVDF and electret are compared. Figure 5.4 (a) compares the maximum PD magnitudes and Figure 5.4 (b) compares the PD repetition rate per cycle with PVDF and electrets at different *dV/dt*. It is observed in Figure 5.3 that, there is a noteworthy increase in the PD magnitude as well as PD occurrence when PDVF is replaced with positive polarity electret when negative polarity voltage is applied. In Figure 5.4, it is observed that although PD magnitude and repletion rate increases as *dV/dt* increases with uncharged PVDF film, when replacing with the electret fabricated under an optimum condition described in Table 5.1, there is a significant increase in the PD magnitude as well as in the repetition rate per cycle. These implies that under negative voltage stress, positive polarity electret is unable to mitigate PD and increases the dielectric risk.

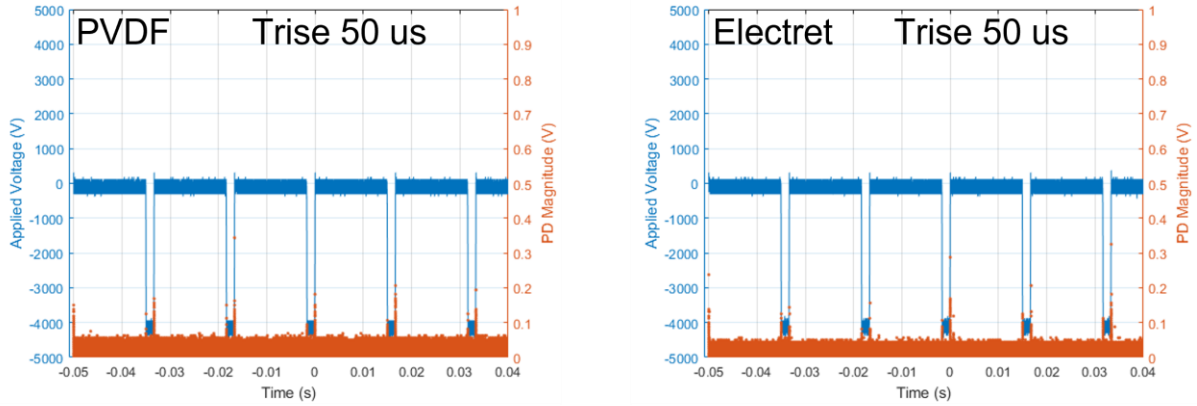

Figure 5.3 PD signal caused by surface discharge under square voltage stimuli with magnitude - 4 kV_{pp}, rise time 50 µs, and duty cycle 90 %. (a) Uncharged PVDF, (b) Positive polarity electret

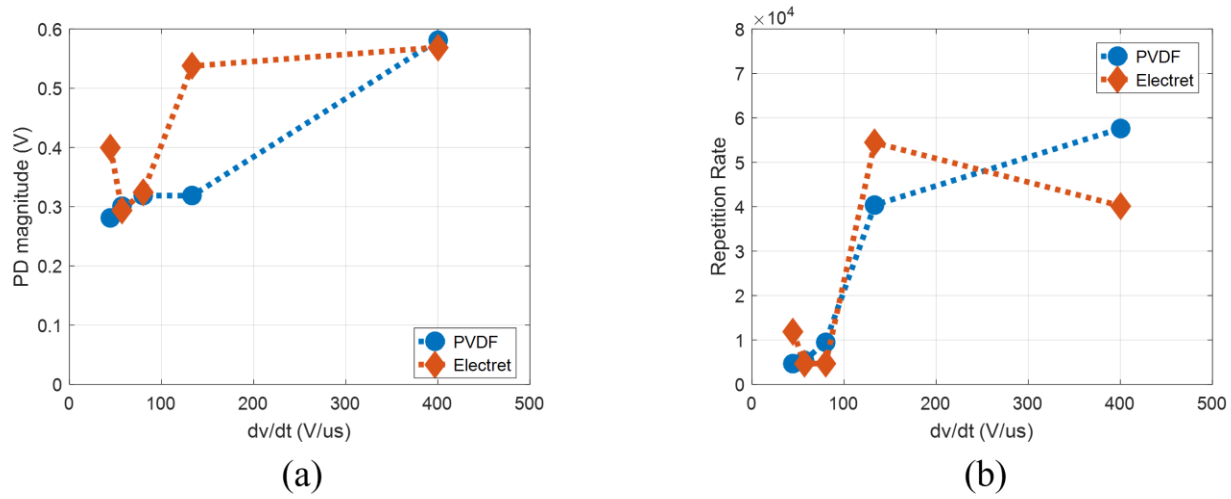

Figure 5.4 Comparison of surface discharge performance of uncharged PVDF and positively charged electret at various *dVdt* under negative voltage. (a) Maximum PD magnitude, (b) Repetition rate.

c) Bipolar stress

An uncharged PVDF and positively charged electret are stressed under bipolar square voltage stimuli with magnitude varying between -2 kV to 2 kV at distinct *dV/dt.* Figure 5.5 shows the PD discharge achieved with uncharged PVDF (Figure 5.5 (a)) and electret (Figure 5.5 (b)) where the square voltage has the rise time of 50 μs and duty cycle of 90 %. To evaluate electrets performance, both maximum PD magnitudes and repetition rate with PVDF and electret are compared. Figure 5.6 (a) compares the maximum PD magnitudes, and Figure 5.6 (b) compares the PD repetition rate per cycle with PVDF and electrets at distinct *dV/dt*. It is observed in Figure 5.5 that, there is a noteworthy increase in the PD magnitude as well as PD occurrence when PDVF is replaced with positive polarity electret when bipolar voltage is applied. In Figure 5.6, it is observed that although PD magnitude and repletion rate increases as *dV/dt* increases with uncharged PVDF film, when replacing with the electret fabricated under an optimum condition described in Table 5.1, there is a significant increase in the PD magnitude as well as in the repetition rate per cycle. These results imply that under bipolar voltage stress, positive polarity electret is unable to mitigate PD and increases the dielectric risk.

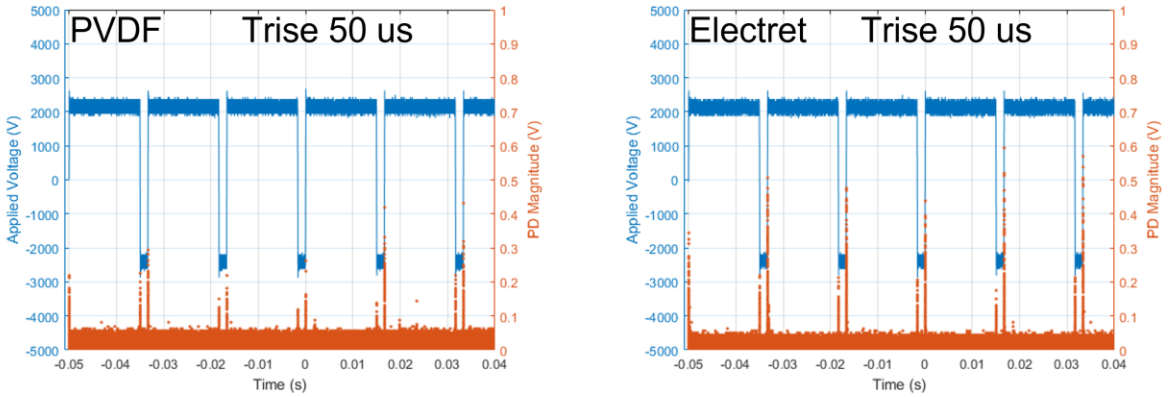

(a) (b)

Figure 5.5 PD signal caused by surface discharge under square voltage stimuli with magnitude 4 kV_{pp} (bipolar), rise time 50 µs, and duty cycle 90 %. (a) Uncharged PVDF, (b) Positive polarity electret

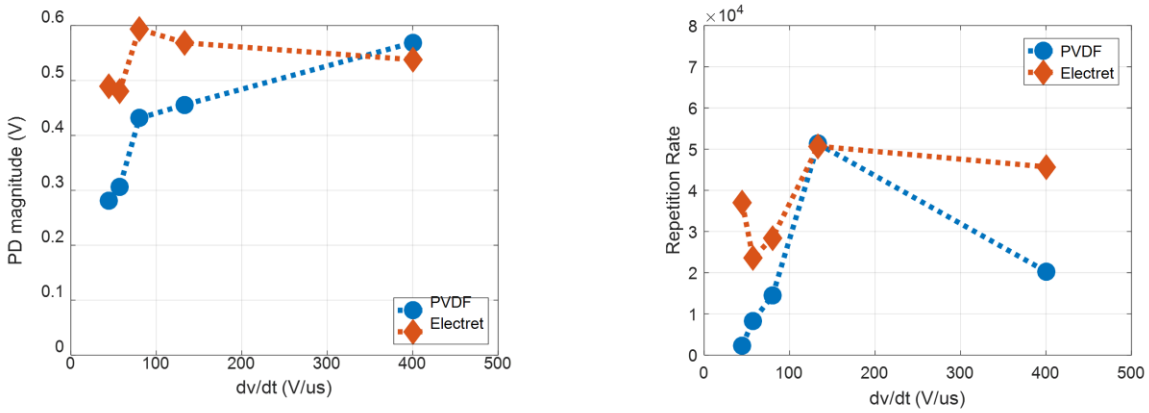

(a) (b)

Figure 5.6 Comparison of surface discharge performance of uncharged PVDF and positively charged electret at various *dVdt* under bipolar voltage. (a) Maximum PD magnitude, (b) Repetition rate.

5.2.1.2 Negative polarity electret

In this case, electrets are fabricated based on the triode corona charging method with PVDF film of thickness 25.4 µm. For fabricating electrets, the charging conditions maintained are described in the Table 5.2. PD magnitude and repetition achieved with both uncharged PVDF and electrets are compared under various voltage polarity stresses.

Table 5.2 Electret fabrication conditions

Needle Voltage	20 kV
Grid Voltage	600 V
Charging Polarity	- ve
Charging Temperature	120 ^{o}C

a) Positive polarity stress

An uncharged PVDF and negatively charged electret are stressed under positive polarity square voltage stimuli with magnitude varying between 0 to 4 kV at distinct *dV/dt.* Figure 5.7 shows the PD achieved with uncharged PVDF (Figure 5.7 (a)) and electret (Figure 5.7 (b)) where the square voltage has the rise time of 50 µs and duty cycle of 90 %. To evaluate electrets performance, both maximum PD magnitudes and repetition rate with PVDF and electret are compared. Figure 5.8(a) compares the maximum PD magnitudes and Figure 5.8(b) compares the PD repetition rate per cycle with PVDF and electrets at different *dV/dt*. It is observed in Figure 5.8 that there is a noteworthy increase in the PD magnitude as well as PD occurrence when PDVF is replaced with negative polarity electret when positive polarity voltage is applied. In Figure 5.8, it is observed that although PD magnitude and repletion rate increases as *dV/dt* increases with uncharged PVDF film, when replacing with the electret fabricated under an optimum condition

described in Table 5.2, there is a significant increase in the PD magnitude as well as in the repetition rate per cycle. These implies that under positive voltage stress, negative polarity electret is unable to mitigate PD and increases the dielectric risk.

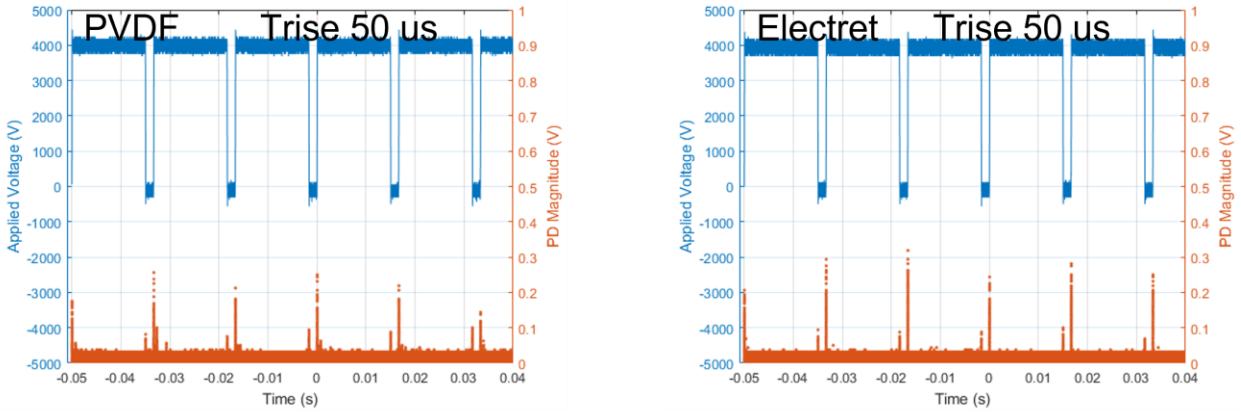

(a) (b)

Figure 5.7 PD signal caused by surface discharge under square voltage stimuli with magnitude 4 kV_{pp}, rise time 50 µs, and duty cycle 90 %. (a) Uncharged PVDF, (b) Negative polarity electret

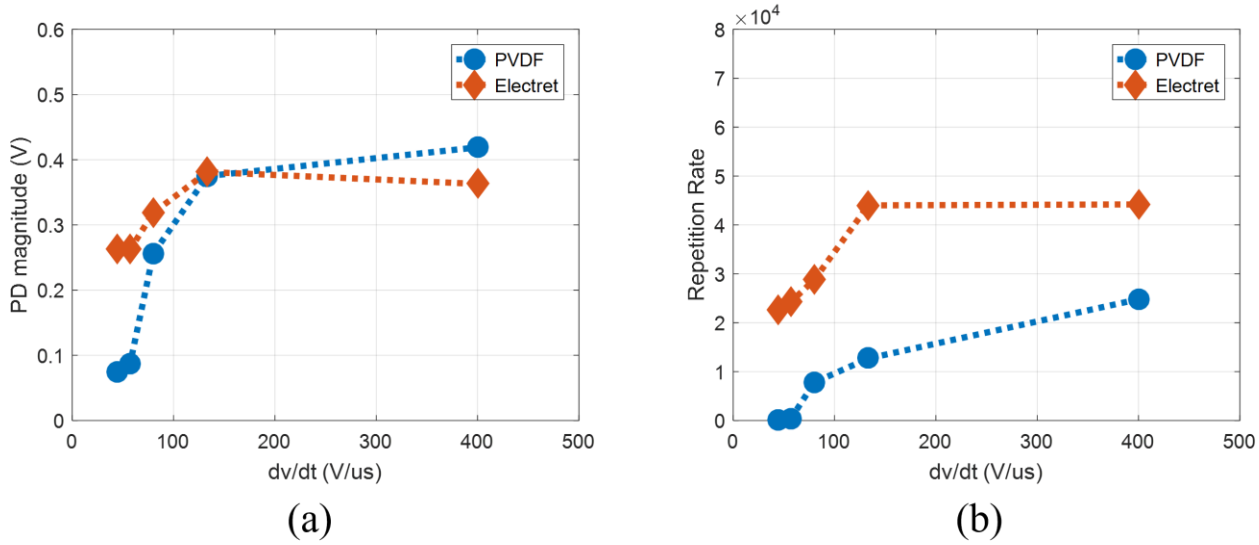

Figure 5.8 Comparison of surface discharge performance of uncharged PVDF and negatively charged electret at various *dVdt* under positive voltage. (a) Maximum PD magnitude, (b) Repetition rate

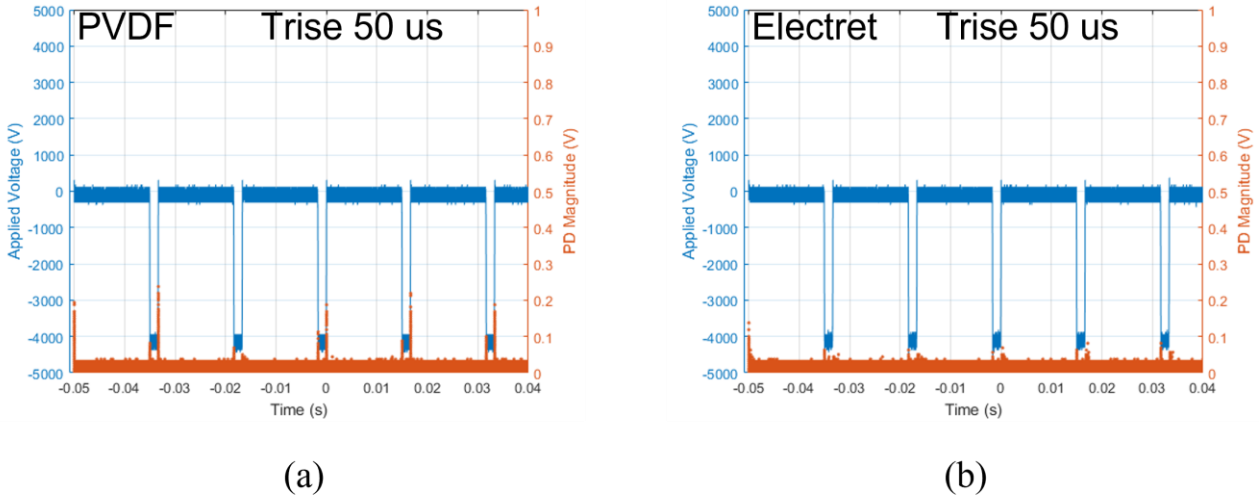

Figure 5.9 PD signal caused by surface discharge under square voltage stimuli with magnitude -4 kV_{pp}, rise time 50 µs, and duty cycle 90 %. (a) Uncharged PVDF, (b) Negative polarity electret

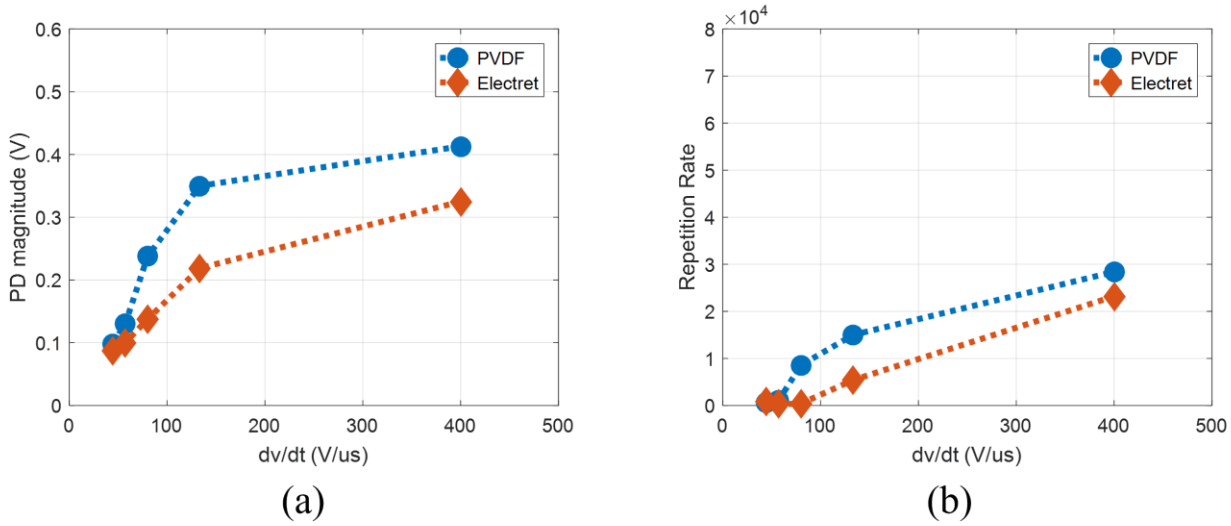

Figure 5.10 Comparison of surface discharge performance of uncharged PVDF and negatively charged electret at various *dVdt* under negative voltage. (a) Maximum PD magnitude, (b) Repetition rate

b) Negative polarity stress

An uncharged PVDF and negatively charged electret are stressed under negative polarity square voltage stimuli with magnitude varying between 0 to -4 kV at distinct *dV/dt*. Figure 5.9 shows the PD discharge achieved with uncharged PVDF (Figure 5.9(a)) and electret (Figure 5.9(b)) where the square voltage has the rise time of 50 µs and duty cycle of 90 %. To evaluate electrets performance, both maximum PD magnitudes and repetition rate with PVDF and electret are compared. Figure 5.10(a) compares the maximum PD magnitudes and Figure 5.10(b) compares the PD repetition rate per cycle with PVDF and electrets at distinct *dV/dt*. It is observed in Figure 5.9 that, there is a substantial reduction in the PD magnitude as well as PD occurrence when PDVF is replaced with negative polarity electret when negative polarity voltage is applied. Figure 5.10 shows that as the *dV/dt* increases, both PD magnitudes and repetition rate show increasing trend. This phenomenon is previously recognized in the literature that as the *dV/dt* increases, dielectric

materials are more stressed and their life time decreases. In Figure 5.10, it is observed that although PD magnitude and repletion rate increases as *dV/dt* increases with uncharged PVDF film, when replacing with the electret fabricated under an optimum condition described in Table 5.2, there is a significant reduction in the PD magnitude as well as in the repetition rate per cycle.

c) Bipolar stress

An uncharged PVDF and negatively charged electret are stressed under bipolar square voltage stimuli with magnitude varying between -2 kV to -2 kV at distinct *dV/dt.* Figure 5.11shows the PD discharge achieved with uncharged PVDF (Figure 5.11 (a)) and electret (Figure 5.11(b)) where the square voltage has the rise time of 50 µs and duty cycle of 90 %. To evaluate electrets performance, both maximum PD magnitudes and repetition rate with PVDF and electret are compared. Figure 5.12(a) compares the maximum PD magnitudes and Figure 5.12(b) compares the PD repetition rate per cycle with PVDF and electrets at distinct *dV/dt*. It is observed in Figure 5.11 that, there is a noteworthy increase in the PD magnitude as well as PD occurrence when PDVF is replaced with negative polarity electret when bipolar voltage is applied. In Figure 5.12, it is observed that although PD magnitude and repletion rate increases as *dV/dt* increases with uncharged PVDF film, when replacing with the electret fabricated under an optimum condition described in Figure 5.12, there is a significant increase in the PD magnitude as well as in the repetition rate per cycle. These implies that under bipolar voltage stress, negative polarity electret is unable to mitigate PD and increases the dielectric risk.

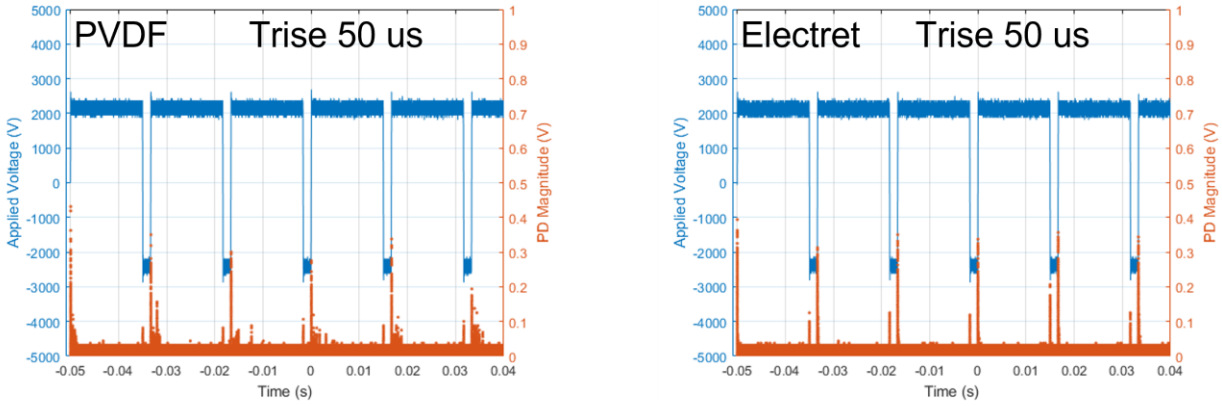

Figure 5.11 PD signal caused by surface discharge under square voltage stimuli with magnitude 4 kV_{pp} (bipolar), rise time 50 µs, and duty cycle 90 %. (a) Uncharged PVDF, (b) Negative polarity electret

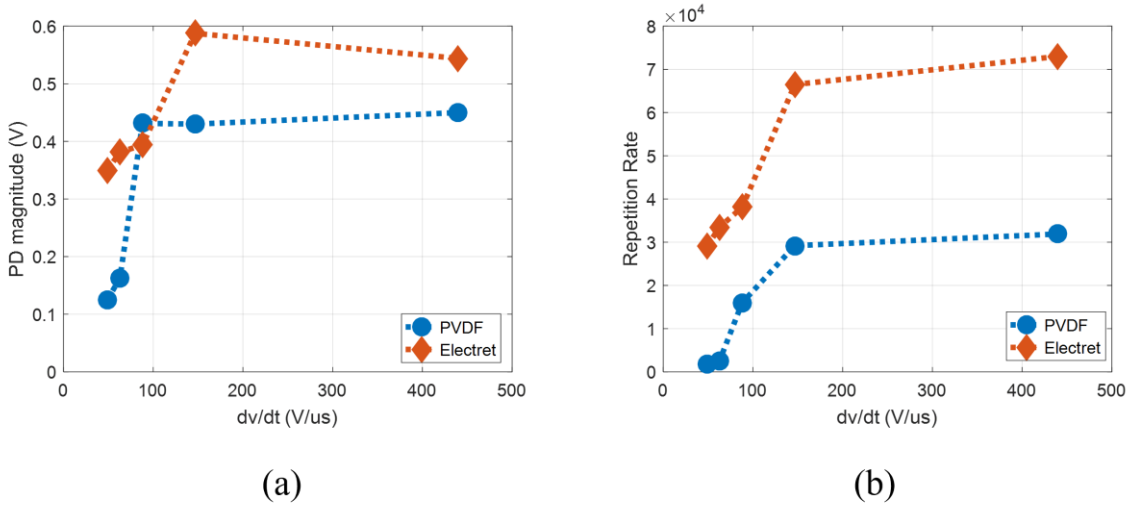

Figure 5.12 Comparison of surface discharge performance of uncharged PVDF and negatively charged electret at various *dVdt* under bipolar voltage. (a) Maximum PD magnitude, (b) Repetition rate.

5.2.2 Cavity discharge

Cavity discharge experiments are conducted with same testbed as described in Chapter V in Figure 3.5. In this case, the solid 3D printed insulator has thickness 2 mm and 20% infill density. Both positive and negative polarity electrets are fabricated, and their PD mitigation performance is compared with the uncharged PVDF films. The *dV/dt* is varied from 100 V/µs to 1000 V/µs by varying the rise time from 10 µs to 90 µs with a step of 20 µs and keeping the square voltage magnitude at 9.6 kV_{pp}. To observe the performance of electret under various voltage polarity stress, both positive polarity and negative polarity electrets are stressed under positive, negative, and bipolar voltage stress.

5.2.2.1 Positive polarity electret

In this case, electrets are fabricated based on the triode corona charging method with PVDF film of thickness 25.4 µm. For fabricating electrets, the charging conditions maintained are described in the Table 5.1. PD magnitude and repetition achieved with both uncharged PVDF and electrets are compared under various voltage polarity stress.

a) Positive polarity stress

An uncharged PVDF and positively charged electret are stressed under positive polarity square voltage stimuli with magnitude varying between 0 to 9.6 kV at different *dV/dt.* Figure 5.13 shows the PD achieved with uncharged PVDF (Figure 5.13 (a)) and electret (Figure 5.13 (b)) where the square voltage has the rise time of 50 µs and duty cycle of 10 %. To evaluate electrets performance, both maximum PD magnitudes and repetition rate with PVDF and electret are compared. Figure 5.14 (a) compares the maximum PD magnitudes and Figure 5.14 (b) compares the PD repetition rate per cycle with PVDF and electrets at different *dV/dt*. It is observed in Figure

5.13 that, there is a substantial reduction in the PD magnitude as well as PD occurrence when PDVF is replaced with positive polarity electret when positive polarity voltage is applied. Figure 5.14 shows that as the *dV/dt* increases, both PD magnitudes and repetition rate shows increasing trend. In Figure 5.14, it is observed that although PD magnitude and repletion rate increases as *dV/dt* increases with uncharged PVDF film, when replacing with the electret fabricated under an optimum condition described in Table 5.1, there is a significant reduction in the PD magnitude as well as in the repetition rate per cycle.

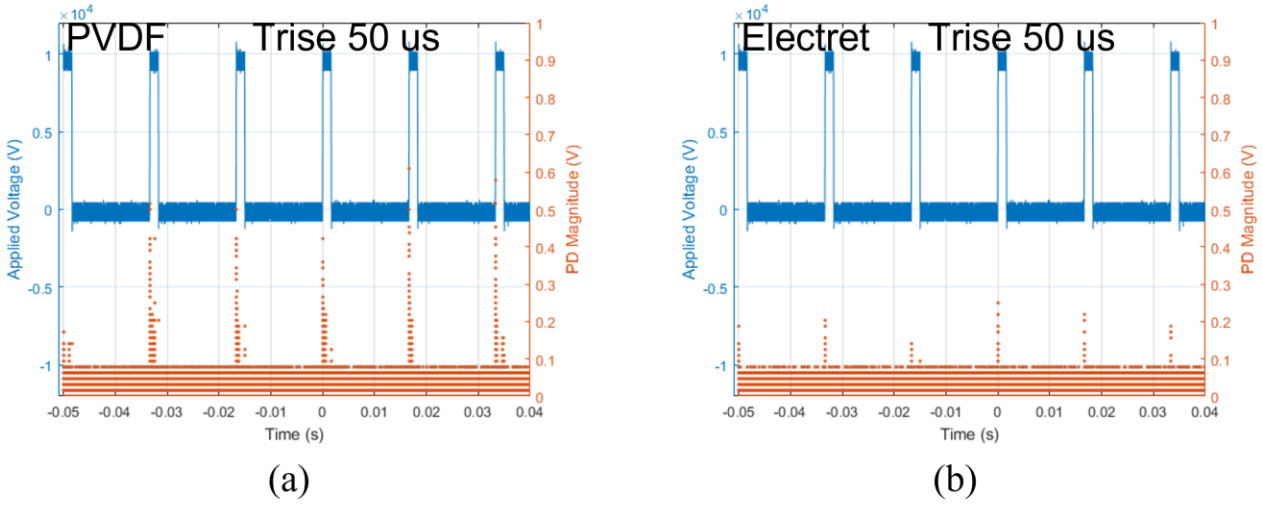

Figure 5.13 PD signal caused by cavity discharge under square voltage stimuli with magnitude 9.6 kV_{pp}, rise time 50 µs, and duty cycle 10 %. (a) Uncharged PVDF, (b) Positive polarity electret

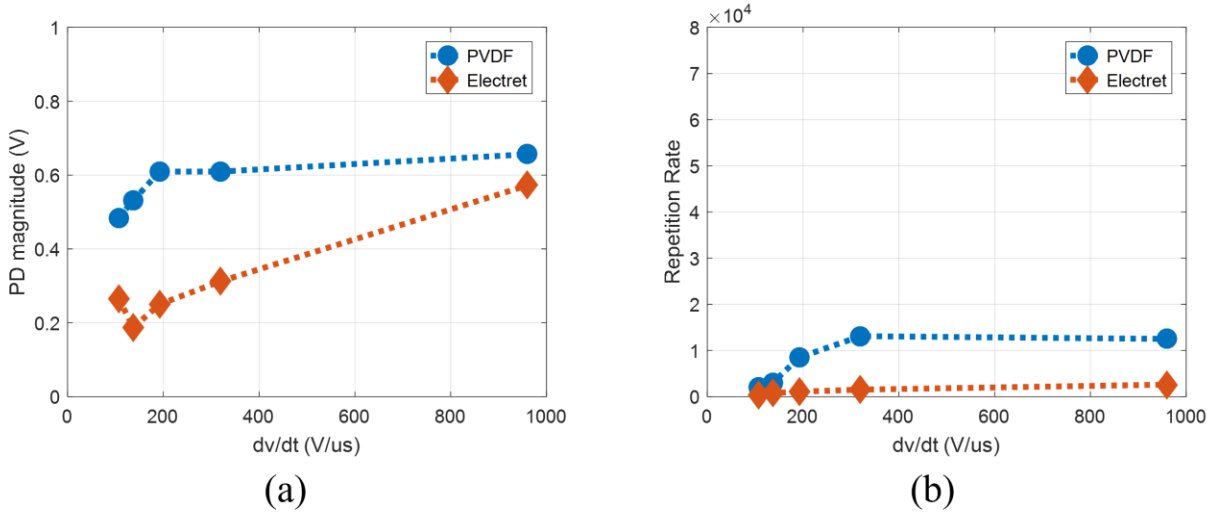

Figure 5.14 Comparison of cavity discharge performance of uncharged PVDF and positively charged electret at various *dVdt* under positive voltage. (a) Maximum PD magnitude, (b) Repetition rate.

b) Negative polarity stress

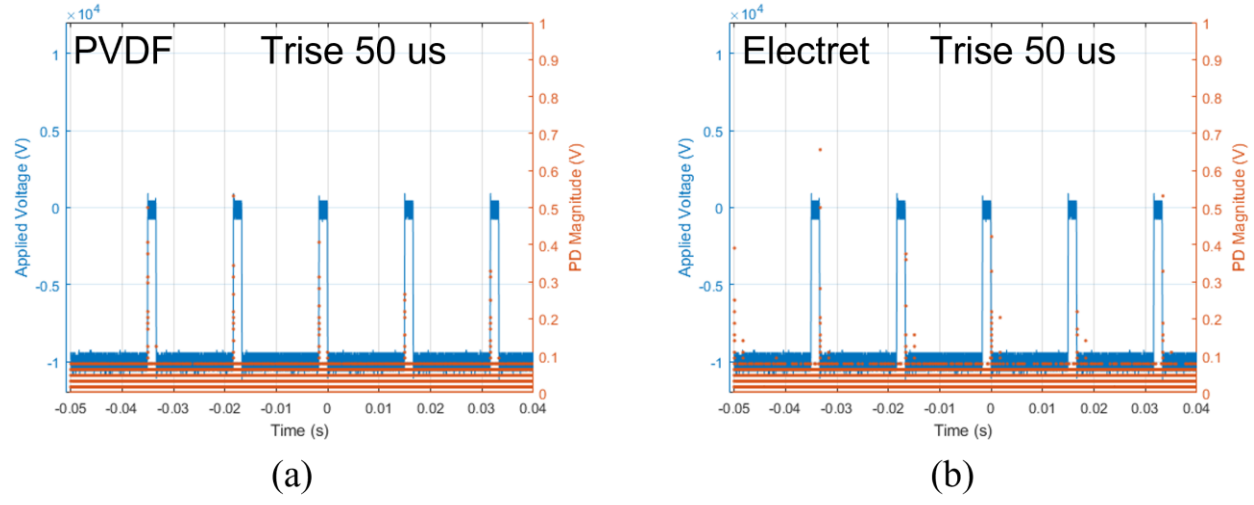

Figure 5.15 PD signal caused by cavity discharge under square voltage stimuli with magnitude -9.6 kV_{pp}, rise time 50 µs, and duty cycle 10 %. (a) Uncharged PVDF, (b) Positive polarity electret

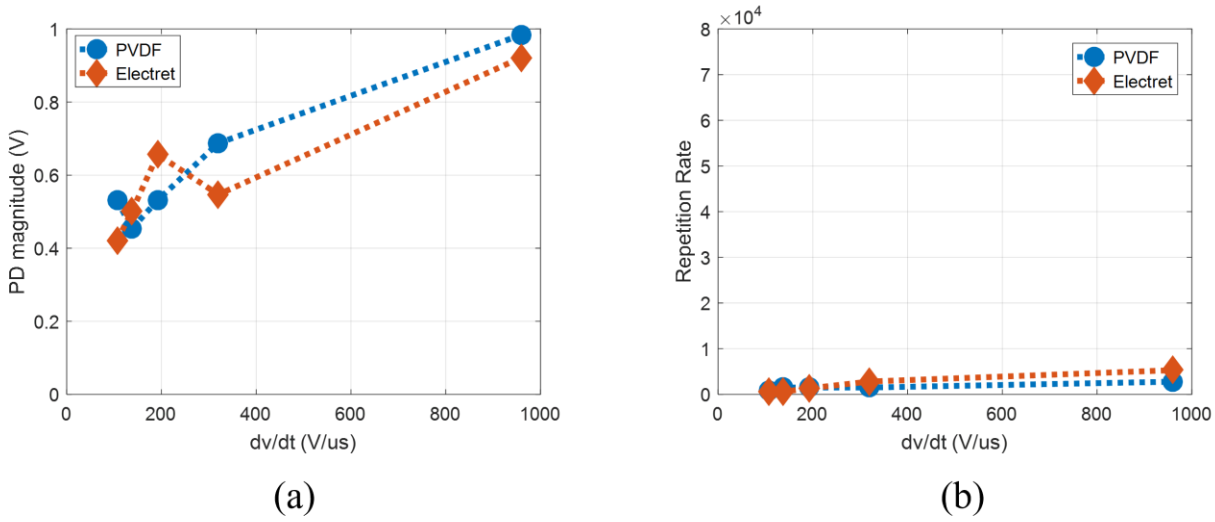

Figure 5.16 Comparison of cavity discharge performance of uncharged PVDF and positively charged electret at various *dVdt* under negative voltage. (a) Maximum PD magnitude, (b) Repetition rate

An uncharged PVDF and positively charged electret are stressed under negative polarity square voltage stimuli with magnitude varying between 0 to -9.6 kV at different *dV/dt*. Figure 5.15 shows the PD discharge achieved with uncharged PVDF (Figure 5.15 (a)) and electret (Figure 5.15 (b)) where the square voltage has the rise time of 50 µs and duty cycle of 10 %. To evaluate electrets performance, both maximum PD magnitudes and repetition rate with PVDF and electret are compared. Figure 5.16 (a) compares the maximum PD magnitudes and Figure 5.16 (b) compares the PD repetition rate per cycle with PVDF and electrets at different *dV/dt*. It is observed in Figure 5.15 that, there is a noteworthy increase in the PD magnitude as well as PD occurrence when PDVF is replaced with positive polarity electret when negative polarity voltage is applied. In Figure 5.16, it is observed that although PD magnitude and repletion rate increases as *dV/dt* increases with uncharged PVDF film, when replacing with the electret fabricated under an optimum condition described in Table 5.1, there is a significant increase in the PD magnitude as

well as in the repetition rate per cycle. These implies that under negative voltage stress, positive polarity electret is unable to mitigate PD and increases the dielectric risk.

c) Bipolar stress

An uncharged PVDF and positively charged electret are stressed under bipolar square voltage stimuli with magnitude varying between -4.8 kV to 4.8 kV at different *dV/dt.* Figure 5.17 shows the PD discharge achieved with uncharged PVDF (Figure 5.17(a)) and electret (Figure 5.17(b)) where the square voltage has the rise time of 50 μs and duty cycle of 10 %. To evaluate electrets performance, both maximum PD magnitudes and repetition rate with PVDF and electret are compared. Figure 5.18(a) compares the maximum PD magnitudes and Figure 5.18(b) compares the PD repetition rate per cycle with PVDF and electrets at different *dV/dt*. It is observed in Figure 5.17 that, there is a noteworthy increase in the PD magnitude as well as PD occurrence when PDVF is replaced with positive polarity electret when a bipolar voltage is applied. In Figure 5.18, it is observed that although PD magnitude and repletion rate increases as *dV/dt* increases with uncharged PVDF film, when replacing with the electret fabricated under an optimum condition described in Table 5.1, there is a significant increase in the PD magnitude as well as in the repetition rate per cycle. These implies that under bipolar voltage stress, positive polarity electret is unable to mitigate PD and increases the dielectric risk.

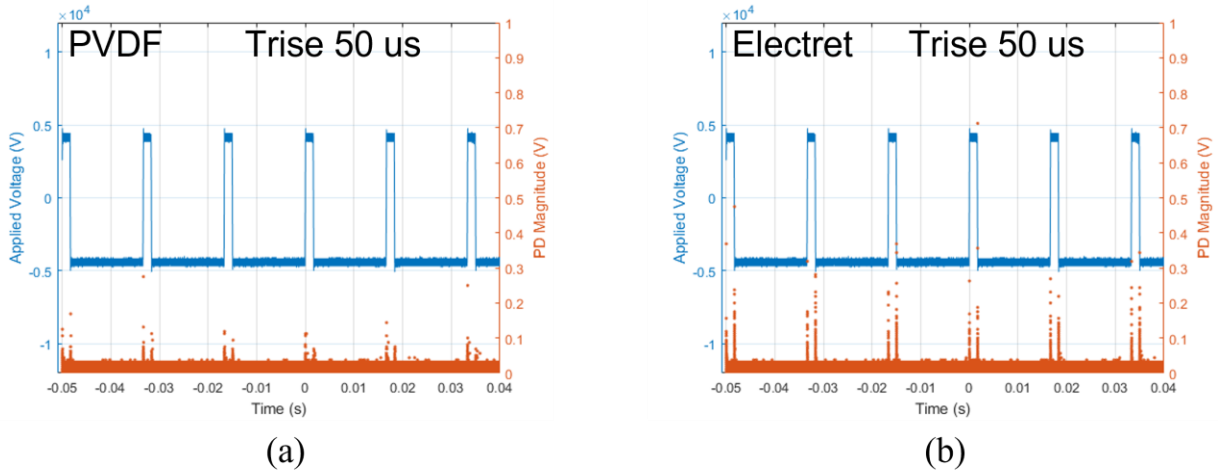

(a) (b)

Figure 5.17 PD signal caused by cavity discharge under square voltage stimuli with magnitude 9.6 kV_{pp} (bipolar), rise time 50 µs, and duty cycle 10 %. (a) Uncharged PVDF, (b) Positive polarity electret

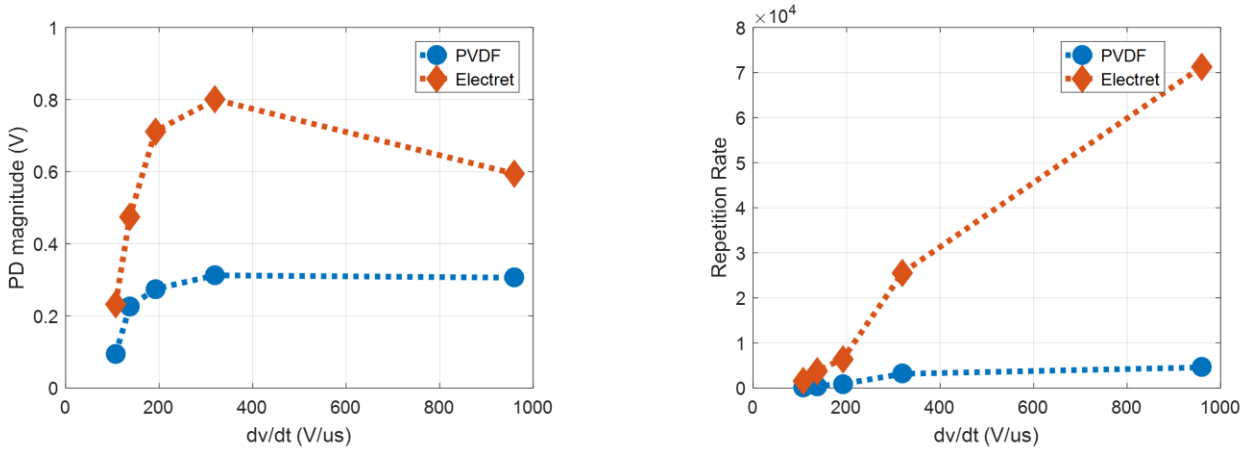

(a) (b)

Figure 5.18 Comparison of cavity discharge performance of uncharged PVDF and positively charged electret at various *dVdt* under bipolar voltage. (a) Maximum PD magnitude, (b) Repetition rate.

5.2.2.2 Negative polarity electret

In this case, electrets are fabricated based on the triode corona charging method with PVDF film of thickness 25.4 μm. For fabricating electrets, the charging conditions maintained are described in the Table 5.2. PD magnitude and repetition achieved with both uncharged PVDF and electrets are compared under various voltage polarity stress.

a) Positive polarity stress

An uncharged PVDF and negatively charged electret are stressed under positive polarity square voltage stimuli with magnitude varying between 0 to 9.6 kV at different *dV/dt.* Figure 5.19 shows the PD discharge achieved with uncharged PVDF (Figure 5.19(a)) and electret (Figure 5.19(b)) where the square voltage has the rise time of 50 μs and duty cycle of 10 %. To evaluate electrets performance, both maximum PD magnitudes and repetition rate with PVDF and electret are compared. Figure 5.20(a) compares the maximum PD magnitudes and Figure 5.20(b) compares the PD repetition rate per cycle with PVDF and electrets at different *dV/dt*. It is observed in Figure 5.19 that, there is a noteworthy increase in the PD magnitude as well as PD occurrence when PDVF is replaced with negative polarity electret when positive polarity voltage is applied. In Figure 5.20, it is observed that although PD magnitude and repletion rate increases as *dV/dt* increases with uncharged PVDF film, when replacing with the electret fabricated under an optimum condition described in Table 5.2, there is a significant increase in the PD magnitude as well as in the repetition rate per cycle. These implies that under positive voltage stress, negative polarity electret is unable to mitigate PD and increases the dielectric risk.

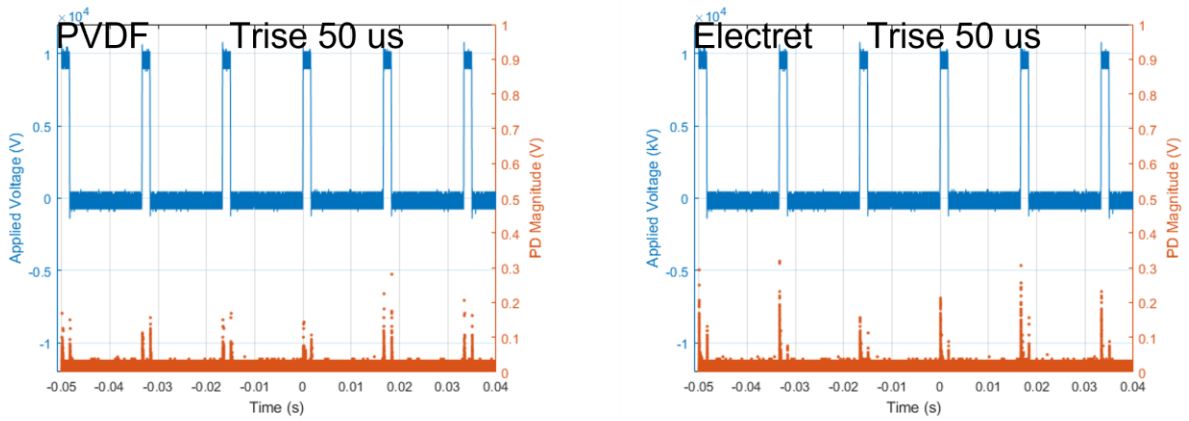

(a) (b)

Figure 5.19 PD signal caused by cavity discharge under square voltage stimuli with magnitude 9.6 kV_{pp}, rise time 50 µs, and duty cycle 10 %. (a) Uncharged PVDF, (b) Negative polarity electret

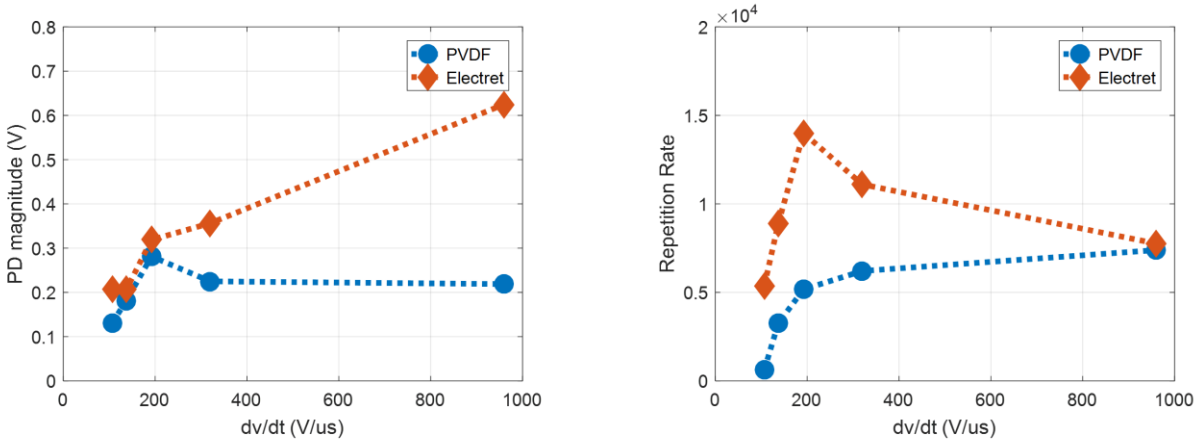

(a) (b)

Figure 5.20 Comparison of cavity discharge performance of uncharged PVDF and negatively charged electret at various *dVdt* under positive voltage. (a) Maximum PD magnitude, (b) Repetition rate.

b) Negative polarity stress

An uncharged PVDF and negatively charged electret are stressed under negative polarity square voltage stimuli with magnitude varying between 0 to -9.6 kV at different *dV/dt*. Figure 5.21 shows the PD discharge achieved with uncharged PVDF (Figure 5.21(a)) and electret (Figure 7.21 (b)) where the square voltage has the rise time of 50 µs and duty cycle of 10 %. To evaluate electrets performance, both maximum PD magnitudes and repetition rate with PVDF and electret are compared. Figure 5.22(a) compares the maximum PD magnitudes and Figure 5.22(b) compares the PD repetition rate per cycle with PVDF and electrets at different *dV/dt*. It is observed in Figure 5.21 that, there is a substantial reduction in the PD magnitude as well as PD occurrence when PDVF is replaced with negative polarity electret when negative polarity voltage is applied. Figure 5.22 shows that as the *dV/dt* increases, both PD magnitudes and repetition rate shows increasing trend. This phenomenon is previously recognized in the previous literatures, that as the *dV/dt* increases, dielectric materials are more stressed and their life time decreases. In Figure 5.22, it is observed that although PD magnitude and repletion rate increases as *dV/dt* increases with uncharged PVDF film, when replacing with the electret fabricated under an optimum condition described in Table 5.2, there is a significant reduction in the PD magnitude as well as in the repetition rate per cycle.

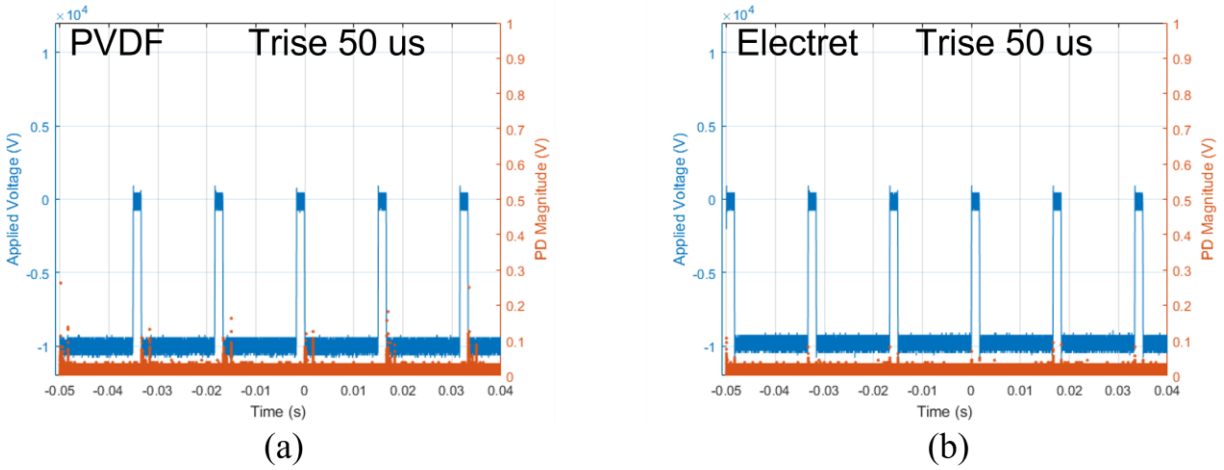

Figure 5.21 PD signal caused by cavity discharge under square voltage stimuli with magnitude -9.6 kV_{pp}, rise time 50 µs, and duty cycle 10 %. (a) Uncharged PVDF, (b) Negative polarity electret

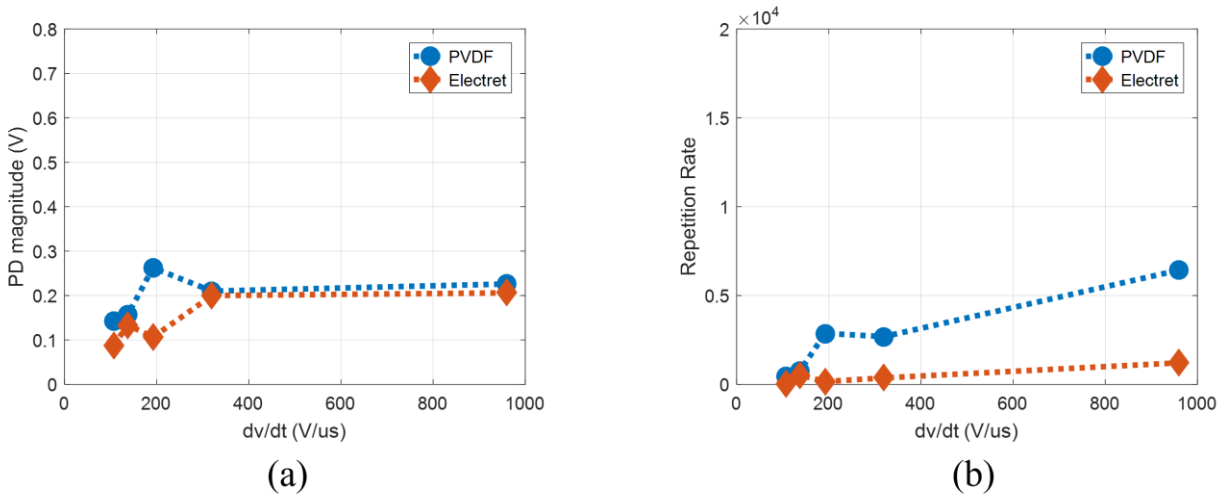

Figure 5.22 Comparison of cavity discharge performance of uncharged PVDF and negatively charged electret at various *dVdt* under negative voltage. (a) Maximum PD magnitude, (b) Repetition rate.

c) Bipolar stress

An uncharged PVDF and negatively charged electret are stressed under bipolar square voltage stimuli with magnitude varying between -4.8 kV to 4.8 kV at different *dV/dt.* Figure 5.23 shows the PD discharge achieved with uncharged PVDF (Figure 5.23(a)) and electret (Figure 5.23(b)) where the square voltage has the rise time of 50 μs and duty cycle of 10 %. To evaluate electrets performance, both maximum PD magnitudes and repetition rate with PVDF and electret are compared. Figure 5.24(a) compares the maximum PD magnitudes and Figure 5.24(b) compares the PD repetition rate per cycle with PVDF and electrets at different *dV/dt*. It is observed in Figure 5.23 that, there is a noteworthy increase in the PD magnitude as well as PD occurrence when PDVF is replaced with negative polarity electret when a bipolar voltage is applied. In Figure 5.24, it is observed that although PD magnitude and repletion rate increases as *dV/dt* increases with uncharged PVDF film, when replacing with the electret fabricated under an optimum condition described in Table 5.2, there is a significant increase in the PD magnitude as well as in the repetition rate per cycle. These implies that under bipolar voltage stress, negative polarity electret is unable to mitigate PD and increases the dielectric risk.

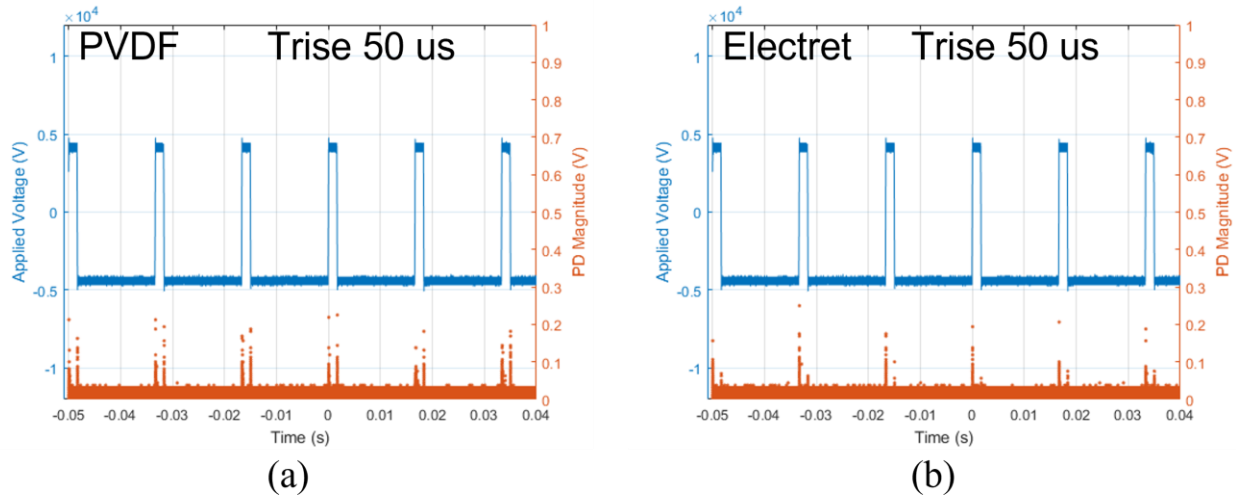

Figure 5.23 PD signal caused by cavity discharge under square voltage stimuli with magnitude 9.6 kV_{pp} (bipolar), rise time 50 µs, and duty cycle 10 %. (a) Uncharged PVDF, (b) Negative polarity electret

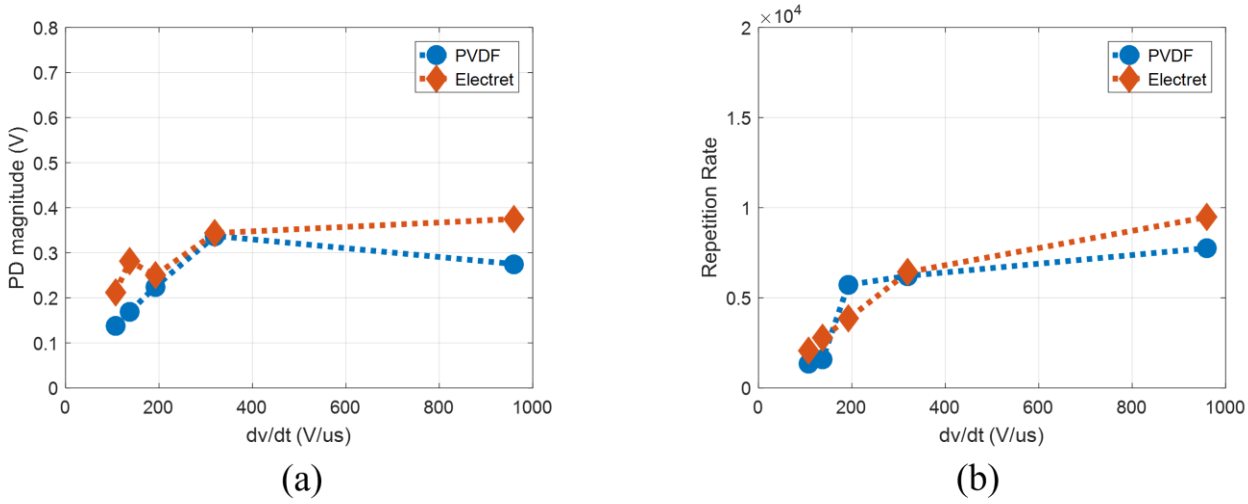

Figure 5.24 Comparison of cavity discharge performance of uncharged PVDF and positively charged electret at various *dVdt* under bipolar voltage. (a) Maximum PD magnitude, (b) Repetition rate.

5.3 Impact of duty cycle

PD experiments with and without electrets are conducted under square voltage of duty cycle varying from 10 µs to 90 µs and a constant voltage level (4 kV_{pp} for surface discharge and 9.6 kV_{pp} for cavity discharge) to analyses the electret-based PD mitigation performance for various duty cycle. In this section electrets are fabricated from the PVDF film in the optimum charging conditions described in the previous section. Both positive polarity electret and negative polarity electret are utilized for the experiments to evaluate their PD mitigation performance at different duty cycle under various voltage polarity stress, i.e., positive, negative, and bipolar voltage stress.

5.3.1 Surface discharge

Surface discharge experiments are conducted with same testbed as described in Chapter V in Figure 3.3. Both positive and negative polarity electrets are fabricated, and their PD mitigation performance is compared with the uncharged PVDF films. The duty cycle is varied from 10% to 90% with a step of 20 %. The square voltage magnitude is kept at 4 kV_{pp}. To observe the performance of electret under various voltage polarity stress, both positive polarity and negative polarity electrets are stressed under positive, negative, and bipolar voltage stress.

5.3.1.1 Positive polarity electret

In this case, electrets are fabricated based on the triode corona charging method with PVDF film of thickness 25.4 µm. For fabricating electrets, the charging conditions maintained are described in the Table 5.1. PD magnitude and repetition achieved with both uncharged PVDF and electrets are compared under various voltage polarity stress.

a) Positive polarity stress

An uncharged PVDF and positively charged electret are stressed under positive polarity square voltage stimuli with magnitude varying between 0 to 4 kV at different duty cycle Figure 5.25 shows the PD discharge achieved with uncharged PVDF (Figure 5.25(a)) and electret (Figure 5.25(b)) where the square voltage has the rise time of 50 μs and duty cycle of 50 %. To evaluate electrets performance, both maximum PD magnitudes and repetition rate with PVDF and electret are compared. Figure 5.26(a) compares the maximum PD magnitudes and Figure 5.26(b) compares the PD repetition rate per cycle with PVDF and electrets at different duty cycle. It is observed in Figure 5.25 that, there is a substantial reduction in the PD magnitude as well as PD occurrence when PDVF is replaced with positive polarity electret when positive polarity voltage is applied. In Figure 5.26, it is observed that PD magnitude and repletion rate do not follow any trend as the duty cycle increase from 10 % to 90% when uncharged PVDF is used. When the uncharged PVDF is replaced with the electret fabricated under an optimum condition described in Table 5.1 there is a significant reduction in the PD magnitude as well as in the repetition rate per cycle.

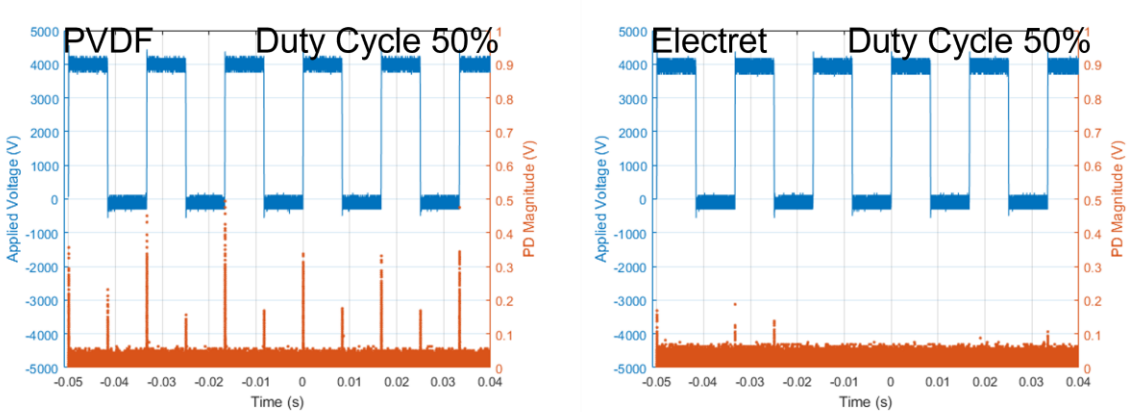

(a) (b)

Figure 5.25 PD signal caused by surface discharge under square voltage stimuli with magnitude 4 kV_{pp}, rise time 50 µs, and duty cycle 50 %. (a) Uncharged PVDF, (b) Positive polarity electret

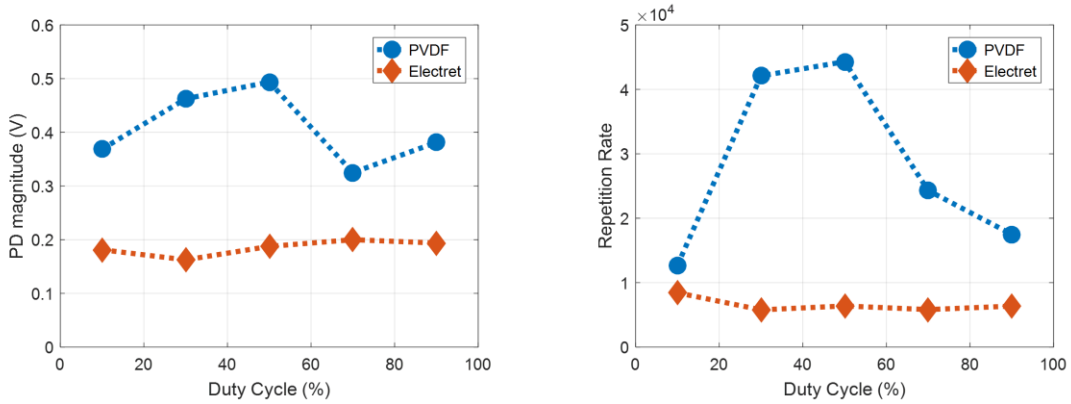

(a) (b)

Figure 5.26 Comparison of surface discharge performance of uncharged PVDF and positively charged electret at various duty cycle under positive voltage. (a) Maximum PD magnitude, (b) Repetition rate.

b) Negative polarity stress

An uncharged PVDF and positively charged electret are stressed under negative polarity square voltage stimuli with magnitude varying between 0 to -4 kV at different duty cycle. Figure 5.27 shows the PD discharge achieved with uncharged PVDF (Figure 5.27(a)) and electret (Figure 5.27(b)) where the square voltage has the rise time of 50 μs and duty cycle of 50 %. To evaluate electrets performance, both maximum PD magnitudes and repetition rate with PVDF and electret are compared. Figure 5.28(a) compares the maximum PD magnitudes and Figure 5.28(b) compares the PD repetition rate per cycle with PVDF and electrets at different duty cycle. It is observed in Figure 5.27 that, there is a noteworthy increase in the PD magnitude as well as PD occurrence when PDVF is replaced with positive polarity electret when negative polarity voltage is applied. In Figure 5.28, it is observed that PD magnitude and repletion rate do not follow any trend as the duty cycle increase from 10 % to 90% when uncharged PVDF is used. When the uncharged PVDF is replaced with the electret fabricated under an optimum condition described in Table 5.1, the PD magnitude and repetition rate either increase or keep same when compared with the uncharged one.

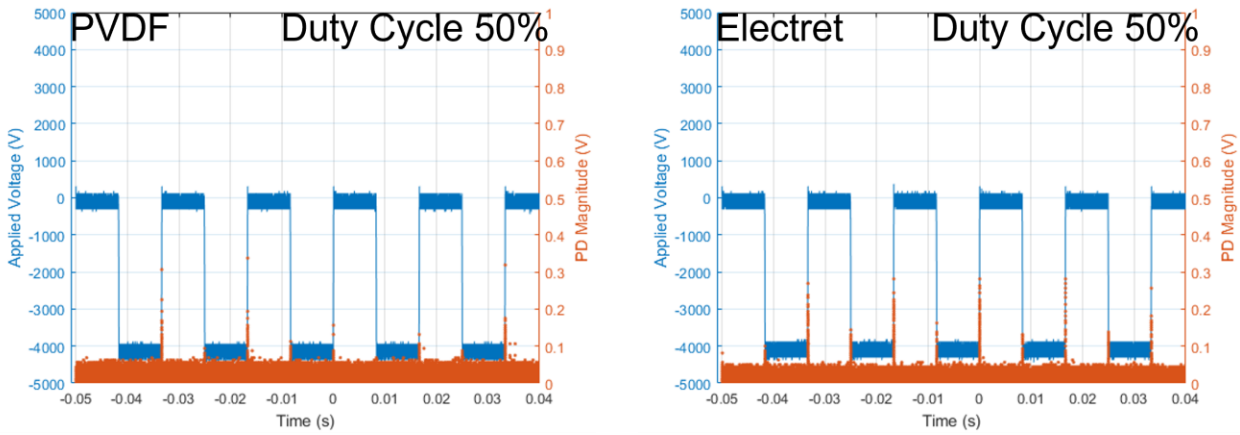

(a) (b)

Figure 5.27 PD signal caused by surface discharge under square voltage stimuli with magnitude -4 kV_{pp}, rise time 50 µs, and duty cycle 50 %. (a) Uncharged PVDF, (b) Positive polarity electret

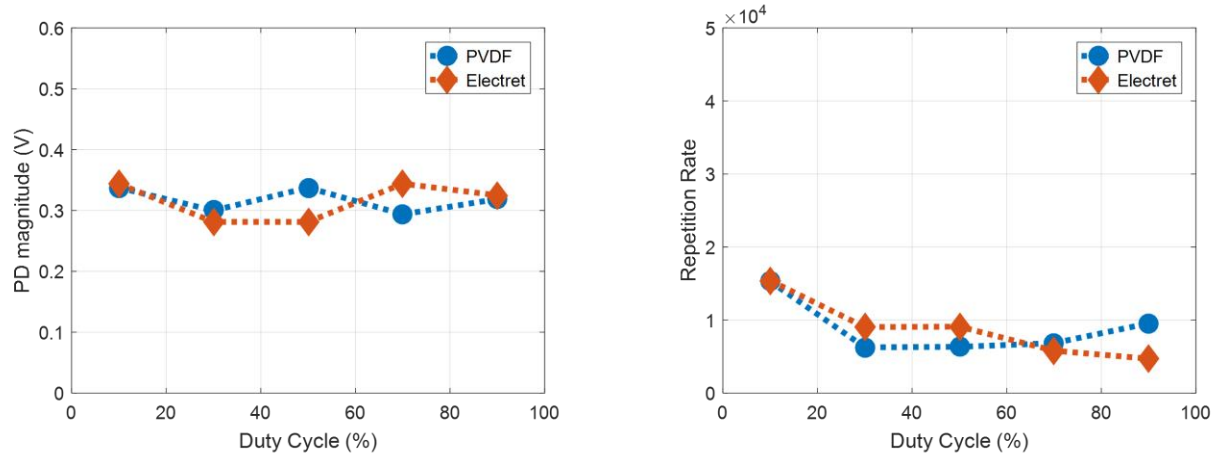

(a) (b)

Figure 5.28 Comparison of surface discharge performance of uncharged PVDF and positively charged electret at various duty cycle under neagtive voltage. (a) Maximum PD magnitude, (b) Repetition rate.

c) Bipolar stress

An uncharged PVDF and positively charged electret are stressed under bipolar square voltage stimuli with magnitude varying between -2 kV to 2 kV at different duty cycle. Figure 5.29 shows the PD discharge achieved with uncharged PVDF (Figure 5.29(a)) and electret (Figure 5.29(b)) where the square voltage has the rise time of 50 μs and duty cycle of 50 %. To evaluate electrets performance, both maximum PD magnitudes and repetition rate with PVDF and electret are compared. Figure 5.30(a) compares the maximum PD magnitudes and Figure 5.30(b) compares the PD repetition rate per cycle with PVDF and electrets at different duty cycle. It is observed in Figure 5.29 that, there is a noteworthy increase in the PD magnitude as well as PD occurrence when PDVF is replaced with positive polarity electret when bipolar voltage is applied. In Figure 5.30, it is observed that PD magnitude and repletion rate do not follow any trend as the duty cycle increase from 10 % to 90% when uncharged PVDF is used. When the uncharged PVDF is replaced with the electret fabricated under an optimum condition described in Table 5.1, the PD magnitude and repetition rate either increase significantly or keep same when compared with the uncharged one.

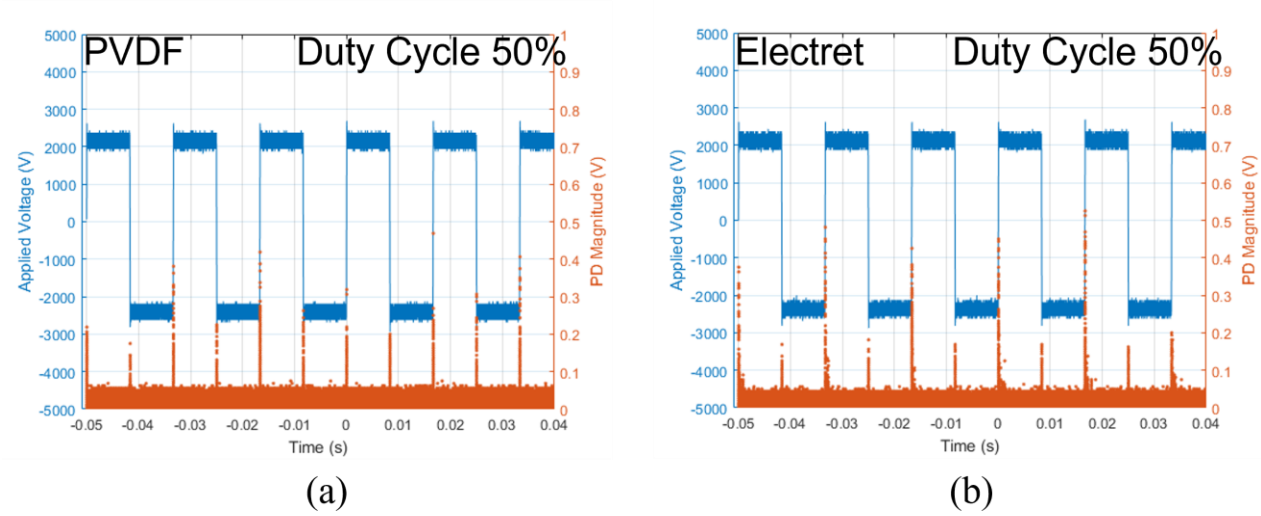

(a) (b)

Figure 5.29 PD signal caused by surface discharge under square voltage stimuli with magnitude 4 kV_{pp} (bipolar), rise time 50 µs, and duty cycle 50 %. (a) Uncharged PVDF, (b) Positive polarity electret

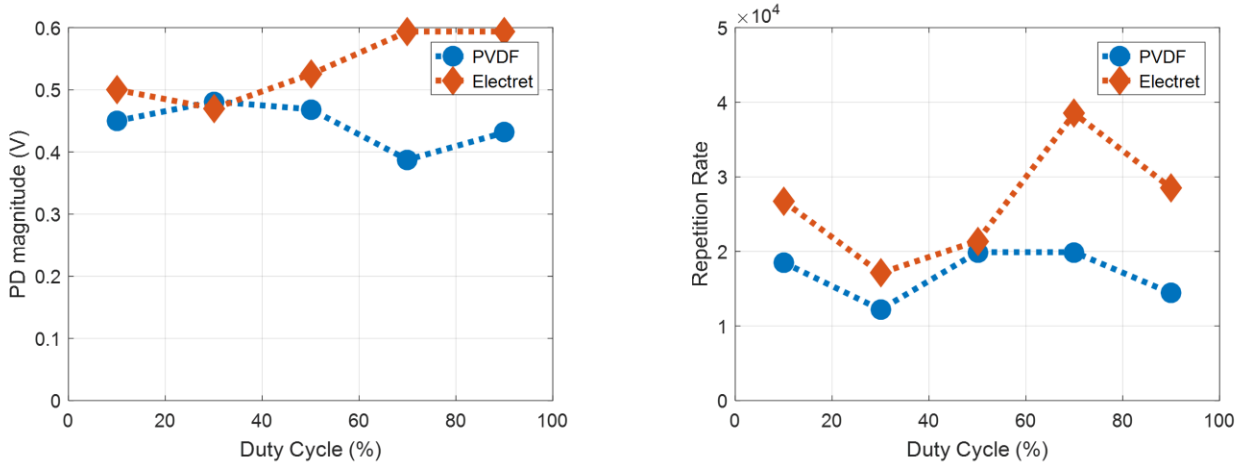

(a) (b)

Figure 5.30 Comparison of surface discharge performance of uncharged PVDF and positively charged electret at various duty cycle under bipolar voltage. (a) Maximum PD magnitude, (b) Repetition rate.

5.3.1.2 Negative polarity electret

In this case, electrets are fabricated based on the triode corona charging method with PVDF film of thickness 25.4 µm. For fabricating electrets, the charging conditions maintained are described in the Table 5.2. PD magnitude and repetition achieved with both uncharged PVDF and electrets are compared under various voltage polarity stresses.

a) Positive polarity stress

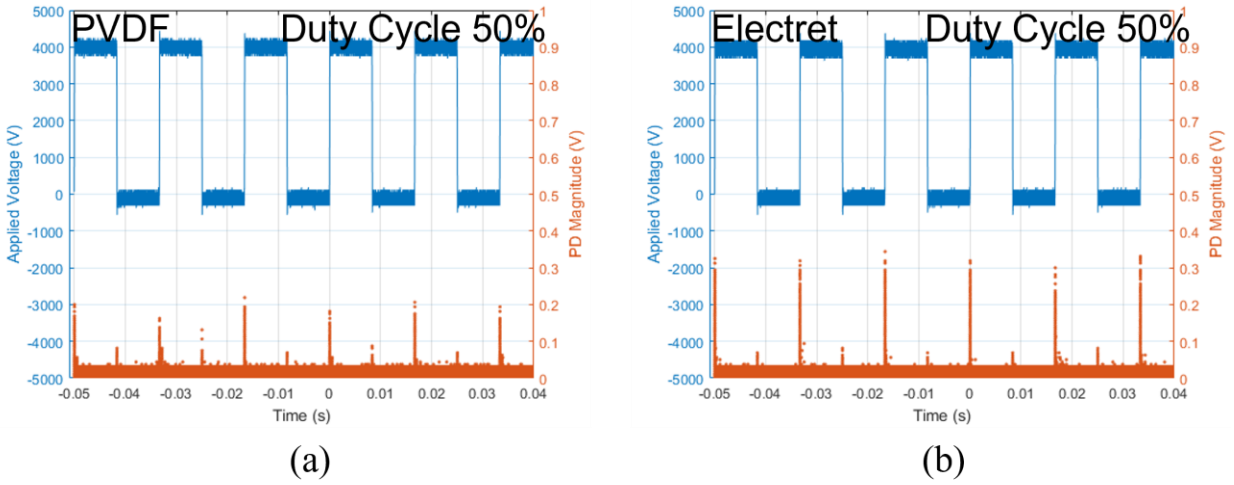

Figure 5.31 PD signal caused by surface discharge under square voltage stimuli with magnitude 4 kV_{pp}, rise time 50 µs, and duty cycle 50 %. (a) Uncharged PVDF, (b) Negative polarity electret

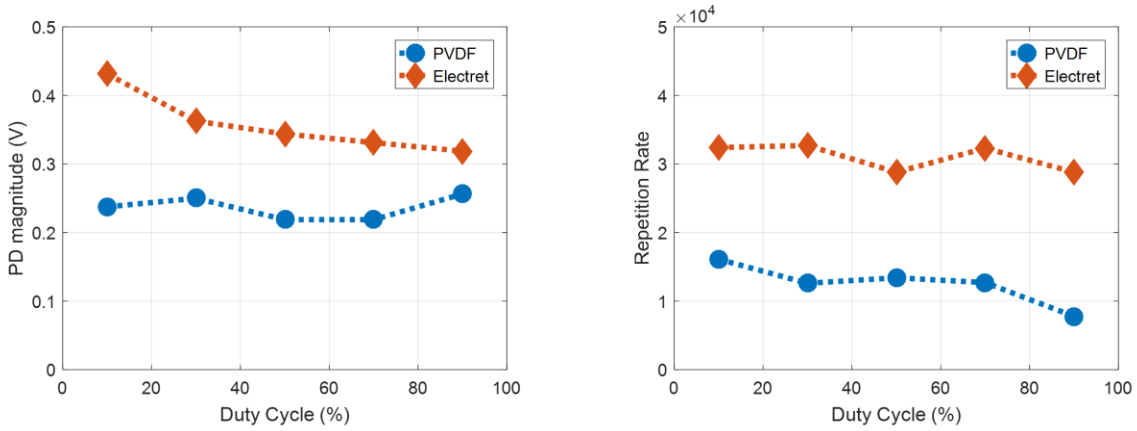

Figure 5.32 Comparison of surface discharge performance of uncharged PVDF and negatively charged electret at various duty cycle under positive voltage. (a) Maximum PD magnitude, (b) Repetition rate

An uncharged PVDF and negatively charged electret are stressed under positive polarity square voltage stimuli with magnitude varying between 0 to 4 kV at different duty cycle. Figure 5.31 shows the PD discharge achieved with uncharged PVDF (Figure 5.31(a)) and electret (Figure 5.31(b)) where the square voltage has the rise time of 50 µs and duty cycle of 50 %. To evaluate electrets performance, both maximum PD magnitudes and repetition rate with PVDF and electret are compared. Figure 5.32(a) compares the maximum PD magnitudes and Figure 5.32(b) compares the PD repetition rate per cycle with PVDF and electrets at different duty cycle. It is observed in Figure 5.31 that, there is a noteworthy increase in the PD magnitude as well as PD occurrence when PDVF is replaced with positive polarity electret when negative polarity voltage is applied. In Figure 5.32, it is observed that PD magnitude and repletion rate do not follow any trend as the duty cycle increase from 10 % to 90% when uncharged PVDF is used. When the uncharged PVDF is replaced with the electret fabricated under an optimum condition described in

Table 5.2, the PD magnitude and repetition rate increase significantly compared with the uncharged one.

b) Negative polarity stress

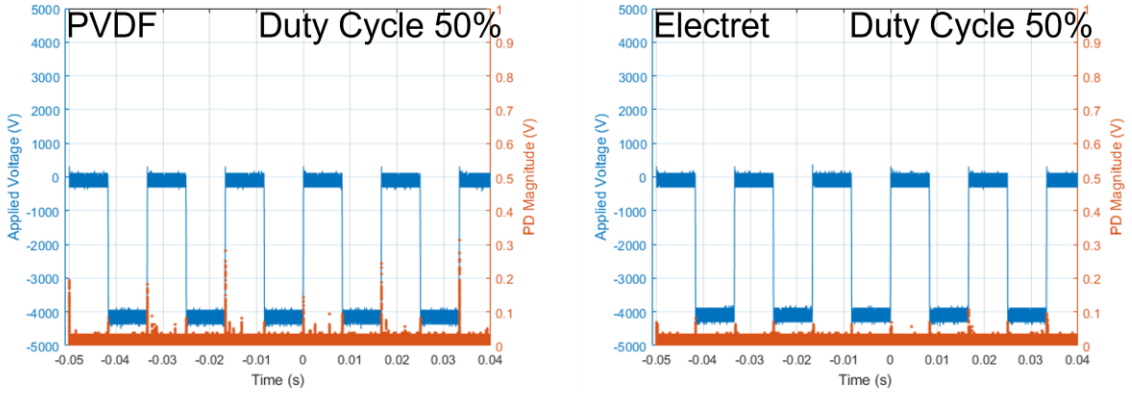

Figure 5.33 PD signal caused by surface discharge under square voltage stimuli with magnitude -4 kV_{pp}, rise time 50 µs, and duty cycle 50 %. (a) Uncharged PVDF, (b) Negative polarity electret

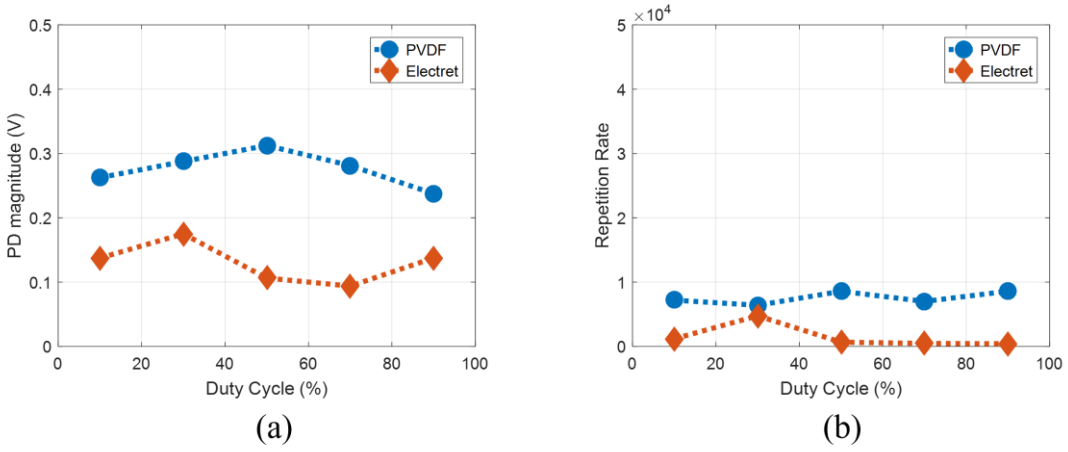

Figure 5.34 Comparison of surface discharge performance of uncharged PVDF and negatively charged electret at various duty cycle under negative voltage. (a) Maximum PD magnitude, (b) Repetition rate

An uncharged PVDF and negatively charged electret are stressed under negative polarity square voltage stimuli with magnitude varying between 0 to -4 kV at different duty cycle Figure 5.33 shows the PD discharge achieved with uncharged PVDF (Figure 5.33(a)) and electret (Figure 5.33(b)) where the square voltage has the rise time of 50 μs and duty cycle of 50 %. To evaluate electrets performance, both maximum PD magnitudes and repetition rate with PVDF and electret are compared. Figure 5.34(a) compares the maximum PD magnitudes and Figure 5.34(b) compares the PD repetition rate per cycle with PVDF and electrets at different duty cycle. It is observed in Figure 5.33 that, there is a substantial reduction in the PD magnitude as well as PD occurrence when PDVF is replaced with negative polarity electret when negative polarity voltage is applied. In Figure 5.34, it is observed that PD magnitude and repletion rate do not follow any trend as the duty cycle increase from 10 % to 90% when uncharged PVDF is used. When the uncharged PVDF is replaced with the electret fabricated under an optimum condition described in Table 5.2, there is a significant reduction in the PD magnitude as well as in the repetition rate per cycle.

c) Bipolar stress

An uncharged PVDF and negatively charged electret are stressed under bipolar square voltage stimuli with magnitude varying between -2 kV to 2 kV at different duty cycle. Figure 5.35 shows the PD discharge achieved with uncharged PVDF (Figure 5.35(a)) and electret (Figure 5.35(b)) where the square voltage has the rise time of 50 μs and duty cycle of 50 %. To evaluate electrets performance, both maximum PD magnitudes and repetition rate with PVDF and electret are compared. Figure 5.36(a) compares the maximum PD magnitudes and Figure 5.36(b) compares the PD repetition rate per cycle with PVDF and electrets at different duty cycle. It is observed in

Figure 5.35 that, there is a noteworthy increase in the PD magnitude as well as PD occurrence when PDVF is replaced with negative polarity electret when bipolar voltage is applied. In Figure 5.36, it is observed that PD magnitude and repletion rate do not follow any trend as the duty cycle increase from 10 % to 90% when uncharged PVDF is used. When the uncharged PVDF is replaced with the electret fabricated under an optimum condition described in Table 5.2, the PD magnitude and repetition rate either increase significantly or keep same when compared with the uncharged one.

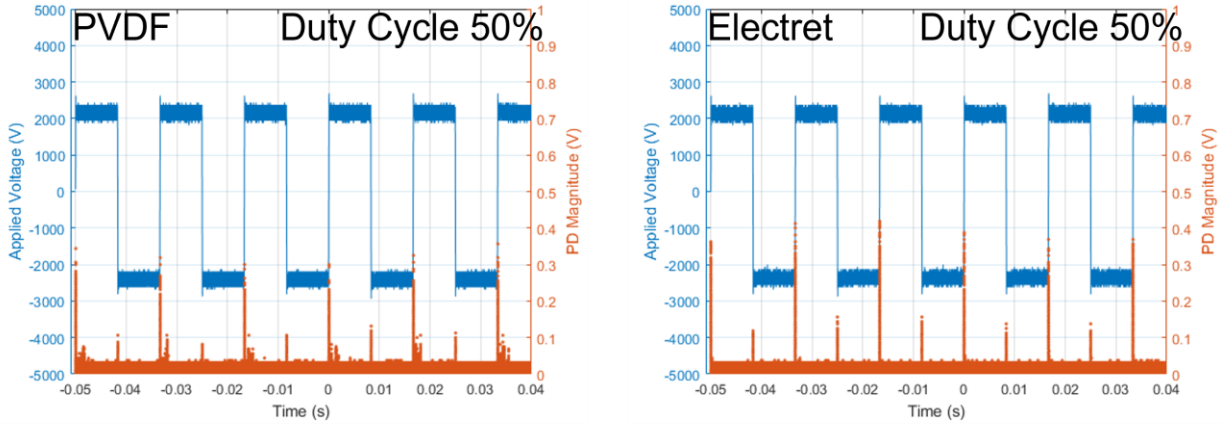

Figure 5.35 PD signal caused by surface discharge under square voltage stimuli with magnitude 4 kV_{pp} (bipolar), rise time 50 µs, and duty cycle 50 %. (a) Uncharged PVDF, (b) Negative polarity electret

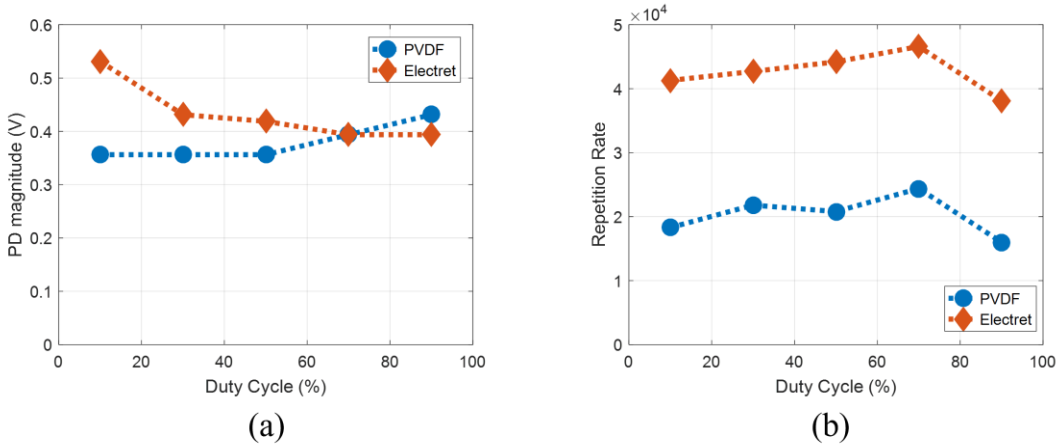

Figure 5.36 Comparison of surface discharge performance of uncharged PVDF and negatively charged electret at various duty cycle under bipolar voltage. (a) Maximum PD magnitude, (b) Repetition rate

5.3.2 Cavity discharge

Cavity discharge experiments are conducted with same testbed as described in Chapter V in Figure 3.5. In this case, the solid 3D printed insulator has thickness 2 mm and 20% infill density. Both positive and negative polarity electrets are fabricated, and their PD mitigation performance is compared with the uncharged PVDF films. The duty cycle is varied from 10% to 90% with a step of 20 µs. The square voltage magnitude is kept at 9.6 kV_{pp}. To observe the performance of electret under various voltage polarity stress, both positive polarity and negative polarity electrets are stressed under positive, negative, and bipolar voltage stress.

5.3.2.1 Positive polarity electret

In this case, electrets are fabricated based on the triode corona charging method with PVDF film of thickness 25.4 µm. For fabricating electrets, the charging conditions maintained are

described in the Table 5.1. PD magnitude and repetition achieved with both uncharged PVDF and electrets are compared under various voltage polarity stress.

a) Positive polarity stress

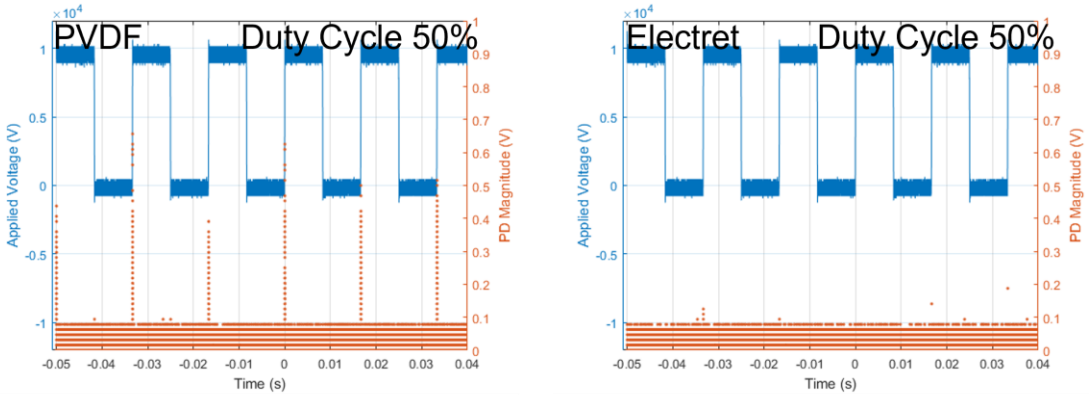

(a) (b)

Figure 5.37 PD signal caused by cavity discharge under square voltage stimuli with magnitude 9.6 kV_{pp}, rise time 50 µs, and duty cycle 50 %. (a) Uncharged PVDF, (b) Positive polarity electret

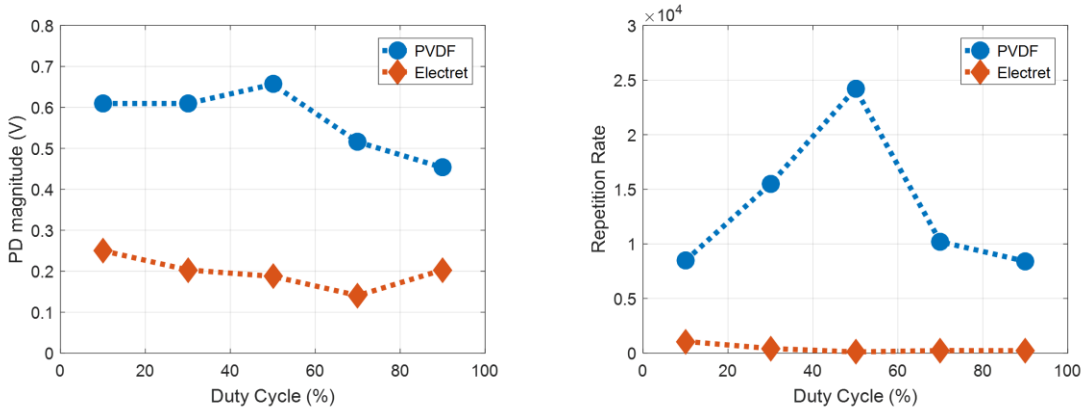

(a) (b)

Figure 5.38 Comparison of cavity discharge performance of uncharged PVDF and positively charged electret at various duty cycle under positive voltage. (a) Maximum PD magnitude, (b) Repetition rate.

An uncharged PVDF and positively charged electret are stressed under positive polarity square voltage stimuli with magnitude varying between 0 to 9.6 kV at different duty cycle Figure 5.37 shows the PD discharge achieved with uncharged PVDF (Figure 5.37(a)) and electret (Figure 5.37 (b)) where the square voltage has the rise time of 50 μs and duty cycle of 50 %. To evaluate electrets performance, both maximum PD magnitudes and repetition rate with PVDF and electret are compared. Figure 5.38 (a) compares the maximum PD magnitudes and Figure 5.38 (b) compares the PD repetition rate per cycle with PVDF and electrets at different duty cycle. It is observed in Figure 5.37 that, there is a substantial reduction in the PD magnitude as well as PD occurrence when PDVF is replaced with positive polarity electret when positive polarity voltage is applied. In Figure 5.38, it is observed that PD magnitude and repletion rate do not follow any trend as the duty cycle increase from 10 % to 90% when uncharged PVDF is used. When the uncharged PVDF is replaced with the electret fabricated under an optimum condition described in Table 5.1, there is a significant reduction in the PD magnitude as well as in the repetition rate per cycle.

b) Negative polarity stress

An uncharged PVDF and positively charged electret are stressed under negative polarity square voltage stimuli with magnitude varying between 0 to -9.6 kV at different duty cycle. Figure 5.39 shows the PD discharge achieved with uncharged PVDF (Figure 5.39(a)) and electret (Figure 5.39(b)) where the square voltage has the rise time of 50 μs and duty cycle of 50 %. To evaluate electrets performance, both maximum PD magnitudes and repetition rate with PVDF and electret are compared. Figure 5.40(a) compares the maximum PD magnitudes and Figure 5.40(b) compares the PD repetition rate per cycle with PVDF and electrets at different duty

cycle. It is observed in Figure 5.40 that, there is a noteworthy increase in the PD magnitude as well as PD occurrence when PDVF is replaced with positive polarity electret when negative polarity voltage is applied. In Figure 5.40, it is observed that PD magnitude and repletion rate do not follow any trend as the duty cycle increase from 10 % to 90% when uncharged PVDF is used. When the uncharged PVDF is replaced with the electret fabricated under an optimum condition described in Table 5.1, the PD magnitude and repetition rate either increase or keep same when compared with the uncharged one.

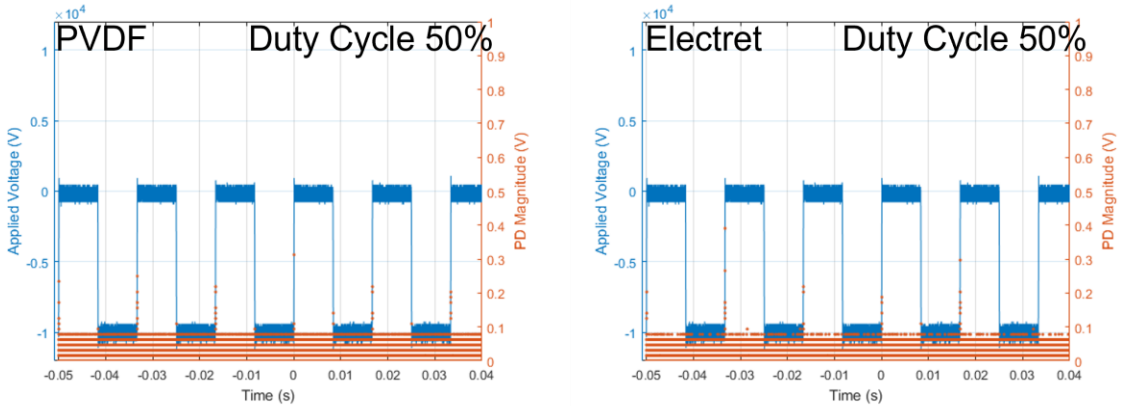

Figure 5.39 PD signal caused by cavity discharge under square voltage stimuli with magnitude -9.6 kV_{pp}, rise time 50 µs, and duty cycle 50 %. (a) Uncharged PVDF, (b) Positive polarity electret

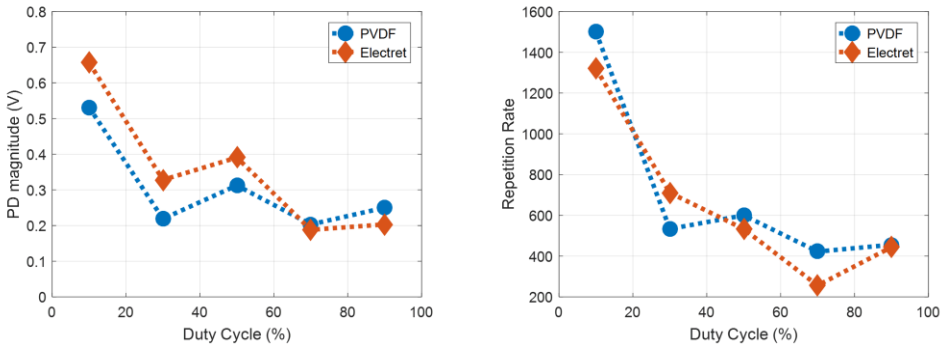

Figure 5.40 Comparison of cavity discharge performance of uncharged PVDF and positively charged electret at various duty cycle under negative voltage. (a) Maximum PD magnitude, (b) Repetition rate.

c) Bipolar stress

An uncharged PVDF and positively charged electret are stressed under bipolar square voltage stimuli with magnitude varying between -4.8 kV to 4.8 kV at different duty cycle. Figure 5.41 shows the PD discharge achieved with uncharged PVDF (Figure 5.41(a)) and electret (Figure 5.41(b)) where the square voltage has the rise time of 50 µs and duty cycle of 50 %. To evaluate electrets performance, both maximum PD magnitudes and repetition rate with PVDF and electret are compared. Figure 5.42(a) compares the maximum PD magnitudes and Figure 5.42(b) compares the PD repetition rate per cycle with PVDF and electrets at different duty cycle. It is observed in Figure 5.41 that, there is a noteworthy increase in the PD magnitude as well as PD occurrence when PDVF is replaced with positive polarity electret when bipolar voltage is applied. In Figure 5.42, it is observed that PD magnitude and repletion rate do not follow any trend as the duty cycle increase from 10 % to 90% when uncharged PVDF is used. When the uncharged PVDF is replaced with the electret fabricated under an optimum condition described in Table 5.1, the PD magnitude

and repetition rate either increase significantly or keep same when compared with the uncharged one.

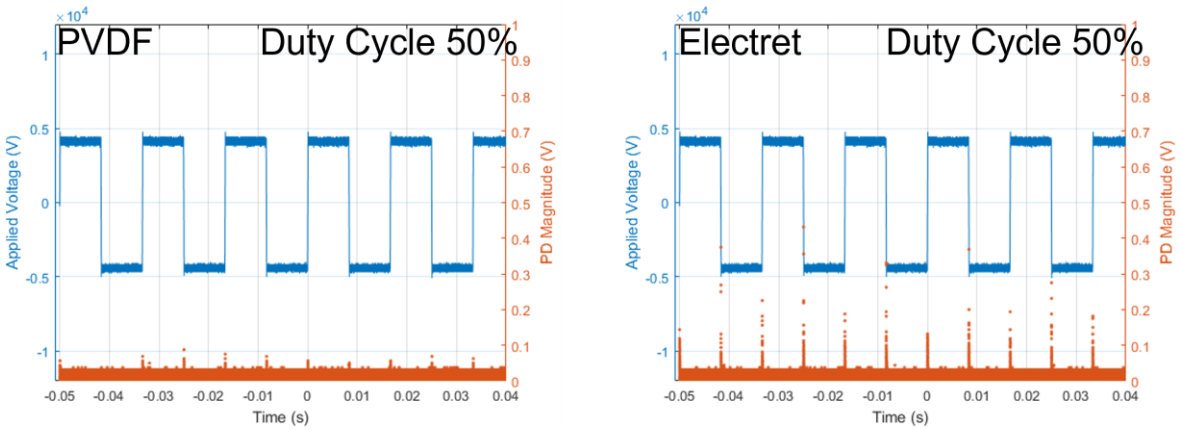

Figure 5.41 PD signal caused by cavity discharge under square voltage stimuli with magnitude -9.6 kV_{pp} (bipolar), rise time 50 µs, and duty cycle 50 %. (a) Uncharged PVDF, (b) Positive polarity electret

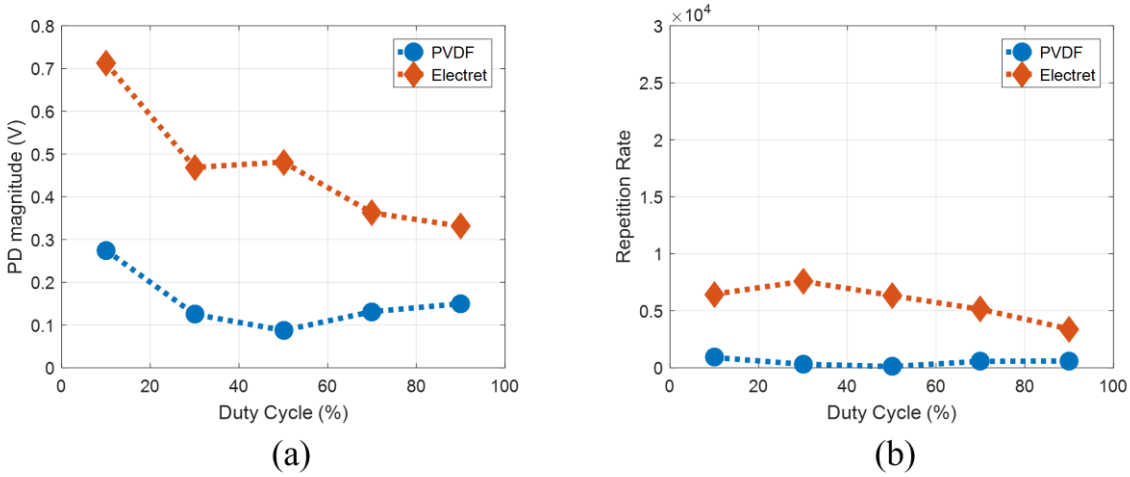

Figure 5.42 Comparison of cavity discharge performance of uncharged PVDF and positively charged electret at various duty cycle under bipolar voltage. (a) Maximum PD magnitude, (b) Repetition rate.

5.3.2.2 Negative polarity electret

In this case, electrets are fabricated based on the triode corona charging method with PVDF film of thickness 25.4 µm. For fabricating electrets, the charging conditions maintained are described in the Table 5.2. PD magnitude and repetition achieved with both uncharged PVDF and electrets are compared under various voltage polarity stress.

a) Positive polarity stress

An uncharged PVDF and negatively charged electret are stressed under positive polarity square voltage stimuli with magnitude varying between 0 to 9.6 kV at different duty cycle. Figure 5.43 shows the PD discharge achieved with uncharged PVDF (Figure 5.43 (a)) and electret (Figure 5.43 (b)) where the square voltage has the rise time of 50 µs and duty cycle of 50 %. To evaluate electrets performance, both maximum PD magnitudes and repetition rate with PVDF and electret are compared. Figure 5.44 (a) compares the maximum PD magnitudes and Figure 5.44 (b)

compares the PD repetition rate per cycle with PVDF and electrets at different duty cycle. It is observed in Figure 5.43 that, there is a noteworthy increase in the PD magnitude as well as PD occurrence when PDVF is replaced with positive polarity electret when negative polarity voltage is applied. In Figure 5.44, it is observed that PD magnitude and repletion rate do not follow any trend as the duty cycle increase from 10 % to 90% when uncharged PVDF is used. When the uncharged PVDF is replaced with the electret fabricated under an optimum condition described in Table 5.2, the PD magnitude and repetition rate increase significantly compared with the uncharged one.

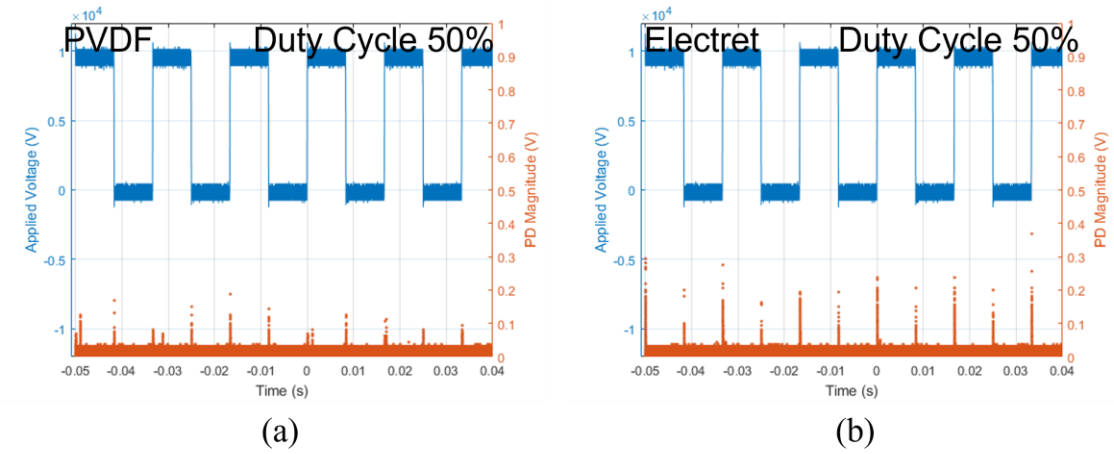

Figure 5.43 PD signal caused by cavity discharge under square voltage stimuli with magnitude 9.6 kV_{pp}, rise time 50 µs, and duty cycle 50 %. (a) Uncharged PVDF, (b) Negative polarity electret

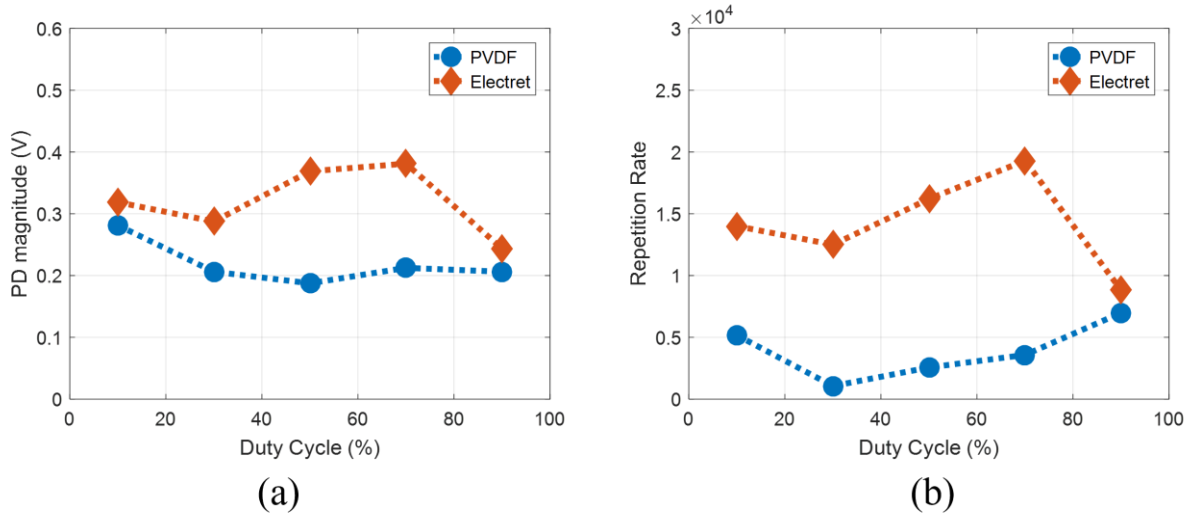

Figure 5.44 Comparison of cavity discharge performance of uncharged PVDF and negatively charged electret at various duty cycle under positive voltage. (a) Maximum PD magnitude, (b) Repetition rate.

b) Negative polarity stress

An uncharged PVDF and negatively charged electret are stressed under negative polarity square voltage stimuli with magnitude varying between 0 to -9.6 kV at different duty cycle Figure 5.45 shows the PD discharge achieved with uncharged PVDF (Figure 5.45(a)) and electret (Figure 5.45(b)) where the square voltage has the rise time of 50 µs and duty cycle of 50 %. To evaluate electrets performance, both maximum PD magnitudes and repetition rate with PVDF and electret are compared. Figure 5.46(a) compares the maximum PD magnitudes and Figure 5.46(b) compares the PD repetition rate per cycle with PVDF and electrets at different duty cycle. It is observed in Figure 5.45 that, there is a substantial reduction in the PD magnitude as well as PD occurrence when PDVF is replaced with negative polarity electret when negative polarity voltage is applied. In Figure 5.46, it is observed that PD magnitude and repletion rate do not follow any

trend as the duty cycle increase from 10 % to 90% when uncharged PVDF is used. When the uncharged PVDF is replaced with the electret fabricated under an optimum condition described in Table 5.2, there is a significant reduction in the PD magnitude as well as in the repetition rate per cycle.

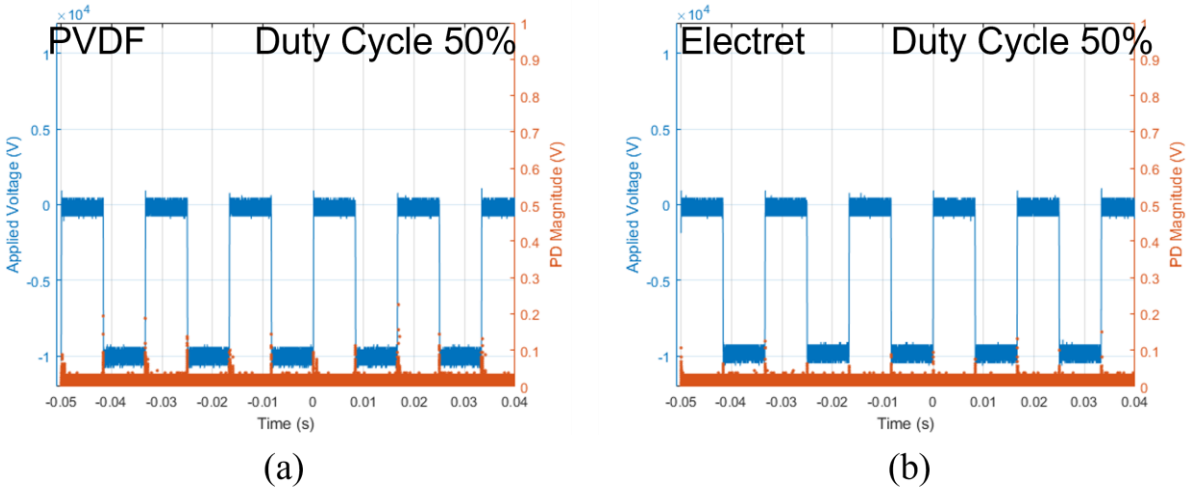

Figure 5.45 PD signal caused by cavity discharge under square voltage stimuli with magnitude -9.6 kV_{pp}, rise time 50 µs, and duty cycle 50 %. (a) Uncharged PVDF, (b) Negative polarity electret

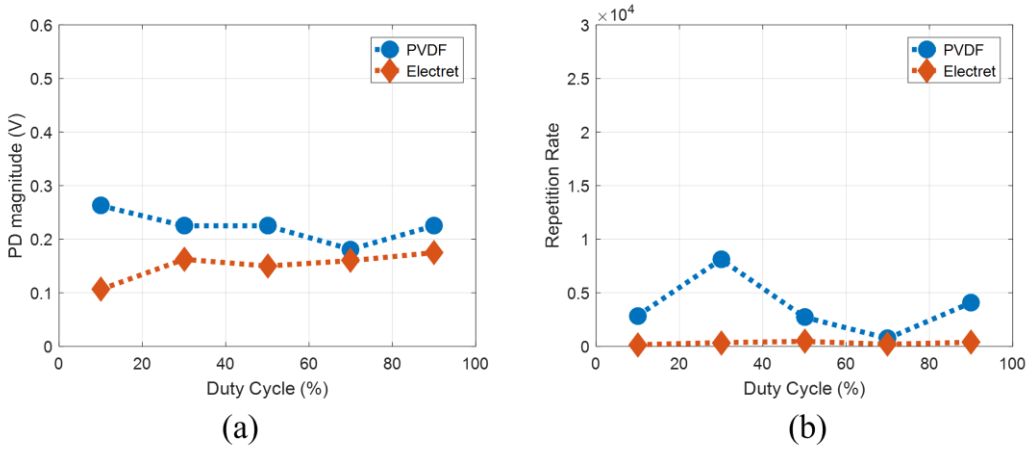

Figure 5.46 Comparison of cavity discharge performance of uncharged PVDF and negatively charged electret at various duty cycle under negative voltage. (a) Maximum PD magnitude, (b) Repetition rate.

c) Bipolar stress

An uncharged PVDF and negatively charged electret are stressed under bipolar square voltage stimuli with magnitude varying between -4.8 kV to 4.8 kV at different duty cycle. Figure 5.47 shows the PD discharge achieved with uncharged PVDF (Figure 5.47(a)) and electret (Figure 5.47(b)) where the square voltage has the rise time of 50 µs and duty cycle of 50 %. To evaluate electrets performance, both maximum PD magnitudes and repetition rate with PVDF and electret are compared. Figure 5.48(a) compares the maximum PD magnitudes and Figure 5.48(b) compares the PD repetition rate per cycle with PVDF and electrets at different duty cycle. It is observed in Figure 5.47 that, there is a noteworthy increase in the PD magnitude as well as PD occurrence when PDVF is replaced with negative polarity electret when bipolar voltage is applied. In Figure 5.48, it is observed that PD magnitude and repletion rate do not follow any trend as the duty cycle increase from 10 % to 90% when uncharged PVDF is used. When the uncharged PVDF is replaced

with the electret fabricated under an optimum condition described in Table 5.2, the PD magnitude and repetition rate either increase significantly or keep same when compared with the uncharged one.

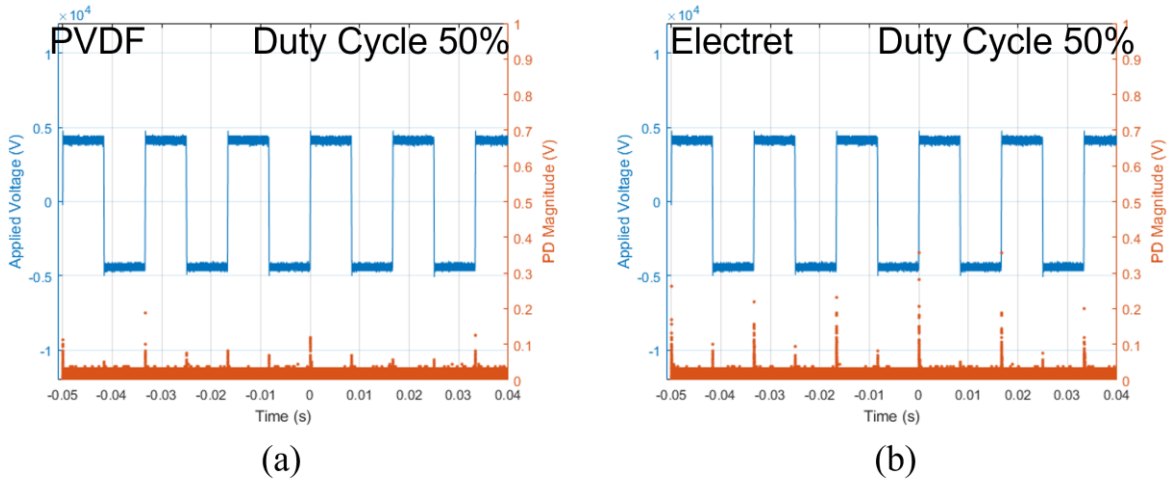

Figure 5.47 PD signal caused by cavity discharge under square voltage stimuli with magnitude 9.6 kV_{pp} (bipolar), rise time 50 µs, and duty cycle 50 %. (a) Uncharged PVDF, (b) Negative polarity electret

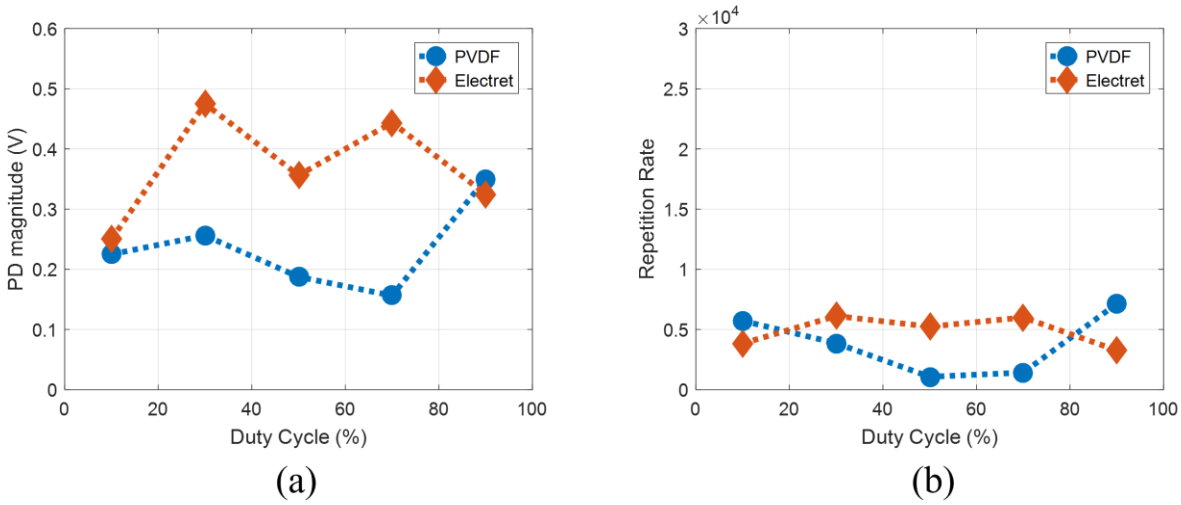

Figure 5.48 Comparison of cavity discharge performance of uncharged PVDF and negatively charged electret at various duty cycle under bipolar voltage. (a) Maximum PD magnitude, (b) Repetition rate.

5.4 Impact of switching frequency

5.4.1 Sinusoidal PWM (SPWM) generation and PD detection

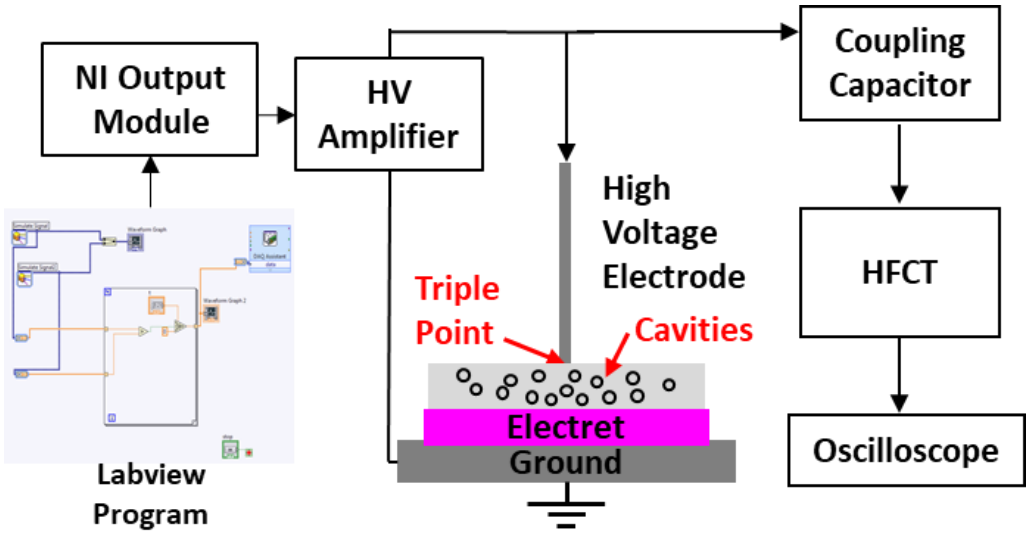

Figure 5.49 PD experiments under sinusoidal PWM signal.

PD experiments are conducted under SPWM voltage stress. The SPWM signal is generated using LabView graphical programming environment. In this graphical program, a 60 Hz sinusoidal signal is modulated with a sawtooth signal of with varying frequency, which is the switching frequency. Figure 5.49 shows the schematic diagram of the PD detection circuit under SPWM signal. The resulting SPWM has amplitude that varies based on the gain factor and rise time 50 µs. An NI voltage output module is used to connect the generated SPWM voltage to PD measurement setup. The SPWM signal generated with LabView graphical program is connected to the high voltage amplifier (Trek Model 20/20 C-HS-L) through NI voltage output module. A

coupling capacitor and high frequency current transformer are used to detect the cavity discharge and surface discharge which is then recorded in high frequency oscilloscope.

5.4.2 Surface discharge

Surface discharge experiments are conducted with same testbed as described in Chapter V in Figure 3.3. Both positive and negative polarity electrets are fabricated, and their PD mitigation performance is compared with the uncharged PVDF films. The switching frequency is varied from 500 Hz to 20,000 Hz (500 Hz, 1000 Hz, 5000 Hz, 10,000 Hz, and 20,000 Hz). The square voltage magnitude is kept at 3.4 kV_{pp}. To observe the performance of electret under various voltage polarity stress, both positive polarity and negative polarity electrets are stressed under positive, negative, and bipolar voltage stresses.

5.4.2.1 Positively charged electret

In this case, electrets are fabricated based on the triode corona charging method with PVDF film of thickness 25.4 μm. For fabricating electrets, the charging conditions maintained are described in the Table 5.1. PD magnitude and repetition achieved with both uncharged PVDF and electrets are compared under various voltage polarity stress.

a) Positive polarity stress

An uncharged PVDF and positively charged electret are stressed under positive polarity square voltage stimuli with magnitude varying between 0 to 3.4 kV at different switching frequency. Figure 5.50 shows the PD discharge achieved with uncharged PVDF (Figure 5.50(a)) and electret (Figure 5.50(b)) where the square voltage has the rise time of 50 μs and switching

frequency of 5000 Hz. To evaluate electrets performance, both maximum PD magnitudes and repetition rate with PVDF and electret are compared. Figure 5.51(a) compares the maximum PD magnitudes and Figure 5.51(b) compares the PD repetition rate per cycle with PVDF and electrets at different frequency. It is observed in Figure 5.50 that, there is a substantial reduction in the PD magnitude as well as PD occurrence when PDVF is replaced with positive polarity electret when positive polarity voltage is applied. In Figure 5.51, it is observed that PD magnitude and repletion rate remains almost same as the switching frequency increase from 500 Hz to 20000 Hz when uncharged PVDF is used. When the uncharged PVDF is replaced with the electret fabricated under an optimum condition described in Table 5.1, there is a significant reduction in the PD magnitude as well as in the repetition rate per cycle.

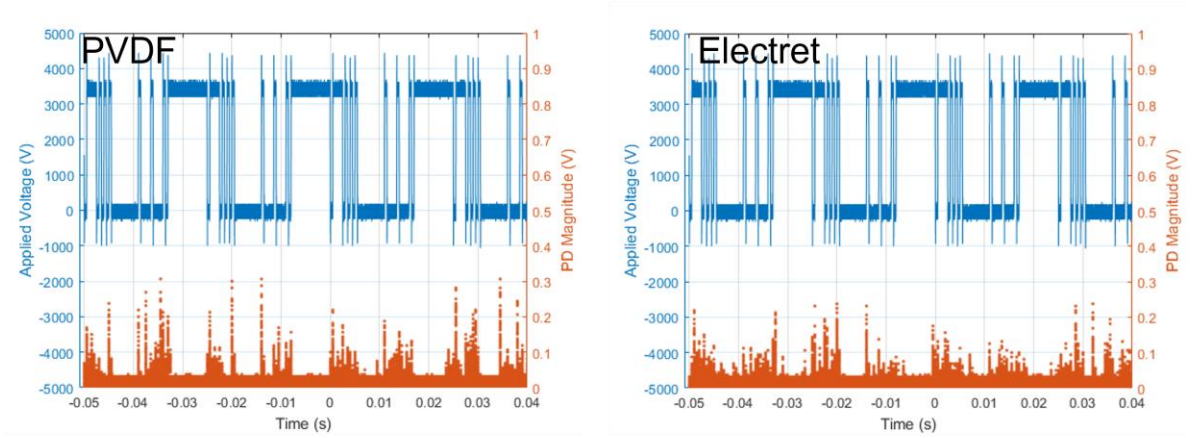

Figure 5.50 PD signal caused by surface discharge under square voltage stimuli with magnitude 3.4 kV_{pp}, rise time 50 µs, and switching frequency 5000 Hz. (a) Uncharged PVDF, (b) Positive polarity electret

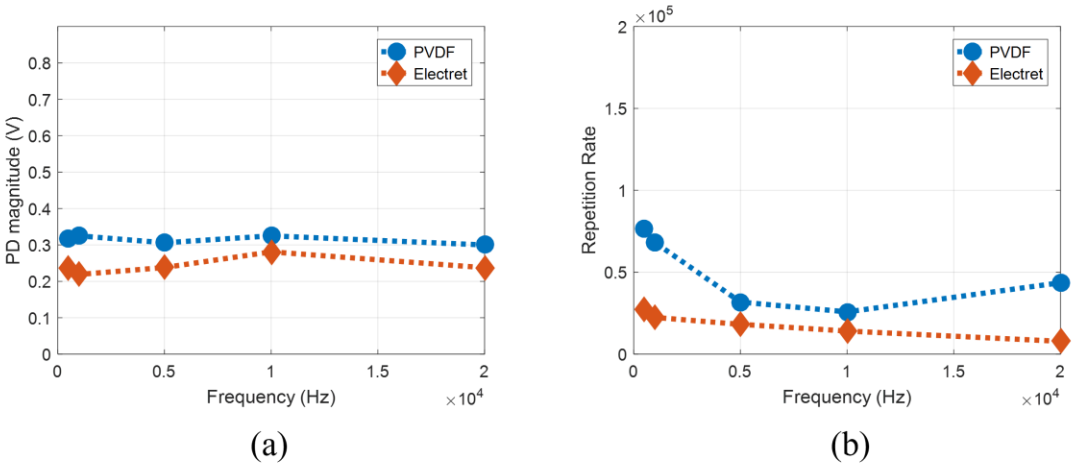

Figure 5.51 Comparison of surface discharge performance of uncharged PVDF and positively charged electret at various switching frequency under positive voltage. (a) Maximum PD magnitude, (b) Repetition rate

b) Negative polarity stress

An uncharged PVDF and positively charged electret are stressed under negative polarity square voltage stimuli with magnitude varying between 0 to -3.4 kV at different switching frequency. Figure 5.52 shows the PD discharge achieved with uncharged PVDF (Figure 5.52(a)) and electret (Figure 5.52(b)) where the square voltage has the rise time of 50 µs and switching frequency of 5000 Hz. To evaluate electrets performance, both maximum PD magnitudes and repetition rate with PVDF and electret are compared. Figure 5.53(a) compares the maximum PD magnitudes and Figure 5.53(b) compares the PD repetition rate per cycle with PVDF and electrets at different frequency. It is observed in Figure 5.52 that, there is a drastic increase in the PD magnitude as well as PD occurrence when PDVF is replaced with positive polarity electret when negative polarity voltage is applied. In Figure 5.53, it is observed that PD magnitude and repletion rate remains almost same as the switching frequency increase from 500 Hz to 20000 Hz when uncharged PVDF is used. When the uncharged PVDF is replaced with the electret fabricated under

an optimum condition described in Table 5.1, there is a substantial increase in the PD magnitude as well as in the repetition rate per cycle.

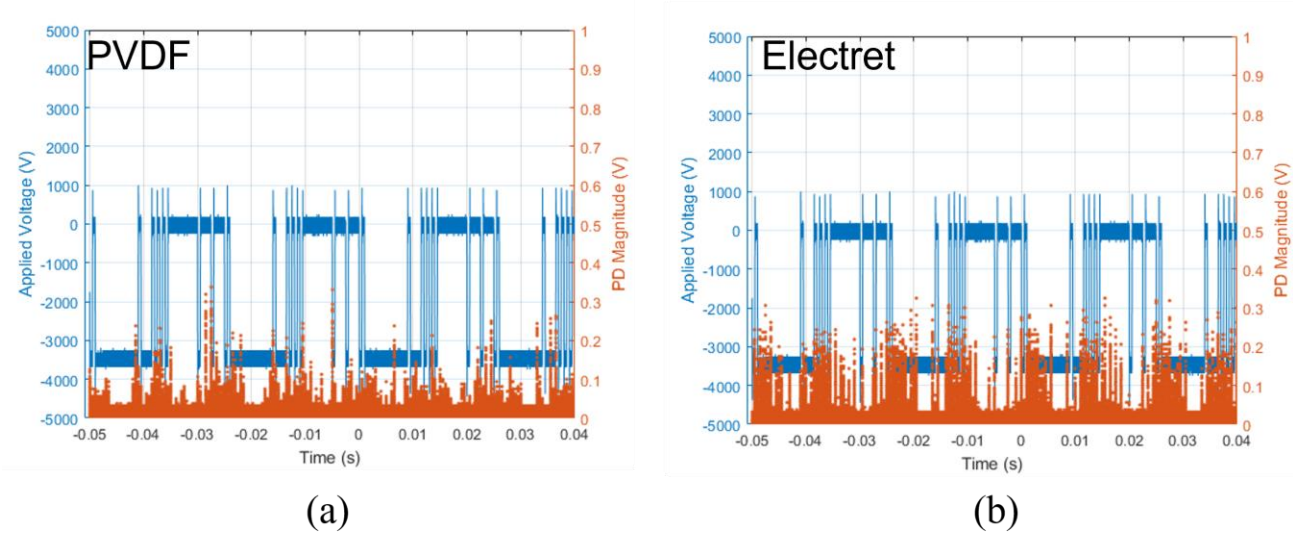

Figure 5.52 PD signal caused by surface discharge under square voltage stimuli with magnitude -3.4 kV_{pp}, rise time 50 µs, and switching frequency 5000 Hz. (a) Uncharged PVDF, (b) Positive polarity electret

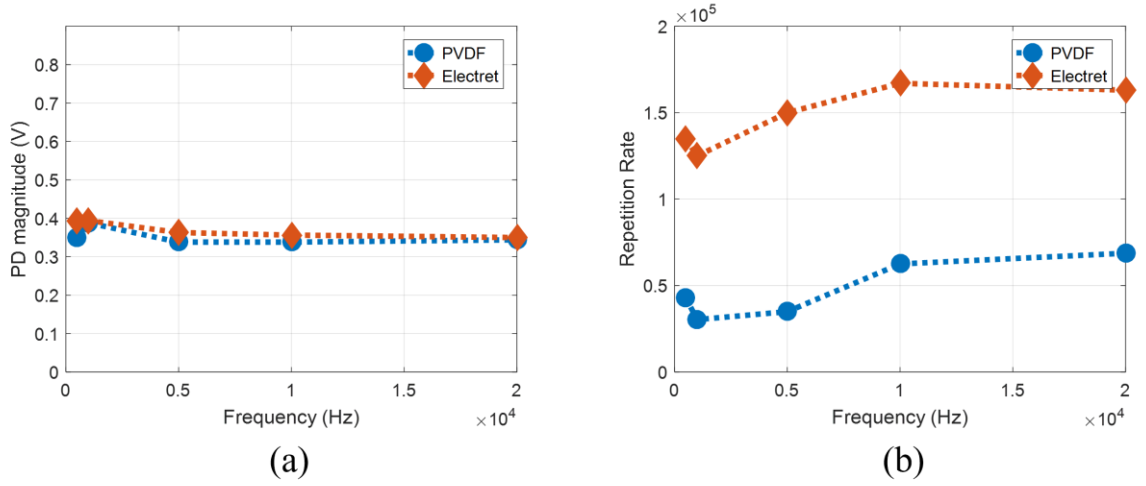

Figure 5.53 Comparison of surface discharge performance of uncharged PVDF and positively charged electret at various switching frequency under negative voltage. (a) Maximum PD magnitude, (b) Repetition rate

c) Bipolar stress

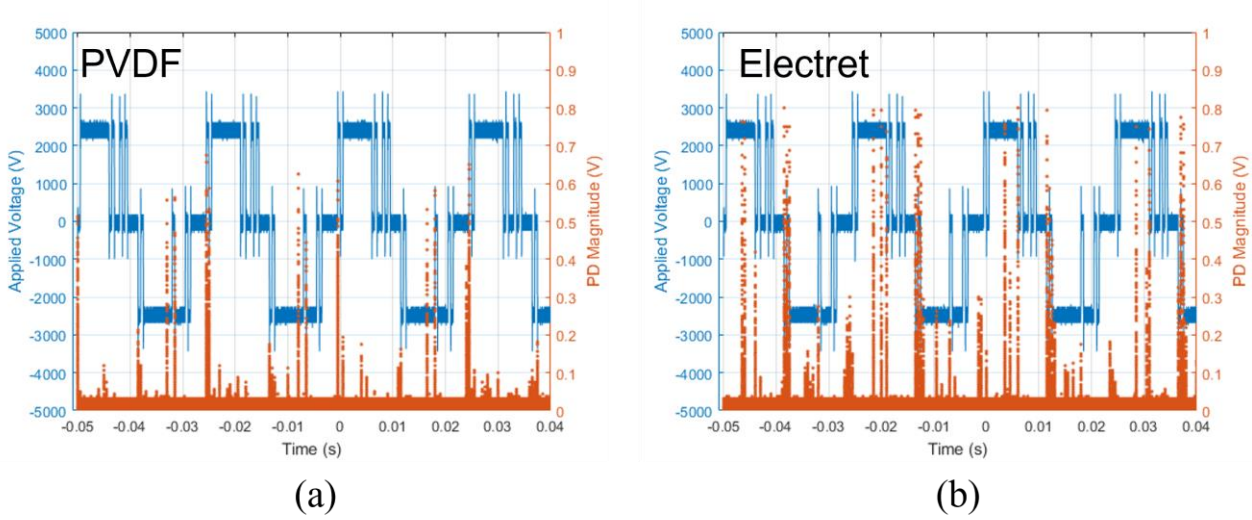

Figure 5.54 PD signal caused by surface discharge under square voltage stimuli with magnitude 2 kV_{pp} (bipolar), rise time 50 µs, and switching frequency 5000 Hz. (a) Uncharged PVDF, (b) Positive polarity electret

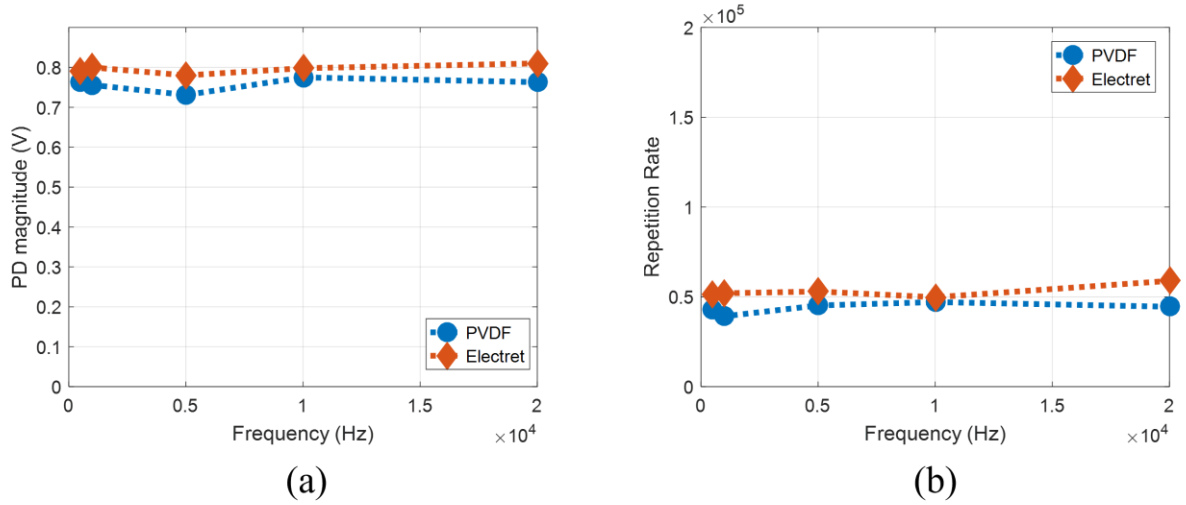

Figure 5.55 Comparison of surface discharge performance of uncharged PVDF and positively charged electret at various switching frequency under negative voltage. (a) Maximum PD magnitude, (b) Repetition rate

An uncharged PVDF and positively charged electret are stressed under bipolar square voltage stimuli with magnitude varying between -2 to -2 kV at different switching frequency. Figure 5.54 shows the PD discharge achieved with uncharged PVDF (Figure 5.54(a)) and electret (Figure 5.54(b)) where the square voltage has the rise time of 50 µs and switching frequency of 5000 Hz. To evaluate electrets performance, both maximum PD magnitudes and repetition rate with PVDF and electret are compared. Figure 5.55(a) compares the maximum PD magnitudes and Figure 5.55(b) compares the PD repetition rate per cycle with PVDF and electrets at different frequency. It is observed in Figure 5.54 that, there is a drastic increase in the PD magnitude as well as PD occurrence when PDVF is replaced with positive polarity electret when bipolar voltage is applied. In Figure 5.55, it is observed that PD magnitude and repletion rate remains almost same as the switching frequency increase from 500 Hz to 20000 Hz when uncharged PVDF is used. When the uncharged PVDF is replaced with the electret fabricated under an optimum condition

described in Table 5.1, there is a substantial increase in the PD magnitude as well as in the repetition rate per cycle.

5.4.2.2 Negatively charged electret

In this case, electrets are fabricated based on the triode corona charging method with PVDF film of thickness 25.4 μm. For fabricating electrets, the charging conditions maintained are described in the Table 5.2. PD magnitude and repetition achieved with both uncharged PVDF and electrets are compared under various voltage polarity stress.

a) Positive polarity stress

An uncharged PVDF and negatively charged electret are stressed under positive polarity square voltage stimuli with magnitude varying between 0 to 3.4 kV at different switching frequency. Figure 5.56 shows the PD discharge achieved with uncharged PVDF (Figure 5.56 (a)) and electret (Figure 5.56(b)) where the square voltage has the rise time of 50 μs and switching frequency of 5000 Hz. To evaluate electrets performance, both maximum PD magnitudes and repetition rate with PVDF and electret are compared. Figure 5.57(a) compares the maximum PD magnitudes and Figure 5.57(b) compares the PD repetition rate per cycle with PVDF and electrets at different frequency. It is observed in Figure 5.56 that, there is a drastic increase in the PD magnitude as well as PD occurrence when PDVF is replaced with negative polarity electret when positive polarity voltage is applied. In Figure 5.57, it is observed that PD magnitude and repletion rate remains almost same as the switching frequency increase from 500 Hz to 20000 Hz when uncharged PVDF is used. When the uncharged PVDF is replaced with the electret fabricated under an optimum condition described in Table 5.2, there is a substantial increase in the PD magnitude as well as in the repetition rate per cycle.

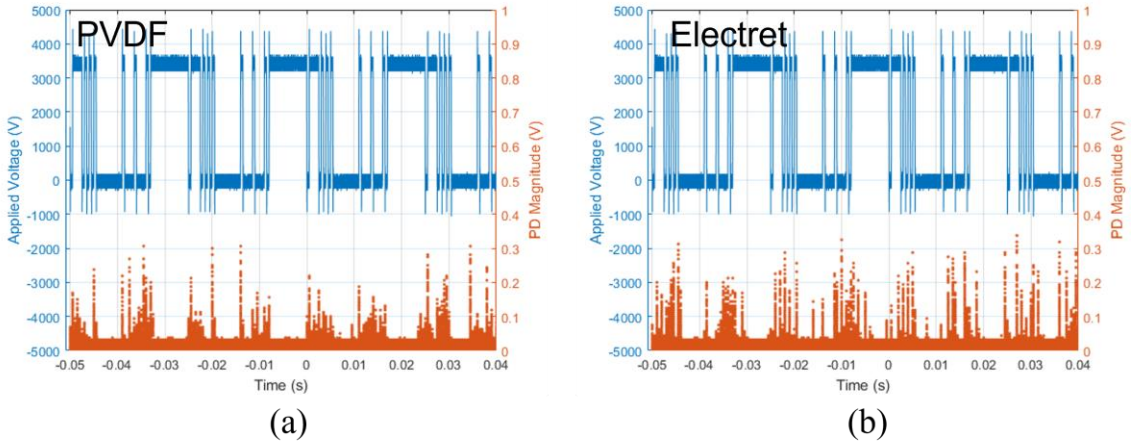

Figure 5.56 PD signal caused by surface discharge under square voltage stimuli with magnitude 3.4 kV_{pp}, rise time 50 µs, and switching frequency 5000 Hz. (a) Uncharged PVDF, (b) Negative polarity electret

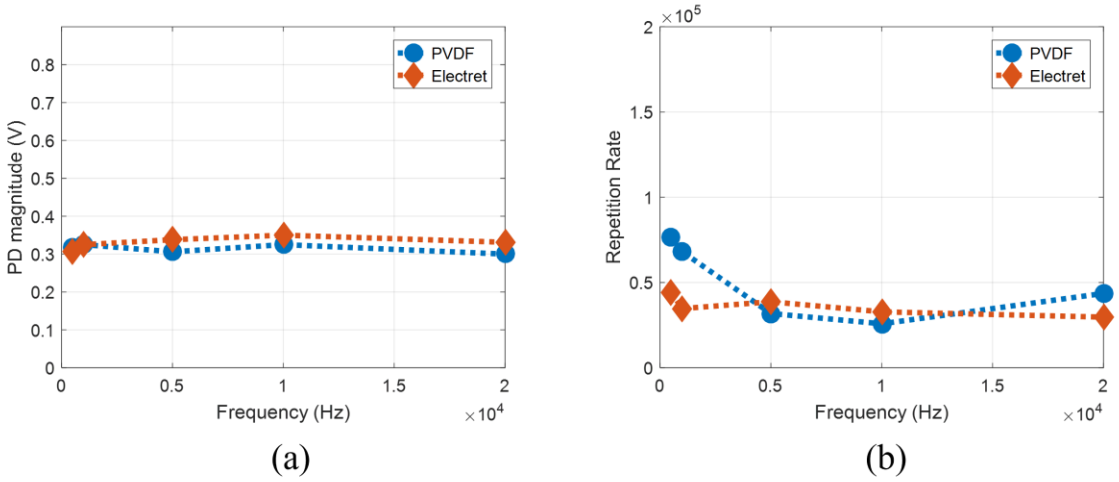

Figure 5.57 Comparison of surface discharge performance of uncharged PVDF and negatively charged electret at various switching frequency under positive voltage. (a) Maximum PD magnitude, (b) Repetition rate

b) Negative polarity stress

An uncharged PVDF and negatively charged electret are stressed under negative polarity square voltage stimuli with magnitude varying between 0 to -3.4 kV at different switching frequency. Figure 5.58 shows the PD discharge achieved with uncharged PVDF (Figure 5.58(a)) and electret (Figure 5.58(b)) where the square voltage has the rise time of 50 μs and switching frequency of 5000 Hz. To evaluate electrets performance, both maximum PD magnitudes and repetition rate with PVDF and electret are compared. Figure 5.59(a) compares the maximum PD magnitudes and Figure 5.59(b) compares the PD repetition rate per cycle with PVDF and electrets at different frequency. It is observed in Figure 5.58 that, there is a substantial reduction in the PD magnitude as well as PD occurrence when PDVF is replaced with negative polarity electret when negative polarity voltage is applied. In Figure 5.59, it is observed that PD magnitude and repletion rate remains almost same as the switching frequency increase from 500 Hz to 20000 Hz when uncharged PVDF is used. When the uncharged PVDF is replaced with the electret fabricated under an optimum condition described in Table 5.2, there is a significant reduction in the PD magnitude as well as in the repetition rate per cycle.

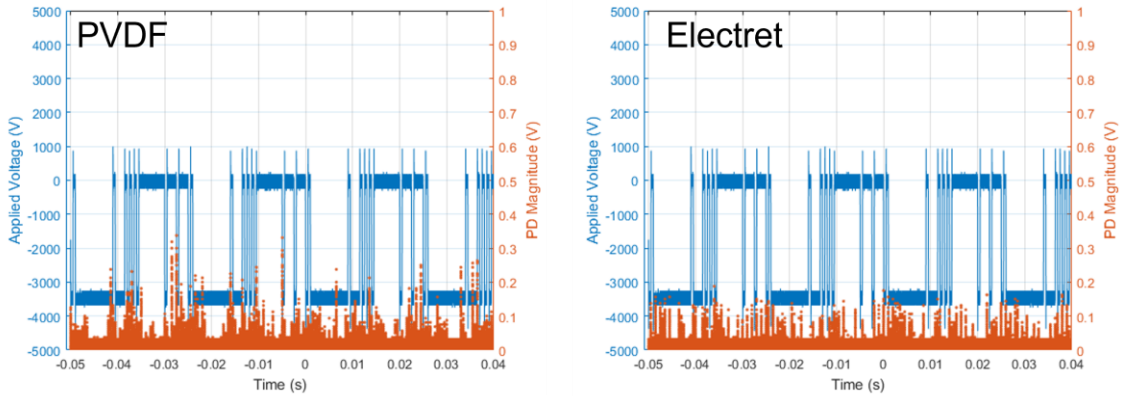

(a) (b)

Figure 5.58 PD signal caused by surface discharge under square voltage stimuli with magnitude -3.4 kV_{pp}, rise time 50 µs, and switching frequency 5000 Hz. (a) Uncharged PVDF, (b) Negative polarity electret

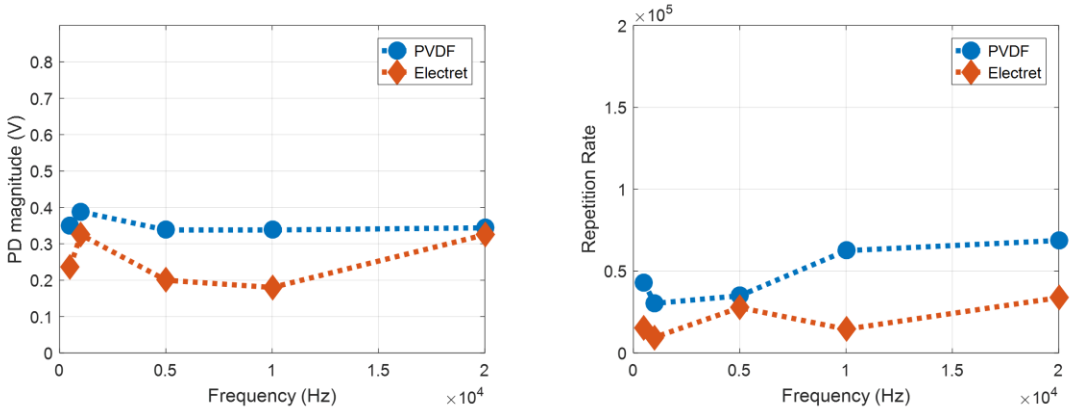

(a) (b)

Figure 5.59 Comparison of surface discharge performance of uncharged PVDF and negatively charged electret at various switching frequency under positive voltage. (a) Maximum PD magnitude, (b) Repetition rate

c) Bipolar stress

An uncharged PVDF and negatively charged electret are stressed under bipolar square voltage stimuli with magnitude varying between -2 to -2 kV at different switching frequency. Figure 5.60 shows the PD discharge achieved with uncharged PVDF (Figure 5.60(a)) and electret (Figure 5.60(b)) where the square voltage has the rise time of 50 μs and switching frequency of 5000 Hz. To evaluate electrets performance, both maximum PD magnitudes and repetition rate with PVDF and electret are compared. Figure 5.61(a) compares the maximum PD magnitudes and Figure 5.61(b) compares the PD repetition rate per cycle with PVDF and electrets at different frequency. It is observed in Figure 5.60 that, there is a drastic increase in the PD magnitude as well as PD occurrence when PDVF is replaced with negative polarity electret when bipolar voltage is applied. In Figure 5.61, it is observed that PD magnitude and repletion rate remains almost same as the switching frequency increase from 500 Hz to 20000 Hz when uncharged PVDF is used. When the uncharged PVDF is replaced with the electret fabricated under an optimum condition described in Table 5.2, there is a substantial increase in the PD magnitude as well as in the repetition rate per cycle.

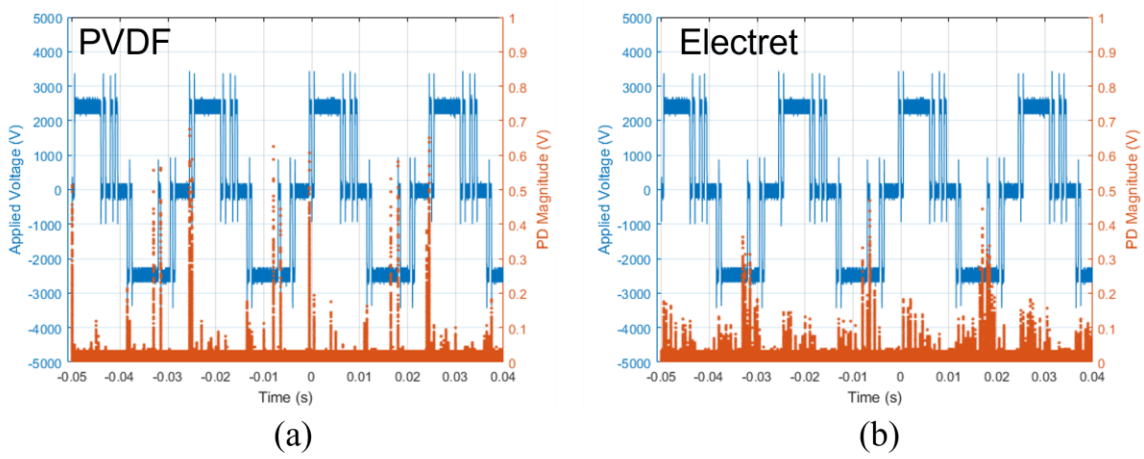

Figure 5.60 PD signal caused by surface discharge under square voltage stimuli with magnitude 2 kV_{pp} (bipolar), rise time 50 µs, and switching frequency 5000 Hz. (a) Uncharged PVDF, (b) Negative polarity electret

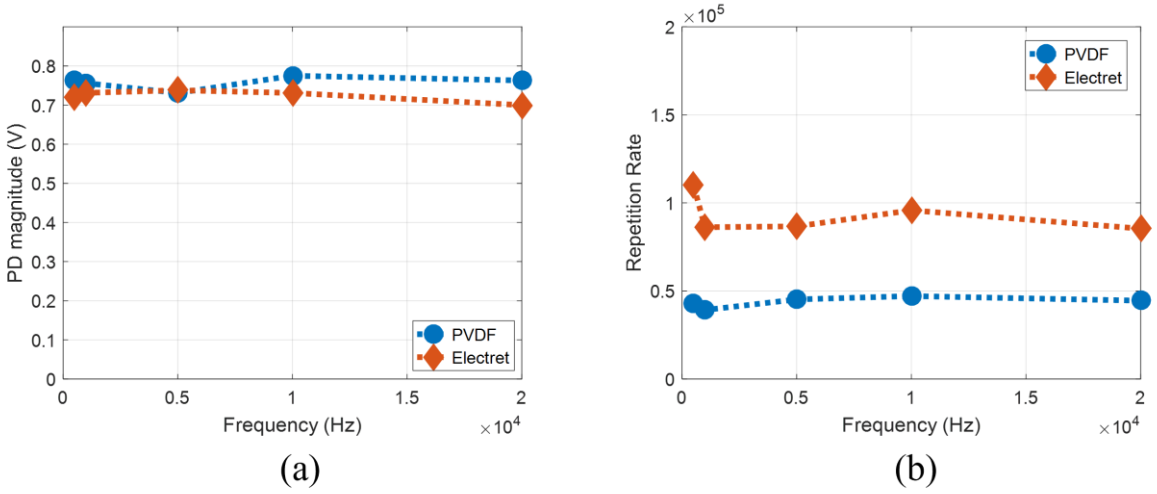

Figure 5.61 Comparison of surface discharge performance of uncharged PVDF and negatively charged electret at various switching frequency under bipolar voltage. (a) Maximum PD magnitude, (b) Repetition rate

5.4.3 Cavity discharge

Cavity discharge experiments are conducted with same testbed as described in Chapter V in Figure 3.5. Both positive and negative polarity electrets are fabricated, and their PD mitigation performance is compared with the uncharged PVDF films. The switching frequency is varied from 500 Hz to 20,000 Hz (500 Hz, 1000 Hz, 5000 Hz, 10,000 Hz, and 20,000 Hz). The square voltage magnitude is kept at 10 kV_{pp}. To observe the performance of electret under various voltage polarity stress, both positive polarity and negative polarity electrets are stressed under positive, negative, and bipolar voltage stress.

5.4.3.1 Positively charged electret

In this case, electrets are fabricated based on the triode corona charging method with PVDF film of thickness 25.4 μm. For fabricating electrets, the charging conditions maintained are described in the Table 5.1. PD magnitude and repetition achieved with both uncharged PVDF and electrets are compared under various voltage polarity stress.

a) Positive polarity stress

An uncharged PVDF and positively charged electret are stressed under positive polarity square voltage stimuli with magnitude varying between 0 to 9 kV at different switching frequency. Figure 5.62 shows the PD discharge achieved with uncharged PVDF (Figure 5.62(a)) and electret (Figure 5.62(b)) where the square voltage has the rise time of 50 μs and switching frequency of 5000 Hz. To evaluate electrets performance, both maximum PD magnitudes and repetition rate with PVDF and electret are compared. Figure 5.63(a) compares the maximum PD magnitudes and Figure 5.63(b) compares the PD repetition rate per cycle with PVDF and electrets at different frequency. It is observed in Figure 5.62 that, there is a substantial reduction in the PD magnitude

as well as PD occurrence when PDVF is replaced with positive polarity electret when positive polarity voltage is applied. In Figure 5.63, it is observed that PD magnitude and repletion rate as the switching frequency increase from 500 Hz to 20000 Hz and both PD magnitude and repetition rate decrease at switching frequency 20000 Hz when uncharged PVDF is used. When the uncharged PVDF is replaced with the electret fabricated under an optimum condition described in Table 5.1, there is a significant reduction in the PD magnitude as well as in the repetition rate per cycle.

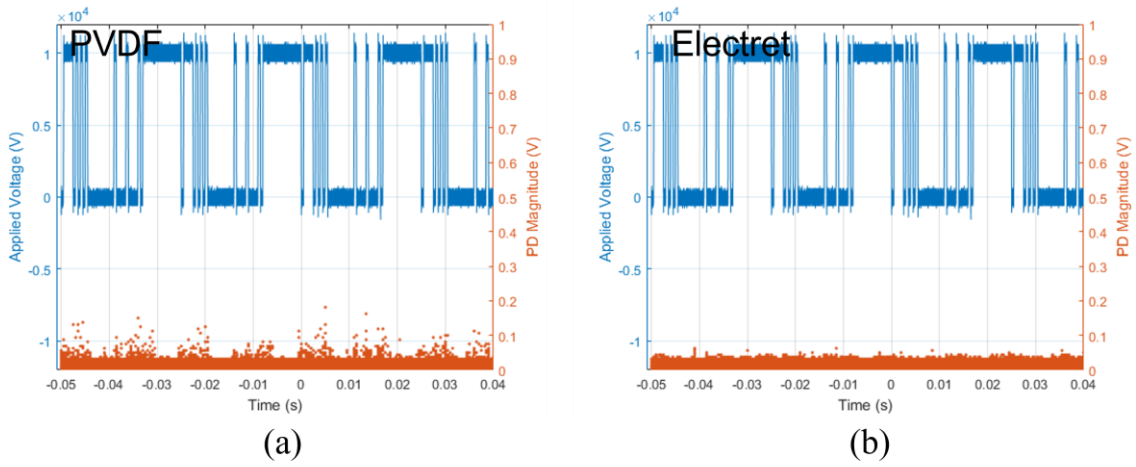

Figure 5.62 PD signal caused by cavity discharge under square voltage stimuli with magnitude 9 kV_{pp}, rise time 50 µs, and switching frequency 5000 Hz. (a) Uncharged PVDF, (b) Positive polarity electret

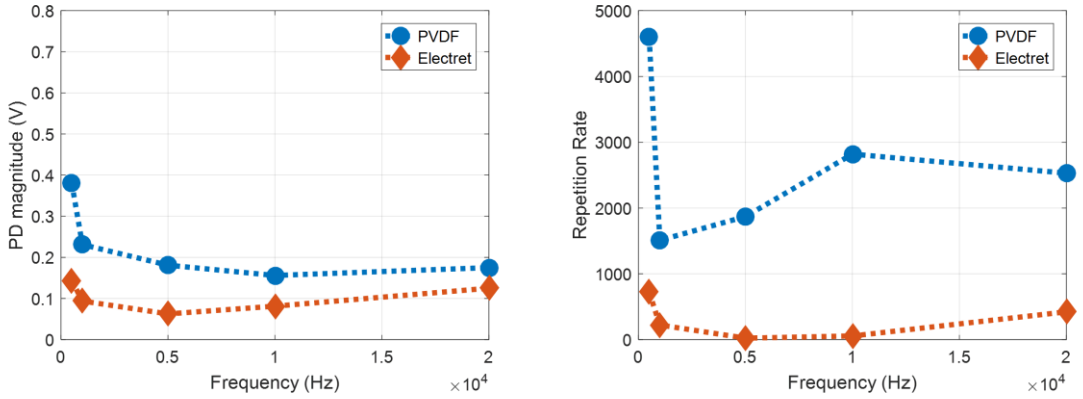

Figure 5.63 Comparison of cavity discharge performance of uncharged PVDF and positively charged electret at various switching frequency under positive voltage. (a) Maximum PD magnitude, (b) Repetition rate

b) Negative polarity stress

An uncharged PVDF and positively charged electret are stressed under negative polarity square voltage stimuli with magnitude varying between 0 to -9 kV at different switching frequency. Figure 5.64 shows the PD discharge achieved with uncharged PVDF (Figure 5.64 (a)) and electret (Figure 5.64 (b)) where the square voltage has the rise time of 50 µs and switching frequency of 5000 Hz. To evaluate electrets performance, both maximum PD magnitudes and repetition rate with PVDF and electret are compared. Figure 5.65 (a) compares the maximum PD magnitudes and Figure 5.65(b) compares the PD repetition rate per cycle with PVDF and electrets at different frequency. It is observed in Figure 5.64 that, there is a drastic increase in the PD magnitude as well as PD occurrence when PDVF is replaced with positive polarity electret when negative polarity voltage is applied. In Figure 5.65, it is observed that PD magnitude and repletion rate as the switching frequency increase from 500 Hz to 20000 Hz and both PD magnitude and repetition rate decrease at switching frequency 20000 Hz when uncharged PVDF is used. When

the uncharged PVDF is replaced with the electret fabricated under an optimum condition described in Table 5.1, there is a substantial increase in the PD magnitude as well as in the repetition rate per cycle.

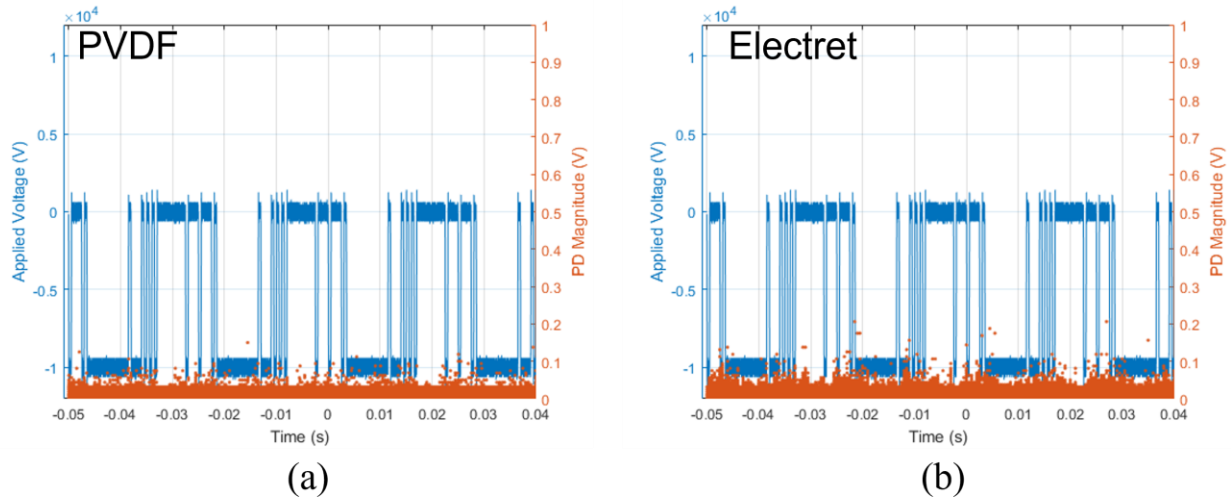

Figure 5.64 PD signal caused by cavity discharge under square voltage stimuli with magnitude -9 kV_{pp}, rise time 50 µs, and switching frequency 5000 Hz. (a) Uncharged PVDF, (b) Positive polarity electret

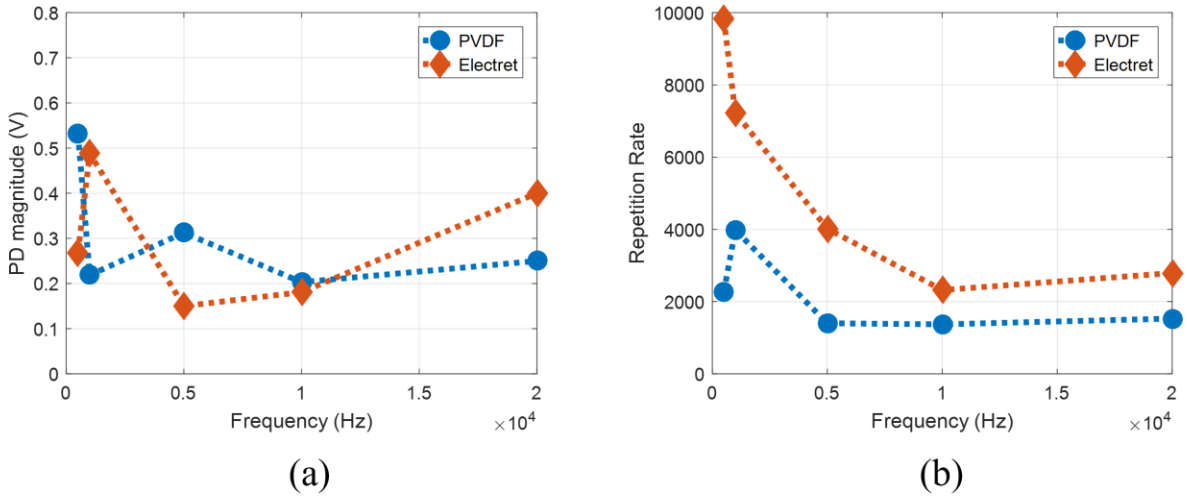

Figure 5.65 Comparison of cavity discharge performance of uncharged PVDF and positively charged electret at various switching frequency under negative voltage. (a) Maximum PD magnitude, (b) Repetition rate

c) Bipolar stress

An uncharged PVDF and positively charged electret are stressed under bipolar square voltage stimuli with magnitude varying between -8 to 8 kV at different switching frequency. Figure 5.66 shows the PD discharge achieved with uncharged PVDF (Figure 5.66 (a)) and electret (Figure 5.66 (b)) where the square voltage has the rise time of 50 µs and switching frequency of 5000 Hz. To evaluate electrets performance, both maximum PD magnitudes and repetition rate with PVDF and electret are compared. Figure 5.67 (a) compares the maximum PD magnitudes and Figure 5.67 (b) compares the PD repetition rate per cycle with PVDF and electrets at different frequency. It is observed in Figure 5.66 that, there is a drastic increase in the PD magnitude as well as PD occurrence when PDVF is replaced with positive polarity electret when bipolar voltage is applied. In Figure 5.67, it is observed that PD magnitude and repletion rate remains almost same as the switching frequency increase from 500 Hz to 20000 Hz both PD magnitude and repetition rate

decrease at switching frequency 20000 Hz when uncharged PVDF is used. When the uncharged PVDF is replaced with the electret fabricated under an optimum condition described in Table 5.1, there is a substantial increase in the PD magnitude as well as in the repetition rate per cycle.

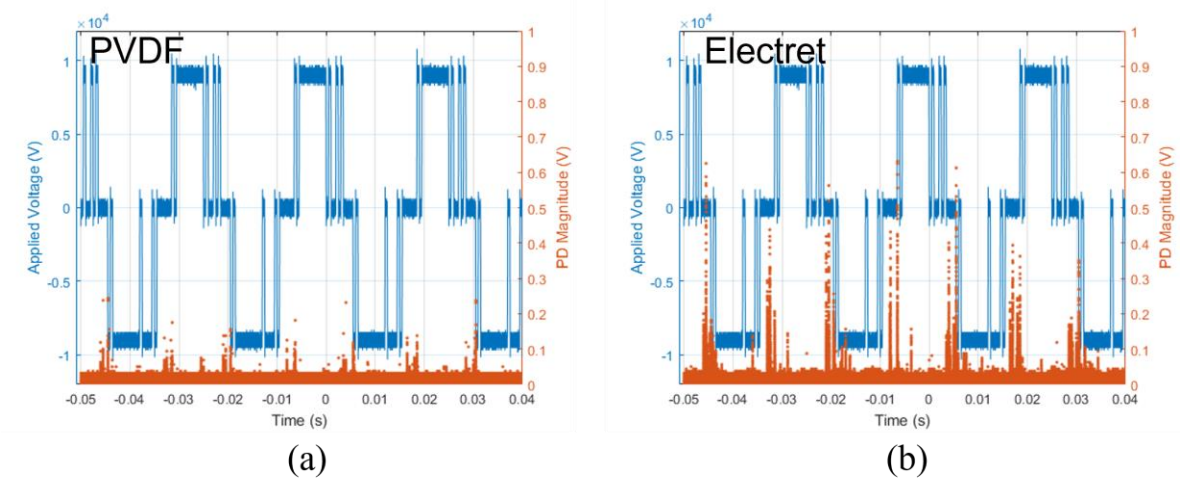

Figure 5.66 PD signal caused by cavity discharge under square voltage stimuli with magnitude 8 kV_{pp} (Bipolar), rise time 50 µs, and switching frequency 5000 Hz. (a) Uncharged PVDF, (b) Positive polarity electret

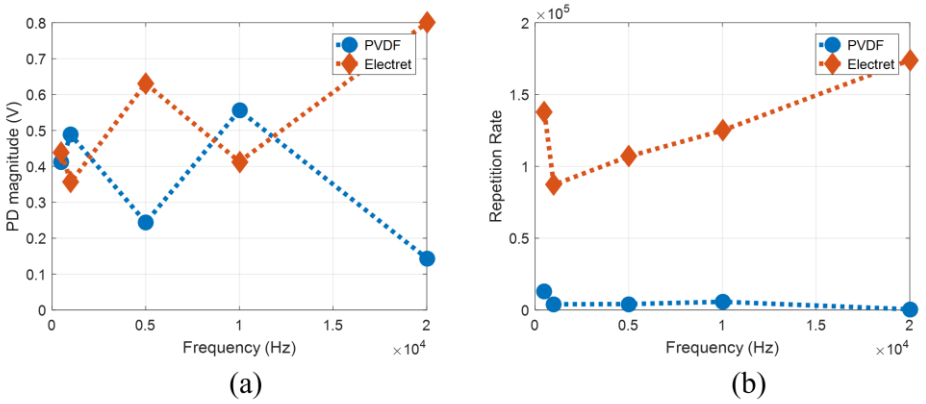

Figure 5.67 Comparison of cavity discharge performance of uncharged PVDF and positively charged electret at various switching frequency under bipolar voltage. (a) Maximum PD magnitude, (b) Repetition rate

5.4.3.2 Negatively charged electret

In this case, electrets are fabricated based on the triode corona charging method with PVDF film of thickness 25.4 µm. For fabricating electrets, the charging conditions maintained are described in the Table 5.2. PD magnitude and repetition achieved with both uncharged PVDF and electrets are compared under various voltage polarity stress.

a) Positive polarity stress

An uncharged PVDF and negatively charged electret are stressed under positive polarity square voltage stimuli with magnitude varying between 0 to 9 kV at different switching frequency. Figure 5.68 shows the PD discharge achieved with uncharged PVDF (Figure 5.68 (a)) and electret (Figure 5.68 (b)) where the square voltage has the rise time of 50 µs and switching frequency of 5000 Hz. To evaluate electrets performance, both maximum PD magnitudes and repetition rate with PVDF and electret are compared. Figure 5.69(a) compares the maximum PD magnitudes and Figure 5.69(b) compares the PD repetition rate per cycle with PVDF and electrets at different frequency. It is observed in Figure 5.68 that, there is a drastic increase in the PD magnitude as well as PD occurrence when PDVF is replaced with negative polarity electret when

positive polarity voltage is applied. In Figure 5.69, it is observed that PD magnitude and repletion rate remains almost same as the switching frequency increase from 500 Hz to 20000 and both PD magnitude and repetition rate decrease at switching frequency 20000 Hz when uncharged PVDF is used. When the uncharged PVDF is replaced with the electret fabricated under an optimum condition described in Table 5.2, there is a substantial increase in the PD magnitude as well as in the repetition rate per cycle.

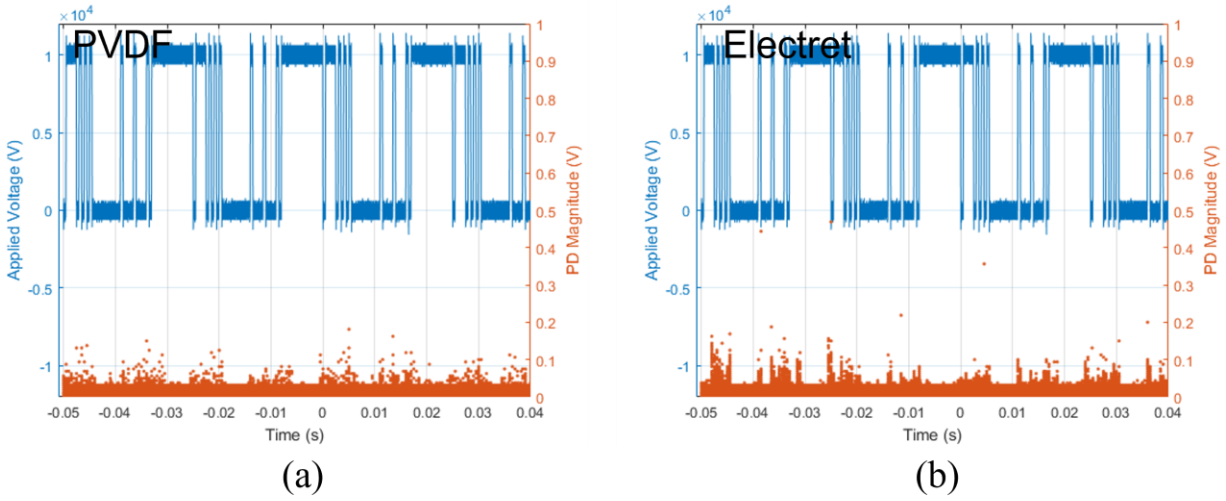

Figure 5.68 PD signal caused by cavity discharge under square voltage stimuli with magnitude 9 kV_{pp}, rise time 50 µs, and switching frequency 5000 Hz. (a) Uncharged PVDF, (b) Negative polarity electret

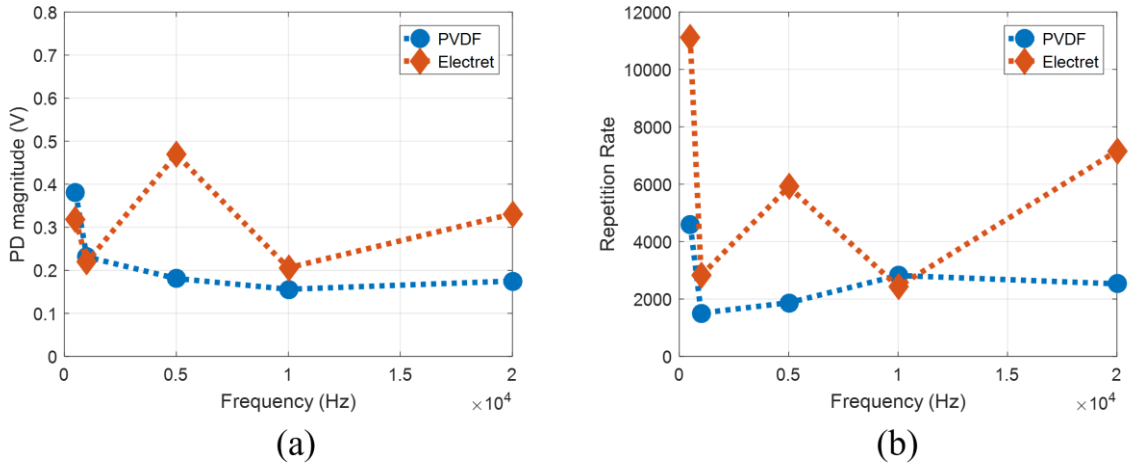

Figure 5.69 Comparison of cavity discharge performance of uncharged PVDF and negatively charged electret at various switching frequency under positive voltage. (a) Maximum PD magnitude, (b) Repetition rate

b) Negative polarity stress

An uncharged PVDF and negatively charged electret are stressed under negative polarity square voltage stimuli with magnitude varying between 0 to -9 kV at different switching frequency. Figure 5.70 shows the PD discharge achieved with uncharged PVDF (Figure 5.70 (a)) and electret (Figure 5.70 (b)) where the square voltage has the rise time of 50 µs and switching frequency of 5000 Hz. To evaluate electrets performance, both maximum PD magnitudes and repetition rate with PVDF and electret are compared. Figure 5.71 (a) compares the maximum PD magnitudes and Figure 7.71 (b) compares the PD repetition rate per cycle with PVDF and electrets at different frequency. It is observed in Figure 7.70 that, there is a substantial reduction in the PD magnitude as well as PD occurrence when PDVF is replaced with negative polarity electret when negative polarity voltage is applied. In Figure 5.71, it is observed that PD magnitude and repletion rate remains almost same as the switching frequency increase from 500 Hz to 20000 Hz and both PD magnitude and repetition rate decrease at switching frequency 20000 Hz when uncharged

PVDF is used. When the uncharged PVDF is replaced with the electret fabricated under an optimum condition described in Table 5.2, there is a significant reduction in the PD magnitude as well as in the repetition rate per cycle.

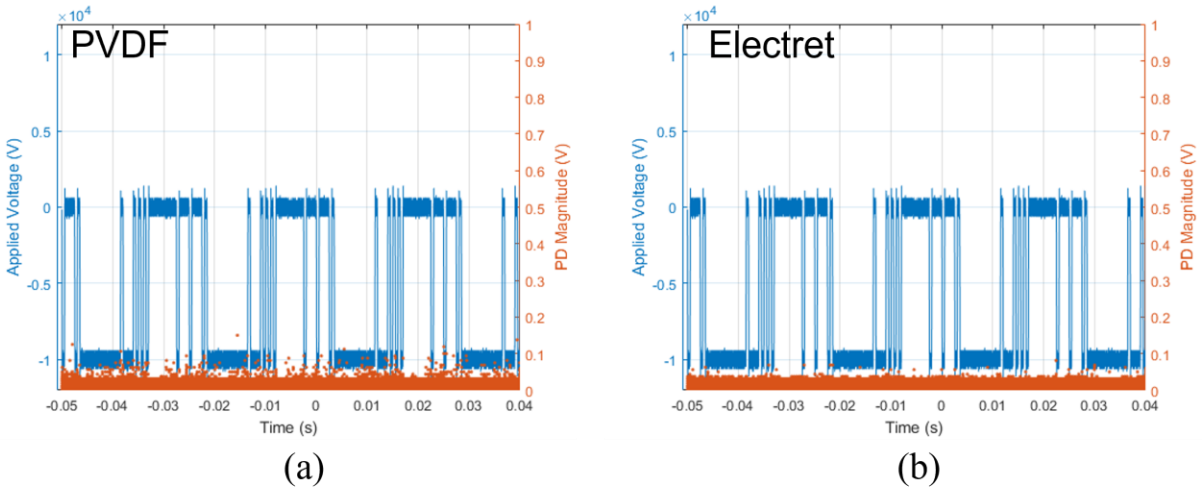

Figure 5.70 PD signal caused by cavity discharge under square voltage stimuli with magnitude -9 kV_{pp}, rise time 50 µs, and switching frequency 5000 Hz. (a) Uncharged PVDF, (b) Negative polarity electret

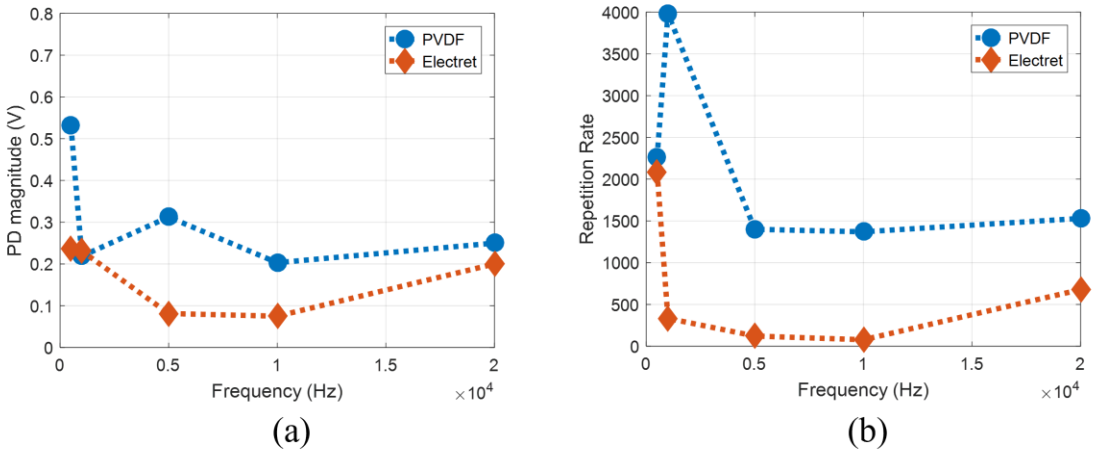

Figure 5.71 Comparison of cavity discharge performance of uncharged PVDF and negatively charged electret at various switching frequency under negative voltage. (a) Maximum PD magnitude, (b) Repetition rate

c) Bipolar stress

An uncharged PVDF and negatively charged electret are stressed under negative polarity square voltage stimuli with magnitude varying between -8 to 8 kV at different switching frequency. Figure 5.72 shows the PD discharge achieved with uncharged PVDF (Figure 5.72 (a)) and electret (Figure 5.72 (b)) where the square voltage has the rise time of 50 µs and switching frequency of 5000 Hz. To evaluate electrets performance, both maximum PD magnitudes and repetition rate with PVDF and electret are compared. Figure 5.73 (a) compares the maximum PD magnitudes and Figure 5.73 (b) compares the PD repetition rate per cycle with PVDF and electrets at different frequency. It is observed in Figure 5.73 that, there is a substantial reduction in the PD magnitude as well as PD occurrence when PDVF is replaced with negative polarity electret when negative polarity voltage is applied. In Figure 5.73, it is observed that PD magnitude and repletion rate remains almost same as the switching frequency increase from 500 Hz to 20000 Hz and both PD magnitude and repetition rate decrease at switching frequency of 20000 Hz when uncharged

PVDF is used. When the uncharged PVDF is replaced with the electret fabricated under an optimum condition described in Table 5.2, there is a significant reduction in the PD magnitude as well as in the repetition rate per cycle.

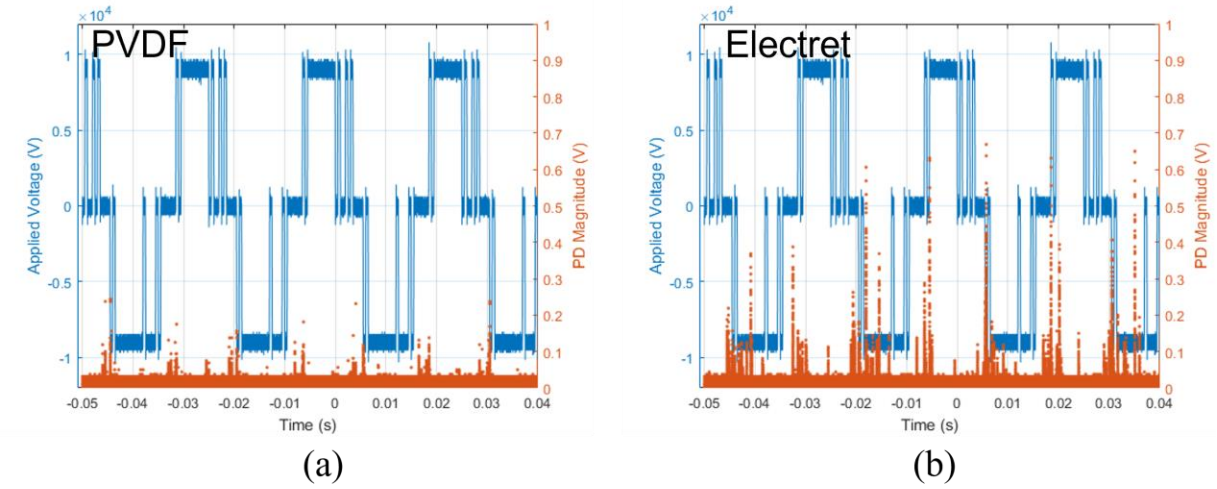

Figure 5.72 PD signal caused by cavity discharge under square voltage stimuli with magnitude 8 kV_{pp} (Bipolar), rise time 50 µs, and switching frequency 5000 Hz. (a) Uncharged PVDF, (b) Negative polarity electret

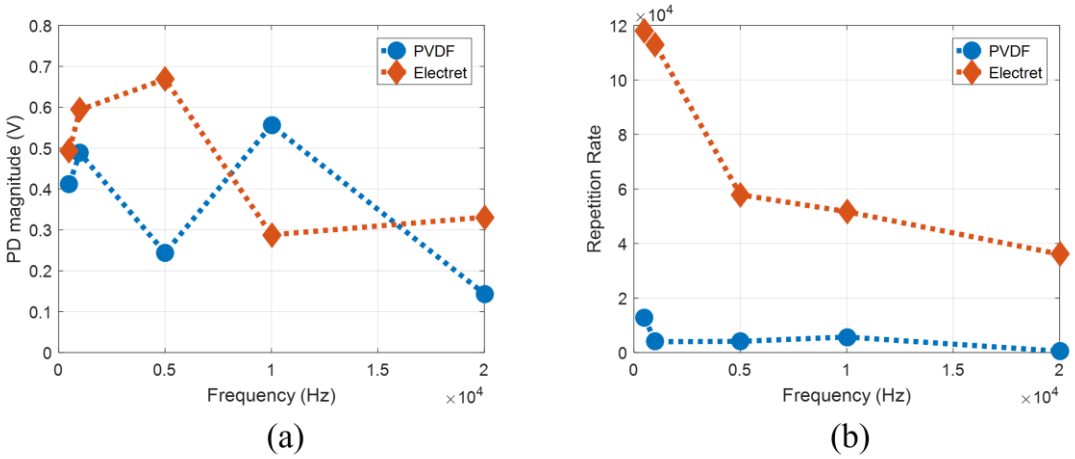

Figure 5.73 Comparison of cavity discharge performance of uncharged PVDF and negatively charged electret at various switching frequency under bipolar voltage. (a) Maximum PD magnitude, (b) Repetition rate

5.5 Summary

In this section, electrets performance in mitigating PD is evaluated under different power electronics voltage parameters, including *dV/dt*, duty cycle, and switching frequency. Both positive polarity electret and negative polarity electrets are fabricated in the optimum charging conditions discussed in Chapter VI and utilized in PD experiments under positive, negative, and bipolar square voltage. The results show that the electret-based PD mitigation approach is only effective for unipolar switching voltage, i.e., a positive polarity electret can mitigate PD when positive voltage is applied. For negative voltage or bipolar voltage, PD magnitude increased. Despite of this limitation, electret-based PD mitigation approach shows noteworthy performance under any power electronics switching frequency, duty cycle, and slew rate. This makes electret-based PD mitigation approach versatile enough for a variety of PEC topologies.

CHAPTER VI

CONCLUSION

This dissertation is focused on modeling the dielectric characteristics of new dielectric medium and developing new dielectric solution to address the emerging dielectric challenges in high-power density applications.

In the first part of this dissertation, the dielectric breakdown characteristics of supercritical fluids were modeled near the critical point based on the electron scattering cross section data of various cluster size. Electron scattering cross section data of SC CO_2, He, and Xe of various cluster size near the critical points were modeled. The modeled cross section data of various cluster size were utilized in Boltzmann analysis to determine electron kinetic process and thus estimate breakdown electric field near the critical point. Sharp decline in the breakdown electric filed were observed near the critical point, which suggest the increase of mean free path due to the formation of clusters and density fluctuations. The agreements achieved between the modeled data using the electron scattering cross sections of CO_2, He, and Xe clusters near the critical point confirm the validity of the modeling approach.

In the second part, a novel electret based electric field neutralization approach was utilized to mitigate PD caused by defects and power electronics driven voltage stimuli. The surface partial discharge in the presence of triple points and cavity discharge due to the presences of cracks, bubbles, and airgaps are effectively mitigated with the inclusion of PVDF based electret layer. In addition, electret-based electric field neutralization approach was utilized to increase the critical

flashover (CFO) voltage associated with dielectric surface flashover phenomena. By the inclusion of an electret layer, CFO significantly increased under unipolar square voltage waveform. This result confirmed that, electret-based approach can increase the dielectric material robustness by reducing the surface flashover occurrence. Moreover, epoxy-based electret was fabricated based on the triode corona charging method and utilized in mitigating PD occurrence in cryogenic conditions. Epoxy-based electret shows promising performance in mitigating PD and thus confirms their application in high-temperature superconducting (HTS) power cables where epoxy spacers are used for electrical insulation.

Electrets were fabricated under various charging conditions, e.g., charging voltage, charging temperature, charging polarity, and charging temperature, based on the triode corona charging method and evaluated through PD experiments under square and pulse width modulated voltage waveform. It was experimentally demonstrated that electrets fabricated under negative polarity and at elevated temperature show better performance in terms of surface charge density, charge stability, and PD mitigation. It was also observed that with high surface charge density, increased charge stability is required for the electret-based PD solution to be useful. The findings of this study serve as useful indicators that point to the next steps required in this research thrust. The impact of the power electronics voltage parameters, e.g., rise time, duty cycle, polarity, and switching frequency, on PD and the effectiveness of electrets in mitigating PD was also discussed. For each of the parameter, surface discharge and cavity discharge experiments were conducted, and electrets-based PD solution was applied for confirmation. The results experimentally demonstrated that with the inclusion of electret, there is a significant reduction in PD magnitude regardless of slew rate, duty cycle, and switching frequency.

CHAPTER VII

FUTURE WORK

The electron scattering cross section data based dielectric breakdown modeling of SCFs estimates the breakdown electric field for each cluster size. However, due to the lack of reported experimental data on the cluster sizes of SCF near the critical point, the cluster sizes had to be assumed near the critical point. For this reason, there is a discrepancy between the modeled data and the reported experimental data which can be minimized with accurately measured cluster size data. Therefore, further investigation of a method to experimentally measure molecular cluster size of SCFs near the critical point is needed. This electron scattering cross section data based dielectric breakdown modeling can further applied to binary and ternary SCF mixtures those are good candidates as dielectric medium.

In this dissertation, electrets were fabricated from PVDF film based on the triode corona charging method under various charging conditions. The surface potential was measured and using equation (5.1), the surface charge density is measured. Equation (5.1) indicates that, surface charge density also depends on the material properties. Therefore, further investigation on PD mitigation performance by electrets that fabricated from other polymer films, e.g., PTFE, Parylene, etc, can be done to achieve both high surface charge density and increased charge stability. Electret-based PD mitigation approach can further be implemented by spray coating and spin coating on the power substrate to evaluate their performance in PD mitigation. Moreover, electret-based electric field neutralization method is a promising solution to charge accumulation.

REFERENCES

[1] Christophorou, Loucas G., James Kenneth Olthoff, and David S. Green. "Gases for electrical insulation and arc interruption: possible present and future alternatives to pure SF6." (1997)

[2] D. T. Meshri, "Industrial Applications of Inorganic Fluorides," in *Advanced Inorganic Fluorides*, Elsevier, 2000, pp. 661–682. doi: 10.1016/B978-044472002-3/50021-1.

[3] A. Beroual and A. (Manu) Haddad, "Recent Advances in the Quest for a New Insulation Gas with a Low Impact on the Environment to Replace Sulfur Hexafluoride (SF6) Gas in High-Voltage Power Network Applications," *Energies*, vol. 10, no. 8, p. 1216, Aug. 2017, doi: 10.3390/en10081216.

[4] R. Ullah, Z. Ullah, A. Haider, S. Amin, and F. Khan, "Dielectric properties of tetrafluoroethane (R134) gas and its mixtures with N 2 and air as a sustainable alternative to SF 6 in high voltage applications," *Electric Power Systems Research*, vol. 163, pp. 532–537, Oct. 2018, doi: 10.1016/j.epsr.2018.04.019.

[5] X. Li, H. Zhao, and A. B. Murphy, "SF $_6$ -alternative gases for application in gas-insulated switchgear," *J. Phys. D: Appl. Phys.*, vol. 51, no. 15, p. 153001, Apr. 2018, doi: 10.1088/1361-6463/aab314.

[6] See http://www.lxcat.laplace.univ-tlse.fr for PHELPS database, retrieved on June 2013.

[7] J. G. Owens, "Greenhouse gas emission reductions through use of a sustainable alternative to SF6," in *2016 IEEE Electrical Insulation Conference (EIC)*, Montreal, QC, Canada, Jun. 2016, pp. 535–538. doi: 10.1109/EIC.2016.7548658.

[8] S. Stauss, H. Muneoka, K. Urabe, and K. Terashima, "Review of electric discharge microplasmas generated in highly fluctuating fluids: Characteristics and application to nanomaterials synthesisa)," *Phys. Plasmas*, vol. 22, no. 5, p. 057103, May 2015, doi: 10.1063/1.4921145.

[9] E. Lemmon, M. McLinden, and D. Friend, NIST Standard Reference Database 23: Reference Fluid Thermodynamic and Transport Properties—REFPROP, Version 9.0 (National Institute of Standards and Technology, Standard Reference DataProgram, Gaithersburg, 2012).

[10] T. Ito and K. Terashima, “Generation of micrometer-scale discharge in a supercritical fluid environment,” *Appl. Phys. Lett.*, vol. 80, no. 16, pp. 2854–2856, Apr. 2002, doi: 10.1063/1.1470695.

[11] T. Ito, H. Fujiwara, and K. Terashima, “Decrease of breakdown voltages for micrometer-scale gap electrodes for carbon dioxide near the critical point: Temperature and pressure dependences,” *J. Appl. Phys.*, vol. 94, no. 8, p. 5411, 2003, doi: 10.1063/1.1611283.

[12] M. Sawada, T. Tomai, T. Ito, H. Fujiwara, and K. Terashima, “Micrometer-scale discharge in high-pressure H2O and Xe environments including supercritical fluid,” *Journal of Applied Physics*, vol. 100, no. 12, p. 123304, Dec. 2006, doi: 10.1063/1.2400802.

[13] H. Muneoka, K. Urabe, S. Stauss, and K. Terashima, “Micrometer-scale electrical breakdown in high-density fluids with large density fluctuations: Numerical model and experimental assessment,” *Phys. Rev. E*, vol. 91, no. 4, p. 042316, Apr. 2015, doi: 10.1103/PhysRevE.91.042316.

[14] J. Wei, C. Park, and L. Graber, “Breakdown characteristics of carbon dioxide–ethane azeotropic mixtures near the critical point,” *Physics of Fluids*, vol. 32, no. 5, p. 053305, May 2020, doi: 10.1063/5.0004030.

[15] J. Wei, A. Cruz, F. Haque, C. Park, and L. Graber, “Investigation of the dielectric strength of supercritical carbon dioxide–trifluoroiodomethane fluid mixtures,” *Physics of Fluids*, vol. 32, no. 10, p. 103309, Oct. 2020, doi: 10.1063/5.0024384.

[16] Ž. Knez, E. Markočič, M. Leitgeb, M. Primožič, M. Knez Hrnčič, and M. Škerget, “Industrial applications of supercritical fluids: A review,” *Energy*, vol. 77, pp. 235–243, Dec. 2014, doi: 10.1016/j.energy.2014.07.044.

[17] J. Wei, A. Cruz, C. Xu, F. Haque, C. Park, and L. Graber, “A Review on Dielectric Properties of Supercritical Fluids,” in *2020 IEEE Electrical Insulation Conference (EIC)*, Knoxville, TN, USA, Jun. 2020, pp. 107–113. doi: 10.1109/EIC47619.2020.9158733.

[18] J. Wei, A. Cruz, F. Haque, C. Park, and L. Graber, “Electrical Breakdown Characteristics of Supercritical Trifluoroiodomethane-Carbon Dioxide (CF3I-CO2) Mixtures,” in *2020 IEEE Conference on Electrical Insulation and Dielectric Phenomena (CEIDP)*, East Rutherford, NJ, USA, Oct. 2020, pp. 427–430. doi: 10.1109/CEIDP49254.2020.9437475.

[19] Y. Tian, J. Wei, C. Park, Z. Wang, and L. Graber, “Modelling of electrical breakdown in supercritical CO2 with molecular clusters formation,” in *2018 12th International Conference on the Properties and Applications of Dielectric Materials (ICPADM)*, Xi’an, May 2018, pp. 992–995. doi: 10.1109/ICPADM.2018.8401205.

[20] F. Haque, J. Wei, L. Graber, and C. Park, “Modeling the dielectric strength variation of supercritical fluids driven by cluster formation near critical point,” *Physics of Fluids*, vol. 32, no. 7, p. 077101, Jul. 2020, doi: 10.1063/5.0008848.

[21] F. Haque, J. Wei, A. Cruz, L. Graber, and C. Park, “Modeling cluster formation driven variations in critical electric field of He and Xe near critical point based on electron scattering cross sections,” *Physics of Fluids*, vol. 32, no. 12, p. 127106, Dec. 2020, doi: 10.1063/5.0028601.

[22] C. Park, S. Pamidi, and L. Graber, “Boltzmann Analysis of Cryogenic He – H_{2} Gas Mixtures as Dielectric Media for High-Temperature Superconducting Power Devices,” *IEEE Trans. Appl. Supercond.*, vol. 27, no. 4, pp. 1–6, Jun. 2017, doi: 10.1109/TASC.2016.2637319.

[23] C. Park, S. Pamidi, and L. Graber, “The critical electric field of gas mixtures over the extended range of cryogenic operating conditions,” *Journal of Applied Physics*, vol. 122, no. 15, p. 153301, Oct. 2017, doi: 10.1063/1.4995663.

[24] C. Park, L. Graber, and S. Pamidi, “The dielectric properties of gaseous cryogen mixtures of He, H_2, Ne, and N_2 in a temperature range of 50–80 K at pressures up to 2.0 MPa,” *Journal of Applied Physics*, vol. 121, no. 8, p. 083304, Feb. 2017, doi: 10.1063/1.4976565.

[25] C. Park, S. Pamidi, and L. Graber, “The dielectric strength of dissociated cryogenic gas media,” *Journal of Applied Physics*, vol. 124, no. 10, p. 104104, Sep. 2018, doi: 10.1063/1.5051769.

[26] L. Graber *et al.*, “Cryogenic power electronics at megawatt-scale using a new type of press-pack IGBT,” *IOP Conf. Ser.: Mater. Sci. Eng.*, vol. 279, p. 012011, Dec. 2017, doi: 10.1088/1757-899X/279/1/012011.

[27] C. Park, M. J. Mauger, T. Damle, J. Huh, S. Steinhoff, and L. Graber, “Cryogenic Power Electronics: Press-Pack IGBT Modules,” *IOP Conf. Ser.: Mater. Sci. Eng.*, vol. 756, p. 012009, Jun. 2020, doi: 10.1088/1757-899X/756/1/012009.

[28] C. Park, O. Obadolagbonyi, and L. Graber, “Cryogenic Power Electronics: Capacitors and Inductors,” *IOP Conf. Ser.: Mater. Sci. Eng.*, vol. 756, p. 012010, Jun. 2020, doi: 10.1088/1757-899X/756/1/012010.

[29] C. Xu, R. Saluja, T. Damle, and L. Graber, “Future cryogenic switchgear technologies for superconducting power systems,” *IOP Conf. Ser.: Mater. Sci. Eng.*, vol. 279, p. 012012, Dec. 2017, doi: 10.1088/1757-899X/279/1/012012.

[30] P. Cheetham *et al.*, “High Temperature Superconducting Power Cables for MVDC Power Systems of Navy Ships,” in *2019 IEEE Electric Ship Technologies Symposium (ESTS)*, Washington, DC, USA, Aug. 2019, pp. 548–555. doi: 10.1109/ESTS.2019.8847830.

[31] S. Pamidi, C. H. Kim, J.-H. Kim, D. Crook, and S. Dale, “Cryogenic helium gas circulation system for advanced characterization of superconducting cables and other devices,” *Cryogenics*, vol. 52, no. 4–6, pp. 315–320, Apr. 2012, doi: 10.1016/j.cryogenics.2011.09.006.

[32] A. Al-Gheilani, W. Rowe, Y. Li, and K. L. Wong, “Stress Control Methods on a High Voltage Insulator: A Review,” *Energy Procedia*, vol. 110, pp. 95–100, Mar. 2017, doi: 10.1016/j.egypro.2017.03.112.

[33] T. Doshi, R. Gorur, and J. Hunt, “Electric field computation of composite line insulators up to 1200 kV AC,” *IEEE Trans. Dielect. Electr. Insul.*, vol. 18, no. 3, pp. 861–867, Jun. 2011, doi: 10.1109/TDEI.2011.5931075.

[34] B. M’hamdi, M. Teguar, and A. Mekhaldi, “Optimal design of corona ring on HV composite insulator using PSO approach with dynamic population size,” *IEEE Trans. Dielect. Electr. Insul.*, vol. 23, no. 2, pp. 1048–1057, Apr. 2016, doi: 10.1109/TDEI.2015.005383.

[35] Yang Qing, Wenxia Sima, Deng Jiazhuo, Yuan Tao, and Chen Lin, “New optimization method on electric field distribution of composite insulator,” in *2010 Annual Report Conference on Electrical Insulation and Dielectic Phenomena*, West Lafayette, IN, Oct. 2010, pp. 1–4. doi: 10.1109/CEIDP.2010.5724046.

[36] Z. Peng, P. Liu, and P. Yu, “Structural Optimization of a New-style Insulator Used in High-Voltage Transmission Lines,” in *2006 IEEE 8th International Conference on Properties and applications of Dielectric Materials*, Bali, Indonesia, Jun. 2006, pp. 832–835. doi: 10.1109/ICPADM.2006.284306.

[37] H. Reynes, C. Buttay, and H. Morel, “Protruding ceramic substrates for high voltage packaging of wide bandgap semiconductors,” in *2017 IEEE 5th Workshop on Wide Bandgap Power Devices and Applications (WiPDA)*, Albuquerque, NM, Oct. 2017, pp. 404–410. doi: 10.1109/WiPDA.2017.8170581.

[38] H. Ye *et al.*, “Review on HVDC cable terminations,” *High Voltage*, vol. 3, no. 2, pp. 79–89, Jun. 2018, doi: 10.1049/hve.2017.0144.

[39] M. Goel, “Electret sensors, filters and MEMS devices: New challenges in materials research,” *CURRENT SCIENCE*, vol. 85, no. 4, p. 11, 2003.

[40] Y. Suzuki, “Recent progress in MEMS electret generator for energy harvesting,” *IEEJ Trans Elec Electron Eng*, vol. 6, no. 2, pp. 101–111, Mar. 2011, doi: 10.1002/tee.20631.

[41] Kao, K. C. (2004). *Dielectric phenomena in solids*. Elsevier.

[42] J. A. Giacometti, S. Fedosov, and M. M. Costa, “Corona charging of polymers: recent advances on constant current charging,” *Braz. J. Phys.*, vol. 29, no. 2, pp. 269–279, Jun. 1999, doi: 10.1590/S0103-97331999000200009.

[43] S. Boisseau, G. Despesse, T. Ricart, E. Defay, and A. Sylvestre, “Cantilever-based electret energy harvesters,” *Smart Mater. Struct.*, vol. 20, no. 10, p. 105013, Oct. 2011, doi: 10.1088/0964-1726/20/10/105013.

[44] A. Kilic, S. Russell, E. Shim, and B. Pourdeyhimi, “The charging and stability of electret filters,” in *Fibrous Filter Media*, Elsevier, 2017, pp. 95–121. doi: 10.1016/B978-0-08-100573-6.00025-3.

[45] K. Tao *et al.*, “Electrostatic/triboelectric hybrid power generator using folded electrets,” in *2017 IEEE 30th International Conference on Micro Electro Mechanical Systems (MEMS)*, Las Vegas, NV, USA, Jan. 2017, pp. 45–48. doi: 10.1109/MEMSYS.2017.7863335.

[46] C. Park, “Electret: An Entirely New Approach of Solving Partial Discharge Caused by Triple Points, Sharp Edges, Bubbles, and Airgaps,” *IEEE Access*, vol. 8, pp. 78354–78366, 2020, doi: 10.1109/ACCESS.2020.2990310.

[47] C. Park, “Electrets: A Remedy for Partial Discharge Caused by Power Electronics Switching,” *IEEE Trans. Ind. Electron.*, pp. 1–1, 2020, doi: 10.1109/TIE.2020.3045707.

[48] F. Haque, J. Wei, L. Graber, and C. Park, “Electron Scattering Cross Section Data of Supercritical CO_2 Clusters,” in *2020 IEEE Electrical Insulation Conference (EIC)*, Knoxville, TN, USA, Jun. 2020, pp. 144–147. doi: 10.1109/EIC47619.2020.9158748.

[49] F. Bottiglioni, J. Coutant, and M. Fois, “Ionization Cross Sections for H 2 , N 2 , and C O 2 Clusters by Electron Impact,” *Phys. Rev. A*, vol. 6, no. 5, pp. 1830–1843, Nov. 1972, doi: 10.1103/PhysRevA.6.1830.

[50] See http://www.lxcat.laplace.univ-tlse.fr for MORGAN database, retrieved on June 2013.

[51] See http://www.lxcat.laplace.univ-tlse.fr for PHELPS database, retrieved on June 2013.

[52] See http://www.lxcat.laplace.univ-tlse.fr for SIGLO database, retrieved on June 2013.

[53] W. Henkes and F. Mikosch, “The effective cross section for ionization by electrons of molecules in hydrogen clusters,” *International Journal of Mass Spectrometry and Ion Physics*, vol. 13, no. 2, pp. 151–161, Feb. 1974, doi: 10.1016/0020-7381(74)80020-3.

[54] A. N. Zavilopulo, A. I. Dolgin, and M. A. Khodorkovsky, “Investigation of argon cluster ionization cross sections by electron impact,” *Phys. Scr.*, vol. 50, no. 6, pp. 696–700, Dec. 1994, doi: 10.1088/0031-8949/50/6/013.

[55] H. Muneoka, K. Urabe, S. Stauss, and K. Terashima, “Breakdown Characteristics of Electrical Discharges in High-Density Helium Near the Critical Point,” *Appl. Phys. Express*, vol. 6, no. 8, p. 086201, Aug. 2013, doi: 10.7567/APEX.6.086201.

[56] G. J. M. Hagelaar and L. C. Pitchford, “Solving the Boltzmann equation to obtain electron transport coefficients and rate coefficients for fluid models,” *Plasma Sources Sci. Technol.*, vol. 14, no. 4, pp. 722–733, Nov. 2005, doi: 10.1088/0963-0252/14/4/011.

[57] F. Haque, O. Faruqe, and C. Park, “Electret: A Solution to Partial Discharge in Power Electronics Applications,” in *2021 IEEE Energy Conversion Congress and Exposition (ECCE)*, Vancouver, BC, Canada, Oct. 2021, pp. 5573–5577. doi: 10.1109/ECCE47101.2021.9595237.

[58] F. Haque, O. Faruqe, and C. Park, “Electret: A Remedy for Partial Discharge and Surface Flashover in Shipboard Power Applications,” in *2021 IEEE Electric Ship Technologies Symposium (ESTS)*, Arlington, VA, USA, Aug. 2021, pp. 1–5. doi: 10.1109/ESTS49166.2021.9512338.

[59] F. Haque and C. Park, “Epoxy Electret: A Remedy for Partial Discharge at Cryogenic Temperature,” p. 6.

[60] A. Thyssen, "Charge distribution and stability in electret materials," Ph.D. dissertation, 2016.

[61] F. Haque and C. Park, “Electret Fabrication Under Various Discharge Conditions of Triode Corona Charging and the Partial Discharge Mitigation Performance,” in *2021 IEEE Electrical Insulation Conference (EIC)*, Denver, CO, USA, Jun. 2021, pp. 289–292. doi: 10.1109/EIC49891.2021.9612314.

[62] F. Haque, O. Faruqe, and C. Park, “Electret Fabrication Under Various Temperatures and Partial Discharge Mitigation Performance,” in *2021 IEEE Conference on Electrical Insulation and Dielectric Phenomena (CEIDP)*, Vancouver, BC, Canada, Dec. 2021, pp. 175–178. doi: 10.1109/CEIDP50766.2021.9705449.

[63] “High-voltage test techniques – Partial discharge measurements,” IEC Standard 60270, p. 61, Dec. 2000.

[64] P. Cheetham, W. Kim, C. H. Kim, S. V. Pamidi, L. Graber, and H. Rodrigo, “Use of partial discharge inception voltage measurements to design a gaseous helium cooled high temperature superconducting power cable,” *IEEE Trans. Dielect. Electr. Insul.*, vol. 24, no. 1, pp. 191–199, Feb. 2017, doi: 10.1109/TDEI.2016.005909.

[65] T. Stamm, P. Cheetham, C. Park, C. H. Kim, L. Graber, and S. Pamidi, “Novel gases as electrical insulation and a new design for gas-cooled superconducting power cables,” *IEEE Electr. Insul. Mag.*, vol. 36, no. 5, pp. 32–42, Sep. 2020, doi: 10.1109/MEI.2020.9165697.

[66] J. R. Harris, “A tutorial on vacuum surface flashover,” *IEEE Trans. Plasma Sci.*, vol. 46, no. 6, pp. 1872–1880, Jun. 2018, doi: 10.1109/TPS.2017.2759248.

[67] O. Faruqe, F. Haque, H. Berdiyev, and C. Park, “Surface Flashover Characteristics of Solid Dielectrics in Shipboard Atmospheric Conditions,” in *2021 IEEE Electric Ship Technologies Symposium (ESTS)*, Arlington, VA, USA, Aug. 2021, pp. 1–5. doi: 10.1109/ESTS49166.2021.9512357.

[68] O. Faruqe, F. Haque, and C. Park, “Electret: A Method to Increase Critical Flashover Voltage in Power Dense Applications,” in *2021 IEEE Conference on Electrical Insulation and Dielectric Phenomena (CEIDP)*, Vancouver, BC, Canada, Dec. 2021, pp. 109–112. doi: 10.1109/CEIDP50766.2021.9705382.

[69] F. Haque and C. Park, “Effects of Fabrication Conditions on the Partial Discharge Mitigation Performance of Electrets for Power Electronic Driven Systems,” *IEEE TRANSACTIONS ON INDUSTRIAL ELECTRONICS*, p. 11.

[70] S. S. Bamji, K. J. Jao, and M. M. Perlman, “Polymer electrets corona charged at high temperature,” *Journal of Electrostatics*, vol. 6, no. 4, pp. 373–379, Sep. 1979, doi: 10.1016/0304-3886(79)90006-8.

[71] P. Romano *et al.*, “Partial discharges at different voltage waveshapes: Comparison between two different acquisition systems,” *IEEE Trans. Dielect. Electr. Insul.*, vol. 25, no. 2, pp. 584–593, Apr. 2018, doi: 10.1109/TDEI.2018.006782.

[72] P. Wang, G. C. Montanari, and A. Cavallini, “Partial Discharge Phenomenology and Induced Aging Behavior in Rotating Machines Controlled by Power Electronics,” *IEEE Trans. Ind. Electron.*, vol. 61, no. 12, pp. 7105–7112, Dec. 2014, doi: 10.1109/TIE.2014.2320226.

[73] M. Borghei and M. Ghassemi, “Partial Discharge Finite Element Analysis under Fast, Repetitive Voltage Pulses,” in *2019 IEEE Electric Ship Technologies Symposium (ESTS)*, Washington, DC, USA, Aug. 2019, pp. 324–328. doi: 10.1109/ESTS.2019.8847797.